LBL-12076
UC-70
CONF-800344

3rd INVITATIONAL WELL-TESTING SYMPOSIUM

"Well Testing in Low Permeability Environments"

Proceedings

March 26-28, 1980 • Berkeley, California

Earth Sciences Division

Lawrence Berkeley Laboratory • University of California
Berkeley, California 94720

This work was supported by the Assistant Secretary for Resource Applications, Office of Industrial and Utility Applications and Operations Division of Geothermal Energy of the U.S. Department of Energy under Contract No. W-7405-ENG-48.

LBL-12076
UC-70
CONF-800344

THIRD INVITATIONAL WELL-TESTING SYMPOSIUM

"Well Testing in Low Permeability Environments"

March 26 - 28, 1980

Thomas W. Doe

and

Werner J. Schwarz

Editors

Earth Sciences Division

University of California

Lawrence Berkeley Laboratory

Berkeley, California

March 1981

This work was supported by the Assistant Secretary for Resource Applications, Office of Industrial and Utility Applications and Operations Division of Geothermal Energy of the U.S. Department of Energy, under Contract No. W-7405-ENG-48.

CONTENTS

WELL TEST DESIGN IN LOW PERMEABILITY FORMATIONS

J. Gale, University of Waterloo, Ontario, Canada - Chairman

ANALYSIS AND INTERPRETATION OF WELL TEST DATA

S. Papadopulos, Potomoc, Maryland - Chairman

INSTRUMENTATION FOR WELL TESTS

T. W. Doe, Lawrence Berkeley Laboratory - Chairman

PREFACE

Thomas W. Doe and Werner J. Schwarz

The goal of the LBL invitational Well Testing Symposiums has been to encourage the interchange of ideas and technology between the fields of Reservoir Engineering, Hydrogeology, Civil Engineering, and energy related Earth Sciences. The initial symposium in 1977 included papers of a wide variety of interests in geothermal well testing. For the second symposium, the subject of injection of fluids underground was selected to focus the symposium proceedings.

Following the precedent of the second symposium, a topic was chosen focusing the proceedings of the third symposium on the testing of low permeability rocks. Unlike the previous symposiums, which were primarily geothermal in nature, the testing of low permeability rocks is a problem common to waste disposal, fossil energy resource development, and underground excavation for civil or mining purposes as well as to geothermal energy development. The development of well-testing in some of these fields has proceeded somewhat independently of the others, hence an interdisciplinary symposium on this topic was felt to be most appropriate.

During the last decade the need for low permeability well-testing has increased significantly. Within the energy resource field there has been the development of hot dry rock geothermal systems, exploitation of tight gas sands, and the development of in situ processing for oil shale and coal. The waste isolation area has seen both radioactive and toxic non radioactive waste disposal in tight formations become an urgent national concern. In the civil and mining areas the use of underground excavations for housing power structures and deep mining for increasingly scarce resources are requiring more and better ground water flow information.

The basic challenge of low permeability well testing is the performance of a test within a reasonable length of time, within the sensitivity of the instrumentation, and affecting a significant volume of rock. Although the governing equations for fluid are not greatly changed by the low value of a rock's permeability, well test techniques

developed for production of fluids in high permeability rocks may not be appropriate due to such factors as the time required for the test or well bore storage. The instrumentation needs are also important as flowmeters and pressure gages need greater reliability and sensitivity for injection tests, interference tests, and other techniques. Although there is much work yet to be done in low permeability well-testing, the papers presented in this volume are a fair representation of the significant progress that has been made in the last few years.

The Earth Sciences Division selected a third symposium organizing committee, under the chairmanship of Professor Paul A. Witherspoon. Members were Thomas W. Doe, T. N. Narasimhan, Ron C. Schroeder and Werner J. Schwarz. The symposium and the proceedings were edited by Thomas W. Doe and Werner J. Schwarz.

The symposium provided a forum for the over 130 participants in which to exchange ideas and present new information on low permeability rocks. The emphasis was on reviewing existing capabilities, identifying current limitations, and generating new ideas for meeting the Department of Energy/Division of Geothermal Energy goals. The opening session was chaired by Ron C. Schroeder and Professor Paul A. Witherspoon who gave the keynote address.

The participants represented the major national laboratories, federal and state governments, industry, utilities, independent consultants, 9 major universities, Canada, England, Germany, Mexico, and Sweden.

Abstracts and papers from non Lawrence Berkeley Laboratory authors are being reproduced unchanged. Lawrence Berkeley Laboratory papers were reviewed by the Earth Sciences Division's Publications Committee and by the Technical Information Department.

ABSTRACT

PERMEABILITY OF DENSE ROCK WITH PARTICULAR RELATION TO THE ISOLATION OF HAZARDOUS WASTE

S. N. Davis

University of Arizona
Tucson, Arizona

During the past decade, the determination of the permeability of very dense rocks has been of increasing importance owing to activities such as 1) the geologic isolation of hazardous wastes, 2) the storage of hydrocarbon fuels, 3) the design of dry-rock geothermal schemes, 4) the study of the distribution of ore deposits, and 5) the investigation of the generating mechanisms of earthquakes.

Hazardous wastes must be isolated for periods of time ranging from a few years to more than 10,000 years. Rock permeability, which controls the rate of redistribution of the waste by groundwater, is not entirely a predictable property over the longer time spans. As a consequence, geochemical techniques of dating water and secondary minerals are being considered as a means to reconstruct the history of permeability changes within a rock with the objective of trying to predict the nature and possible magnitude of future changes.

ABSTRACT

ROLE OF MASSIVE HYDRAULIC FRACTURING IN THE EXPLOITATION AND DEVELOPMENT OF OIL AND GAS RESERVES IN LOW PERMEABILITY FORMATIONS

Ram G. Agarwal
Amoco Production Company
Tulsa, Oklahoma

Massive hydraulic fracturing (MHF) appears to be a proven stimulation technique for commercially developing natural gas resources contained in low permeability formations. This paper briefly reviews the locations of major tight gas basins in the U.S. and points out the limitatons of the conventional analysis methods (normally applied to high permeability formations) in predicting reserves for tight gas wells. Methods are discussed to evaluate and predict the performance of low permeability gas wells stimulated by MHF. Field examples are included to demonstrate the applicability of such methods. Portions of this talk are taken from Reference 1.

Reference

1. Agarwal, R. G., Carter, R. D., and Pollock, C. B.: "Evaluation and Performance Prediction of Low-Permeability Gas Wells Stimulated by Massive Hydraulic Fracturing," J. Pet. Tech. (March, 1979) 362-372D; Trans., AIME, 267.

THE ROLE OF WELL TESTING IN CIVIL ENGINEERING

Don Banks
Chief, Engineering Geology and Rock Mechanics Division
U. S. Army Engineer Waterways Experiment Station
Vicksburg, Mississippi

Civil engineering involves the application of art and science to the investigation, evaluation, design, construction, operation, and maintenance of worthwhile projects. Projects on which well testing results are important to the civil engineer are obviously those in which the subsurface flow of water potentially impacts upon safety and economical considerations. A few examples include: flow of water (a) through foundations and abutments of dams, (b) within slopes, or (c) into subsurface excavations and underground openings; development of underground water supplies; and leakage from reservoirs and canals. Closely akin to the cited examples are control measures to prevent flow (i.e., grouting) and to reduce pore water pressures (i.e., drains) and construction techniques. To the above-listed, more traditional examples of civil engineering projects, new projects of national interest with new needs are being identified. Projects requiring a renewed interest in the understanding of underground flow of water are exampled by needs for underground storage of radioactive or other forms of hazardous wastes; underground storage of energy-producing products; development of alternate forms of energy reserves (i.e., geothermal); and concern over pollutant migration. Significantly, experience has shown that the most successful approach in solving the more traditional projects, thereby indicating a similar approach to the more newly identified projects, has been when the civil engineer works as a team member with engineering geologists, hydrogeologists, and groundwater hydrologists.

The purpose of well testing is to derive a value of the permeability of the geologic medium or to directly measure the velocity or quantity of fluid flow. In the former situation, a change of the in-hole water pressure is created and the resulting response of the system is measured. Through interpretation of the response measurements by means of appropriate conceptual models, the permeability of the medium can be derived. In the latter situation, borehole velocity meters or tracers, as examples, are used to measure the rate at which water is flowing in the medium. Once the tests are analyzed, a site-specific, boundary-valued problem is solved to permit design decisions to be made. Past civil engineering interest has generally focused on flow in the near-surface environment (or, in the case of tunnels, in the new-bore environment). Thus, equipment and procedures were generally developed to operate to nominal depths - say 200 to 300 ft. Secondly, because of traditional interests, pertinent tests have been conducted in the more pervious zones with the result that test equipment has been relatively simple. Thirdly, because the usual use of the data was to make a design decision (e.g., whether or not to grout; the type of draining or dewatering scheme to be employed; sizing of pumps, etc.), relatively simplistic models have been employed. The inherent variability of geologic media and the general application of the results from well testing have given the civil engineer some degree of comfort in satisfying the often quoted "criteria" of determining a measure of the permeability "within an order of magnitude." Perhaps with new projects and more stringent needs, the civil engineer must now work even more closely with the engineering geologist or hydrogeologist to better define the medium in which the tests are being conducted and to improve equipment and analysis procedures for use in geologic media exhibiting much lower permeabilities than were previously of importance.

Civil engineering projects are quite varied by nature, and thus, without the interjection of site-specific considerations or personal preferences, cause a variety of techniques to be employed. The types of tests (with attendant depth of investigation limitations) typically employed on civil engineering projects are:

- Simple borehole tests
  - --Water gain/loss during drilling
  - --Variable or constant head tests in open boreholes
- Packer or pressure tests in boreholes
  - --Single packer assembly
  - --Double (or at times multiple) packer assemblages
- Permeameter tests
  - --Sealed individual piezometers
  - --Continuous borehole piezometers
- Well pumping tests
- In-hole tests using well flow meters or tracer tests

While general, good practice requires records to be maintained by the drilling inspector or on-site geologist of water losses or gains during drilling, the understanding of subsurface flow of water is much more complicated than would be indicated by total reliance on this type "test." In fact, except in cases where there is a total loss of water into cavernous limestones, the observations can lead to an incomplete and erroneous picture.

Variable or constant head tests in open boreholes are frequently conducted in near-surface settings. Generally, these tests are limited to the most pervious of materials. In the case of water flowing into the media, fines may

clog conduits to cause an under-estimate of the permeability of the media; in the case of water flowing from the media, fines may wash from the conduits to cause an over-estimate of the permeability.

Packer tests are normally conducted, either with single, double, or multiple assemblages when (a) distinct stratification of materials is indicated, (b) the number of borings is limited, or (c) the depths of interest indicate that the conduct of interference-type tests (i.e., well pumping) may be exceedingly expensive. In the packer test one or more packers are inflated to isolate the section between the packer and the bottom of the hole or between successive packers. A standpipe, either free or connected to a pump, and a source of water are used to elevate the pressure in the isolated section. Observations of the relationship between the quantity of flow and the active pressure in the isolated section, along with assumptions regarding the geologic media, lead to an estimate of the permeability of the zone being tested. It is often thought that if a sufficient number of tests are conducted, along with detailed geologic observation of the rock core or of the borehole wall, then meaningful, relative information can be obtained. However, it is well known that the test results are strongly influenced if fines in the injected water tend to clog the fractures. Similarly, it is known that the results can be completely misleading depending upon the location of the borehole and packer with respect to the joint system present in the rock mass.

Generally, in civil engineering practice (with variations depending upon the purpose of the project), if the average permeability as deduced from the simple tests described above does not vary over an order of magnitude,

then further testing and definition is not considered to be required. The completion of the project will generally be made with occasional single piezometers installed in selected boreholes to indicate seasonal changes in the groundwater flow or construction related changes as caused by excavation or drainage or as retarded by grouting measures.

Where the results indicate strata of extremely high or low permeabilities, then multiple piezometers are many times installed. These multiple piezometer installations can be of single piezometers located in a close cluster of boreholes, each to a different depth, or several piezometers installed in a single borehole.

Most piezometers are carefully installed with a protecting filter or screening material placed around the tip. Permanent seals are placed both above and below the screen. The piezometer will be developed by bailing, pumping, and surging before being declared operational. Generally, a falling head or rising head test will be performed to give yet another measure of the permeability of the strata in which the piezometer tip is placed. Observation of the piezometric levels with time gives detailed information of the response of the geologic media to changes in flow as caused by excavation or drainage or as retarded by grouting measures.

These type tests are recognized as affecting only a local volume of material and, on projects in which an interpretation of the mass characteristics is sought, may be supplemental or used in conjunction with well pumping tests or tracer tests. When well pumping tests or tracer tests are employed, generally near-surface flows are of concern. Deeper flows are determined only on projects of major importance.

While these types of tests are usually employed, test equipment, test conduct, and interpretation of results are almost as varied as the number of people conducting the tests. A review of the literature will indicate numerous papers describing adaptations or variations of traditional tests purportedly to meet site-specific requirements but at times, it is suspected, to meet the personal preferences of individual engineers. By themselves such adaptations should not be criticized, but where unnecessary, adherence to established guidelines would greatly aid in the portability of data or in establishing meaningful data bases for use in similar situations. Detailed descriptions for various tests can be found in the Earth Manual of the formerly-known Bureau of Reclamation; in the U. S. Army Technical Manual TM 5-818-5 (April 1971), Dewatering and Groundwater Control for Deep Excavations (also numbered NAVFAC P-418 and AFM 88-5, Chap. 6); in Time Lag and Soil Permeability in Groundwater Observations by Hvorslev, WES Bulletin No. 36 (1951); in the suggested procedures of the International Society for Rock Mechanics Commission on Standardization of Laboratory and Field Tests, "Suggested Methods for Determining Hydraulic Parameters and Characteristics of Rock Masses" (Part 5) and "Suggested Method for Determining Permeability by Water Injection Out of Three Cells Separsted by Packers in a Borehole" (Part 6).

Such standardized approaches to obtaining a measure of the flow of water through geologic media have generally been sufficient in past civil engineering applications. However, with new needs, such as previously described, the civil engineer and his coworkers must critically reexamine past approaches. The reexamination must cover the areas of:

a. Flow phenomena.

b. Test equipment and equipment control.

c. Test procedure.

d. Interpretation of test results.

e. Numerical modeling to extend the results over the volume of interest.

f. Well-documented case studies indicating successful applications and importantly, unsuccessful applications with stated reasons.

To a large extent, continuation of symposia, such as this one, will provide the forum for researchers, practitioners, equipment developers, and modelers to assemble and discuss the results of reexamination and improvement in describing fluid flow in geologic media.

New problem needs by their nature imply a determination of flow characteristics at greater depths than generally involved in civil engineering practice and in materials of low permeability. Work being performed by the groundwater hydrologists, engineering geologists, hydrogeologists, civil engineers, petroleum engineers, geothermal engineers, theoreticians, and numerical modelers all have a significant place to play.

If it can be assumed that the fluid flow in the deep, low permeability environment will be dominated by flow through discontinuities, then problems of accurately defining the presence and characteristics of the network of discontinuities are immediately evident. Once descriptions are obtained from core or borehole observation techniques, a major problem involves the extrapolation of the information to unexplored regions of interest, i.e., a description of the heterogeneity of the flow system. Then superimposed upon this boundary description is a description of the response of the system to changes in pressure, temperature, possible mixed fluid flow, possible unsaturated flow,

and possible variable flow laws, i.e., laminar, transitional, and turbulent flow. These considerations must precede the design and selection of equipment, determination of test procedure, interpretation of test results, and application of results to obtain a successful solution of the engineering problem.

The tasks are many. Coordinated reexamination and continued development by many workers in several disciplines will be required to successfully come to grips with the solution of fluid flow in low permeability environments. I, for one, applaud the efforts of personnel at the Lawrence Berkeley Laboratory as individual workers and in hosting this symposium. I am looking forward to hearing of the advances described in the technical papers.

HOT DRY ROCK GEOTHERMAL RESERVOIR ENGINEERING

R. Lee Aamodt
Los Alamos National Laboratory
Resource Engineering, G-5
Los Alamos, NM 87545

History

The Los Alamos Hot Dry Rock Geothermal Energy project is located on the Jemez plateau, in northern New Mexico, about two miles (3.2 km) west of the ring fault which bounds the Valles Caldera. Two wells, GT-2 and EE-1, were originally drilled to a depth of 9600 ft (2.93 km) and 10,000 ft (3.05 km), respectively, and, after some difficulties, including re-drilling of the bottom portion of GT-2, a good fracture connection was made between EE-1 and GT-2B, as the modified GT-2 was called. Water entered this fracture from EE-1 at a depth of 9020 ft (2.75 km) and emerged from several exits in GT-2B. The main exit was located at 8760 ft (2.67 km).

This circulation system was studied extensively for the purpose of establishing a number of fracture properties. Techniques were developed to determine orientation, geometry, heat exchange area, volume, flow impedance and impedance distribution.

A much larger fracture system was then created from a depth of 9620 ft (2.93 km) in EE-1. Similar studies are underway or have been completed on this system. Figure 1 shows schematically the system as it appears today. The techniques used and results obtained in the study of the new and old fracture systems are discussed below.

Fracture Creation

All fractures created in EE-1 and GT-2 by hydraulically pressurizing the wellbore appear to have been weakly cemented natural fractures, as no breakdown-pressure peak has been seen. The fractures may not be oriented at right angles to the least principal horizontal earth stress. They appear to stay partially open after their formation, possibly because of a shear component in the earth stress acting on the fracture, with a resulting displacement of the faces relative to one another.

When the gradient in earth stress is considered, normal hydraulic fracture equations usually do not apply. Quasi 3-D machine calculations by A. Vollan and T. Wacker of Dornier System GmbH, West Germany[1] show that with a fracturing fluid such as water, fractures will generally assume an elongated pear shape, eventually running away in the upward direction. Pumping at high flow rates reduces this effect, maximizes shear displacement of the fracture faces, and opens up the maximum number of joints of various orientations.

Fracture Orientation

Seismic signals accompanying fracture growth delineate regions of high pressure. The signals are observed with a downhole seismometer having three sets of four seismometers oriented at right angles. Signal direction can be determined, with 180° ambiguity, from the first P-wave cycle, while distance is deduced from the time difference between P- and S-wave arrivals. A pressure sensor at a different point in the wellbore can remove the directional ambiguity.

Geometry

Information about joint systems can be derived in a single well by borehole televiewer and dipmeter logs. Correlation of logs in nearby wellbores is also informative. Spinner and temperature logs taken under flowing conditions identify the major entrance and exit points. The top of the fracture can be located by passing sound waves between wellbores, if the fracture lies between them. Since temperature recovery in radial geometry is faster than in plane geometry, the bottom of the fracture can be located after a few weeks of no flow, if it is close enough to one wellbore.

Heat Exchange Area

Figure 2 shows the fit obtained between calculations and observations of temperature drawdown in the old fracture system during the 75-day test. The new fracture is now undergoing a flow test. The heat exchange area is one of the most reliable numbers obtained during a flow test.

Volume

Fracture volume is obtained by injecting a slug of concentrated dye into the reservoir. Figure 3 shows results for both the old and new fractures. The new volume is ~32,000 gallons (122 m^3), if the volume at the peak of the returning dye concentration is used. This is about ten times the volume of the old fracture.

Flow Impedance and Distribution

Flow impedance is defined as the difference in pressure between the exit and entrance points of a flowing well-pair, divided by the flow rate. The overall impedance requires a correction for the difference in pressure of water in the hot and cold legs of the reservoir. An entrance and exit impedance may be derived from the prompt change in pressure when the wells are shut in.

Reference

1. MAGES, Report submitted to the Executive Committee for the Program of Research and Development on Man-Made Geothermal Energy Systems under the auspices of the International Energy Agency, 1979.

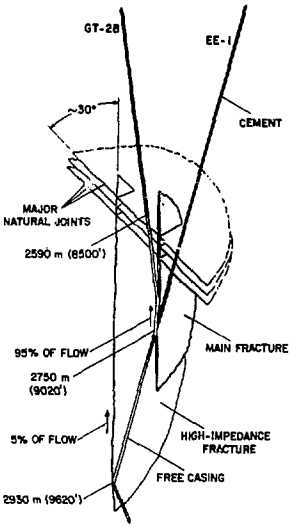

Fig. 1. Present configuration of reservoir (schematic).

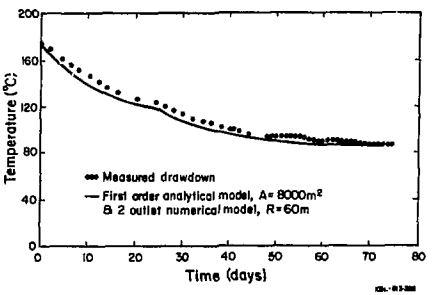

Fig. 2. Calculated and observed temperature drawdown curves.

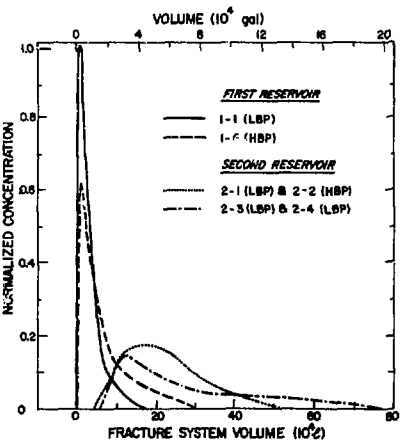

Fig. 3. Dye tracer recovery curves.

ABSTRACT

WELL TESTING IN TIGHT GAS SANDS

L. A. Rogers
Institute of Gas Technology
Chicago, Illinois

Department of Energy tests of geopressured-geothermal wells in Louisiana and Texas are providing data from which reservoir analysis and potential production can be made. IGT is participating in the geopressured-geothermal program in obtaining the reservoir data, making laboratory measurements on core samples, and performing computer simulation of the well production. Computer modeling of the Edna Delcambre well test provided an understanding of the anamolous excess free gas above that dissolved in the brine. Projections based on test data are providing information from which production and economic analyses can be made.

SOME EXPERIENCES FROM WELL TESTING IN PRECAMBRIAN ROCKS OF SWEDEN

K-E. Almen, L. Carlsson, and K. Hansson
Geological Survey of Sweden
Uppsala, Sweden

BACKGROUND

The Swedish Stipulation Law requires that before starting new nuclear reactors it must be shown how and where the high level waste can be handled and stored in a safe way. The KBS:s proposal (KBS 1977, 1978) for final storage of the high level nuclear waste comprises a repository at a depth around 500 meters in Swedish crystalline rock. A great number of drillings, well tests and other investigations were performed to show the existence of sufficiently large volumes of rock with very low groundwater flow suitable for a repository. The well tests performed also gave relevant values of the hydraulic conductivities to be used in model calculations of groundwater flow and transport times (Stokes and Thunvik 1978, Stokes 1979, Axelsson and Carlsson 1979).

In total about 12,000 meters of boreholes were drilled and investigated within the work of KBS. In the two areas Finnsjön and Sternö, see Figure 1, almost 7,700 meters of boreholes were investigated and the results formed the basis for the KBS safety-analysis for a repository in crystalline rock in accordance with the requirements of the Stipulation Law (KBS 1977, 1978). In this paper a brief review will be presented of the hydraulic well-test performed and some experiences from the testing and the results.

AREAS INVESTIGATED

Finnsjön

The Finnsjö area is located in northeastern Uppland, about 120 km north of Stockholm, see Figure 1. The topography is

very flat, characterized by a Subcambrian peneplane formed more than 570 million years ago.

The bedrock is made up of different rock-types found within the Sveco-Fennian area in Sweden. Granodiorite with an age more than 1 800 million years is the dominating rock type. Other rock-types to be found are leptite, granite, metabasite, pegmatite and aplite. The area has a high frequency of fractures, 3 - 4 fractures per meter on the rock surface.

In the area seven fully cored bore-holes with a diameter of 56 mm were drilled to lengths varing between 494 and 691 m. All the bore-holes were core-logged and hydraulic well tested. Some of them were also geophysical well-logged. The location of the bore-holes and major fracturezones is shown in Figure 2.

Sternö

The Sternö area is a peninsula in the Baltic Sea, about 400 km SSW of Stockholm. The peninsula is about 1 500 m wide and the highest point about 50 m above the sea level.

Near the surface the rock type is a fine-grained gneiss, called Coastalgneiss, intersected by veins and bodies of pegmatites and granites. At depths the rock type turns over to a gneissic granite and to a granite called Karlshamnsgranite. The transition from gneiss to granite is gradual and not characterized by any tectonic or other structural zone. The fracture frequency is low, about 0.5 per meter on the rock surface. Through the area a 150 - 250 m wide dolerite-dike runs in north-south direction.

Five bore-holes with lengths between 577 and 803 m were drilled in the area. The same kind of investigations as in the Finnsjö area were performed in the bore-holes in Sternö. The location of the bore-holes and major tectonic features is shown in Figure 3.

HYDRAULIC TESTING

Method

Two types of hydraulic tests were carried out with respect to equipment used, single- and doublepacker water injection tests. Due to the large number of tests to be carried out during a limited time (Carlsson et al 1979) a rather simple method was applied. Water was injected at constant head into a tested section of fixed length (2 or 3 m), with a pressure of 0.2, 0.4 and 0.6 MPa in excess of the hydrostatic head. The flow was measured at the imposed head difference when an apparent steady state had been reached. The hydraulic conductivity was calculated by the formula used by Banks (1972):

$$k = \frac{Q}{2\pi \cdot L \cdot \Delta p} \left(1 + \ln \frac{L}{2r}\right)$$

When k = the hydraulic conductivity of the test section
Q = injection flow rate
r = bore-hole radius
L = length of the test section
Δp = head difference

Transient methods with constant head or constant water injection flow were performed in some sections in order to compare the hydraulic conductivity values obtained by different methods (Carlsson et al 1979).

The values of the hydraulic conductivity thus obtained are values of the rock mass where the sum of the conductivities of each individual fracture in the test section is averaged over the section. With the knowledge of fracture spacing and geometric data the obtained rock mass conductivity can be transformed to a hydraulic conductivity of an equivalent set of hypothetical average fractures and of each individual fracture.

Equipment

The equipment used was constructed in 1977 - 78 and the tests performed until the end of 1979. The same equipment was used in the two types of test, but the single packer tests were made with the two packers placed together and water injected beneath them, see Figure 4.

The packers used were of rubber-type with a length of 0.3 m. They were mechanically expanded by using oil-hydraulics. Water was injected through a stem of steel-pipes with 10 mm inner and 20 mm outer diametres, each pipe 2 m in length. They were joined by inside screwthread and O-ring packing. The packer equipment was held in the hole by the steel-pipes. Water injection flow was monitored by flow-meters of rotameter type. Six different flow-meters were used, which overlapped one another. The lowest measurable flow rate in practice was 0.85 ml/min. The injected water was marked with Rhodamine which made it possible during later pumping and sampling to see whether the water obtained was contaminated by the injection or not.

Results

Double packer measurements

Results of the double and single packer measurements given as hydraulic conductivity versus depth are presented by Hult et al 1978, Gidlund et al 1979, Carlsson et al 1979 and Ekman and

a decrease in hydraulic conductivity over longer sections might be seen below 400 m in the diagrams.

It has sometimes been pointed out that the use of long test section will give a mean value of the rock mass hydraulic conductivity. The length chosen should depend on among other things the fracture frequency and distribution in the borehole. An average hydraulic conductivity of each bore-hole both from single and double packer tests is given in Table 1. Good agreement is obtained for the two types of measurements in Sternö but for Finnsjön the agreement is poor in spite of higher conductivity values.

Table 1. Values of the hydraulic conductivity for each borehole from single packer measurement and from calculations based on double packer measurements based on 3 meters test sections.

Borehole	section m below ground surface	Hydraulic conductivity m/s	
		Double packer	Single packer
Fi 4	52 - 590	$5.4 \cdot 10^{-7}$	$6.2 \cdot 10^{-8}$
Fi 6	100 - 691	$5.8 \cdot 10^{-7}$	$6.8 \cdot 10^{-8}$
Ka 1	30 - 779	$9.3 \cdot 10^{-10}$	$1.3 \cdot 10^{-10}$
Ka 2	100 - 576	$5.4 \cdot 10^{-9}$	$8.4 \cdot 10^{-9}$
Ka 3	50 - 765	$2.6 \cdot 10^{-8}$	$2.0 \cdot 10^{-8}$
Ka 4	48 - 553	$6.1 \cdot 10^{-8}$	$2.9 \cdot 10^{-8}$
Ka 5	100 - 578	$6.3 \cdot 10^{-9}$	$2.6 \cdot 10^{-9}$

Gentzschein 1980.

In Figures 5 and 6 the hydraulic conductivities are shown in groups of half-decade values versus depth together with the fracture frequency obtained from core-logging. In general the high hydraulic conductivity values are combined with high fracture frequency. A slight decrease in hydraulic conductivity with depth is observed for the high fractured zones. The much higher fracture-frequency in the Finnsjö area compared to the Sternö area observed on the rock surface are also observed from the boreholes.

The bore-holes were placed and drilled to illustrate and confirm fracture zones and other geological units or features within the areas. For instance bore-hole № 3 (Sternö) was placed to confirm a fracture zone (tectonic line) and to illustrate its hydraulic conductivity. The bore-hole crossed that tectonic line at the depth of 300 - 350 m which is shown in Figure 6. Thus the distribution of the hydraulic conductivity along the bore-holes and between them differs. Despite that it is assumed that the bore-holes together in each area might show some general distribution of the hydraulic conductivity of the rock mass down to about 500 - 600 m. In Figure 7 zones in a normal distribution diagram are shown of the distribution of the hydraulic conductivity in the two areas Finnsjön and Sternö, calculated from each bore-hole. The diagram thus gives an indication of the hydraulic properties within the areas and a comparison between them.

Figures 8 and 9 show how much of the bore-holes at different depth has hydraulic conductivity lower than 10^{-9} m/s. In some

of the bore-holes in Finnsjön no sections occur with conductivity lower than 10^{-9} m/s. On the other hand some sections in the bore-holes in Sternö have 100 % of their lengths lower than 10^{-9} m/s.

Single packer measurements and comparison between single and double packer measurements.

By using up to about 100 times longer test sections in the single packer measurements compared to the 3 m sections used in double packer measurement, the measuring limit can in theory be lowered about two orders of magnitude.

Most of the single packer measurements were made by lowering the packer 50 m at a time in the boreholes. The obtained transmissivity values from each test gave base-values for calculation of the hydraulic conductivity for each individual 50 m section. Figures 10 and 11 show the results from some of the boreholes both from single and double packer measurements and calculations. In some of the calculated sections a substraction of two very similar transmissivities gave negative values and were excluded in the diagrams of the single packer measurements. The negative values imply that the difference between the two basic flow rate-measurements in question is within the experimental errors at the two packer positions.

Figure 11 shows that in Sternö a marked change in the hydraulic conductivity in general occurs near 300 - 400 meters depth. Above this change values of 10^{-8} m/s are found and below it about 10^{-10} m/s or lower prevail. Such an abrupt change can not clearly be distinguished in the diagrams from Finnsjön, Figure 10. However

The influence of test section length is illustrated in Figures 12 and 13 in which single packer measurements are compared with the calculated values from double packer measurements using 2 or 3 meters sections. For the very low hydraulic conductivity in shorter sections no good agreement exists illustrated at depth in Sternö Ka 3. The same disagreement is found for long sections with high hydraulic conductivity as in Finnsjön Fi 6.

All individual single packer measurements and corresponding calculations from double packer measurements are compared in Figure 14. In general the hydraulic conductivity calculated from double packer measurements is higher than corresponding single packer measurements. It must be kept in mind that the test sections are picked out without any respect to fractures or other tectonic zones, and that leakage is likely to occur both within the rock between the test section and borehole and between the packers and the bore-hole wall. This leakage affects the calculated value of hydraulic conductivity less in single packer measurements than in double packer measurements, because it is spread over a longer section in calculation and also because a longer packer is used in the single packer measurement. The differences showed in Figure 14 might indicate a leakage which corresponds to a hydraulic conductivity of up to 10^{-9} - 10^{-8} m/s, equivalent to 6 - 60 ml/min at double packer measurement with 3 meter test section and a head difference of 0.2 MPa.

DISCUSSION

The leakages observed as disagreements between the two types of measurements might in a theoretical discussion be distinguished in two types. First a very small leakage which probably has to do with insufficient closure between packers and bore-hole wall

and other imperfections in the measuring system. This leakage affects the very low conductivity measurements as shown in the Sternö measurements. Usually this leakage represents the measuring limit of the double packer equipment used. For a continuous set of 75 individual 3 m sections between 350 and 575 m depth in bore-hole Ka 2 in Sternö this leakage was determined as 2.23 ± 1.59 ml/min at 0.2 MPa excess head.

The second type of leakage occurs in rock with a high fracture frequency where water might be transported through the fracture system as short-circuit flow between the test section and the untested part of the bore-hole. As a high frequency of fractures, which also can transport water, indicates high hydraulic conductivity this second type of leakage occurs in and affects the measurements of high hydraulic conductivity when using small test section and short packers. This type of leakage is illustrated by some of the measurements in Finnsjön.

To avoid or minimize the leakages mentioned it is recommended to use longer packers and to use information of the locations of highly fractured parts of the borehole in order to make suitable applications of the instrument and method for measurements of hydraulic conductivity in these parts.

REFERENCES

Axelsson, C-L., Carlsson, L. 1979: Model calculations of groundwater conditions on Sternö peninsula. KBS technical report 79 - 10, Stockholm 1979.

Banks, D. C. 1972: In situ measurements of permeability in basalt. Proceedings of the Symposium on Percolation Through Fissured Rock. Stuttgart 1972, pp. T1 - A.

Carlsson, L., Gentzschein, B., Gidlund, G., Hansson, K., Svensson, T., Thoregren, U. 1979: Supplementary measurements of permeability in the Finnsjö area (In Swedish). KBS technical report (in print). Stockholm Sept. 1979.

Carlsson, L., Gidlund, G., Hansson, K., Klockars, C-E. 1979: Estimation of hydraulic conductivity in Swedish Precambrian crystalline bedrock. Proceedings of the NEA/IAEA Workshop on Low-Flow, Low-Permeability Measurements in Largely Impermeable Rocks, Paris March 1979, pp. 97 - 114.

Ekman, L., Gentzschein, B. 1980: Supplementary geohydrologic investigations in Sternö (In Swedish). KBS technical report 80 - 01 (in print). Stockholm March 1980.

Gidlund, G., Hansson, K., Thoregren, U. 1979: Supplementary hydraulic conductivity measurements in the Karlshamn area (In Swedish). KBS technical report 79 - 06. Stockholm 1979.

Hult, A., Gidlund, G., Thoregren, U. 1978: Measurements of hydraulic conductivity (In Swedish). KBS technical report 61, Stockholm Jan. 1978.

KBS 1977: Handling of spent nuclear fuel and final storage of vitrified high level reprocessing waste. Report in five parts from the Nuclear Fuel Safety Project, KBS, Stockholm 1977.

KBS 1978: Handling and final storage of unreprocessed spent nuclear fuel. Report in two parts from the Nuclear Fuel Safety Project, KBS, Stockholm 1978.

Stokes, J., Thunvik, R. 1978: Investigations of groundwater flow in rock around repositories for nuclear waste. KBS technical report 47. Stockholm May 1978.

Stokes, J. 1979: Calculations of groundwater movement within the Sternö area in Blekinge, preliminary report (In Swedish). KBS technical report 79 - 08, Stockholm 1979.

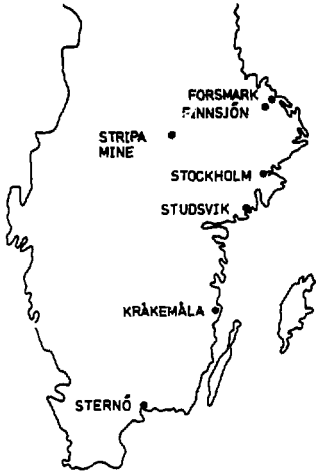

Fig. 1. The location of the Finnsjö and Sternö area in Sweden.

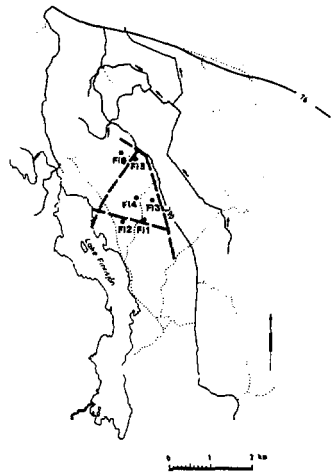

Fig. 2. Map of the Finnsjö area with deep bore-holes and major tectonic lines.

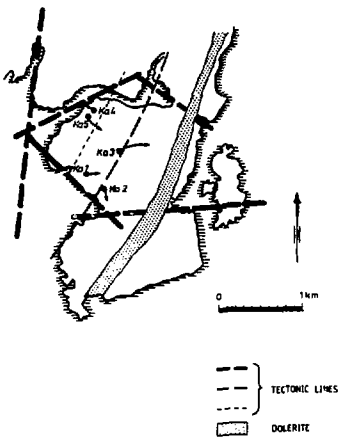

Fig. 3. Map of the Sternö area with deep bore-holes and major tectonic lines.

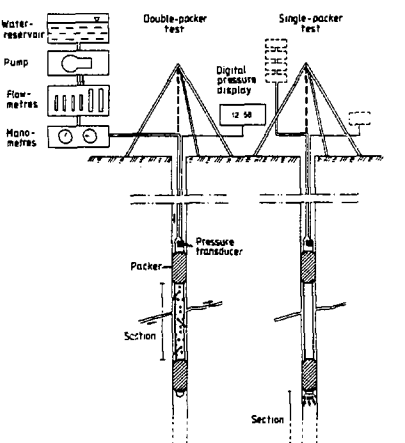

Fig. 4. Equipment used and packer configuration in the double and single packer measurements.

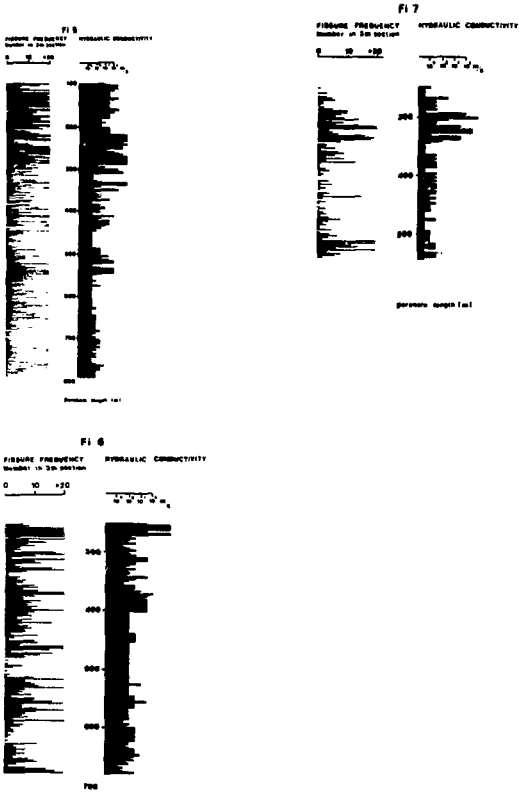

Fig. 5. Hydraulic conductivity versus depth and corresponding fracture frequency in the bore-holes in the Finnsjö area. The hydraulic conductivity is given in groups of half-decades.

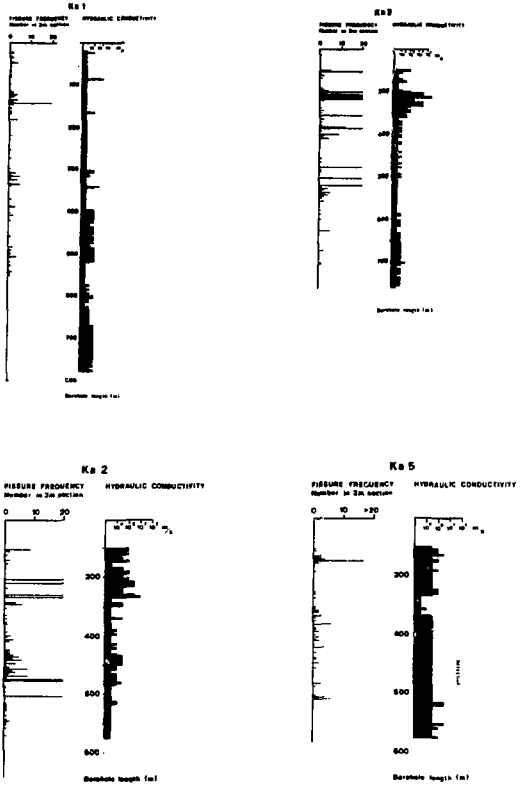

Fig. 6. Hydraulic conductivity versus depth and corresponding fracture frequency in the bore-holes in the Sternö area. The hydraulic conductivity is given in groups of half-decades.

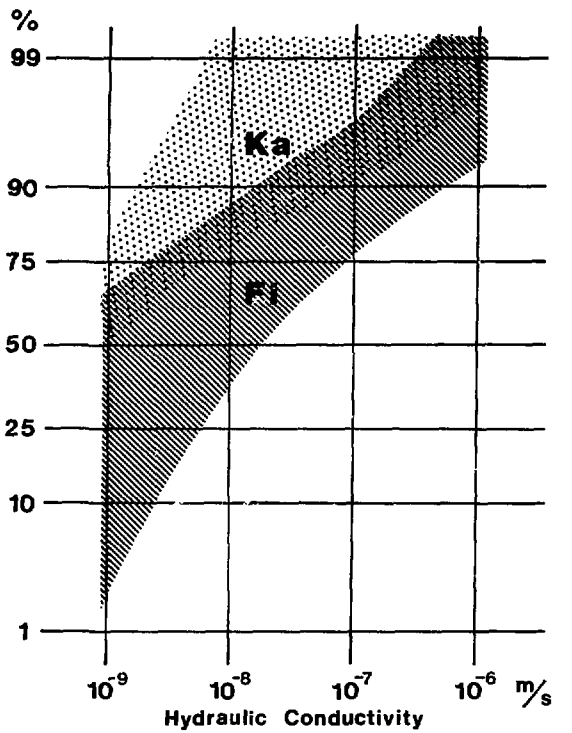

Fig. 7. Zones in a normal distribution diagram illustrating the hydraulic conductivity values obtained from measurements in the borehole in Finnsjön and Sternö.

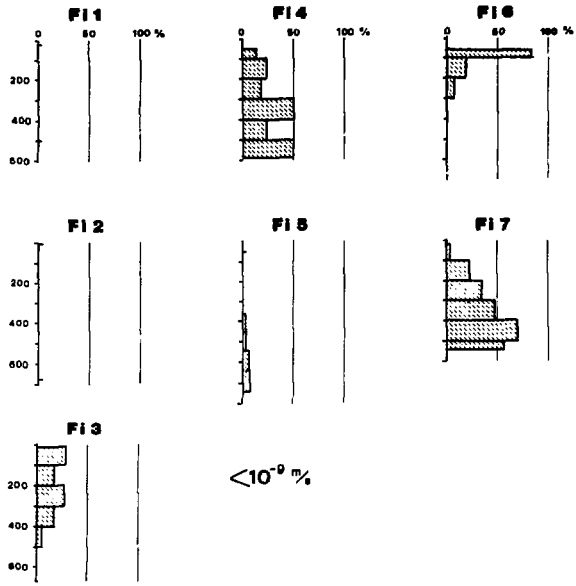

Fig. 8. Percentage of different sections in the bore-holes in Finnsjön with hydraulic conductivity lower than 10^{-9} m/s.

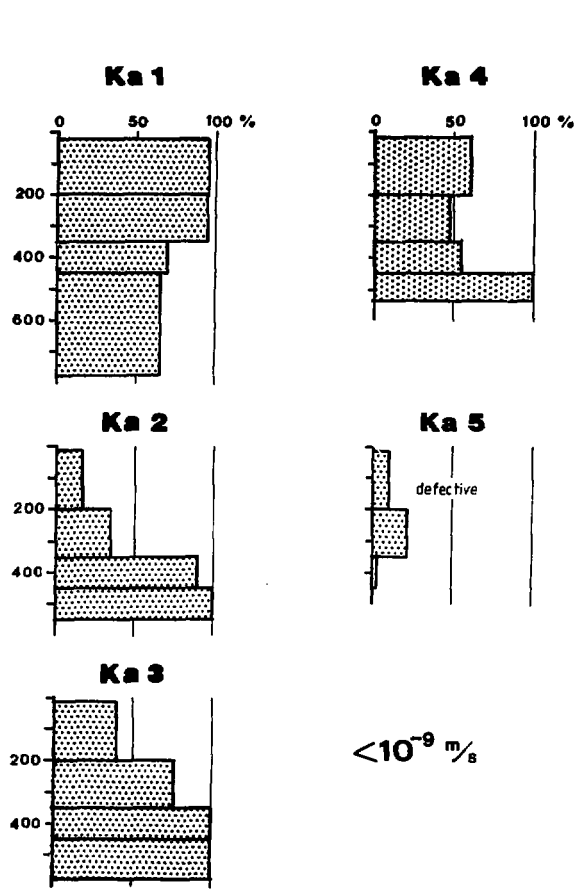

Fig. 9. Percentage of different sections in the bore-holes in Sternö with hydraulic conductivity lower than 10^{-9} m/s.

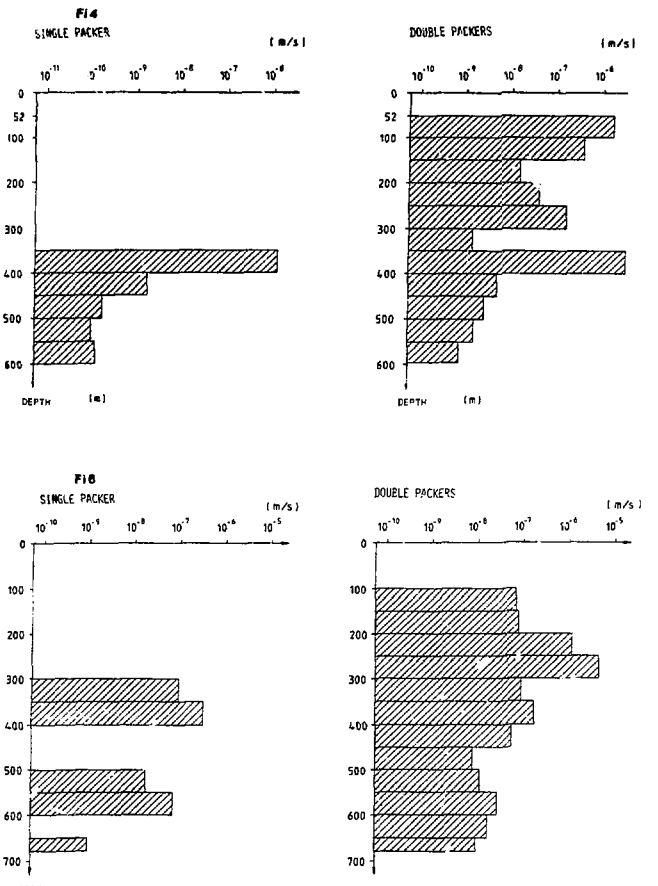

Fig. 10. Hydraulic conductivity calculated from single and double packer measurements in Finnsjön.

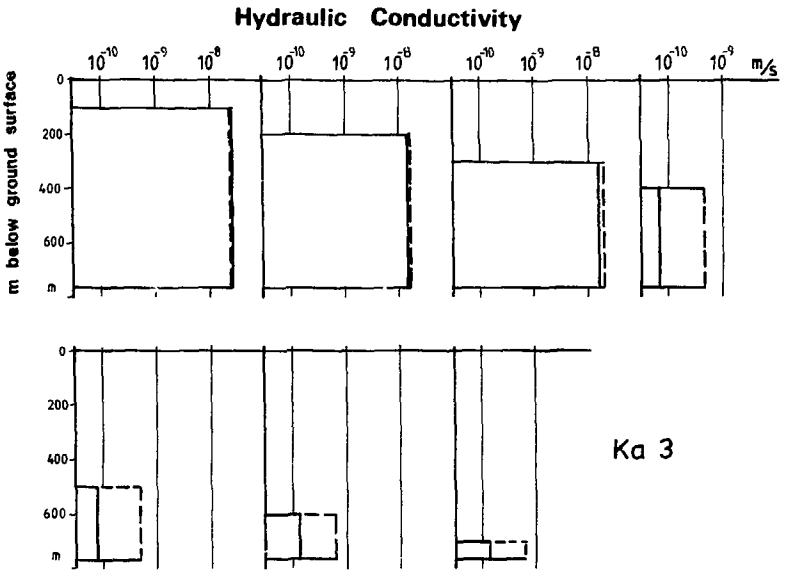

Fig. 13. Hydraulic conductivity from single packer measurements(full line) with different length of the test section and corresponding value from double packer measurements(broken line) in bore-hole Ka 3 in Sternö.

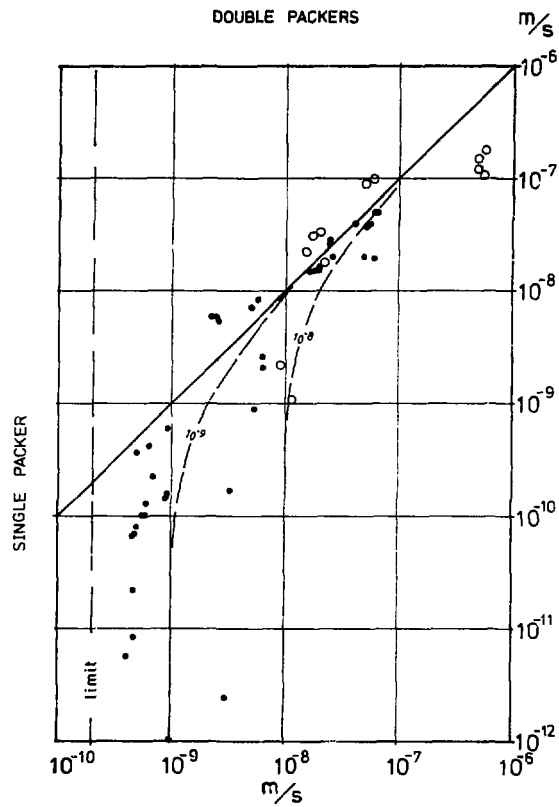

Fig. 14. Hydraulic conductivity from single packer measurements and corresponding value from double packer measurements. Curves are shown indicating leakages corresponding to hydraulic conductivities of 10^{-8} m/s and 10^{-9} m/s in double packer measurements.

LARGE-SCALE PERMEABILITY TESTING AT STRIPA

J. C. S. Long, P. A. Witherspoon, C. R. Wilson, and A. O. DuBois
Lawrence Berkeley Laboratory, University of California
Berkeley, California 94720

The macropermeability experiment at Stripa, Sweden, is an attempt to measure the average permeability of a very large volume of low-permeability, fractured rock. Flow into and pressure surrounding a 33 m drift will be measured. This experiment will also help to determine the size of the representative elementary volume for the Stripa granite. Problems in pressure field characterization include the perturbation resulting from drainage into the rest of the mine and vagaries of the fracture system itself. To measure pressure, 15 boreholes have been drilled from the drift into the surrounding rock and instrumented with 94 packers and 90 pressure gages. Inflow to the drift is measured by evaporating the seepage into the ventilation air while measuring the change in water vapor content between incoming and exhaust air streams. In order to measure this change in water vapor content, the drift has been sealed off and measurements of the barometric pressure, air velocity in the exhaust duct, and the wet and dry bulb temperatures of the inlet and exhaust air are taken. A test at ambient temperature has been completed. Preliminary results estimate a hydraulic conductivity of about 6.5×10^{-11} m/s.

1. MOTIVATION FOR LARGE SCALE TESTING

The prospect of geologic storage of nuclear waste has created a need to determine the hydrologic material properties of low-permeability fractured rock. The macropermeability experiment at the Stripa mine in Sweden is an attempt to improve permeability characterization techniques for the analysis of regional groundwater flow through low permeability rock in the vicinity of a nuclear waste repository. The experiment is part of the Swedish-American Cooperative Program on Radioactive Waste Storage in Mined Caverns in Crystalline Rock[1,2]. At Stripa we are monitoring flow into, and pressure surrounding a 5 m x 5 m x 33 m long drift called the ventilation drift at the 335 m level of the Stripa mine (Figure 1). This paper examines the theoretical problems associated with making such a measurement, and describes the actual experiment now in progress including preliminary results as of November 1979.

Three problems arise in determining flow parameters for low permeability fractured rock. The first is to determine the minimum volume of rock for which the permeability tensor is representative of a larger rock mass and is amenable to a porous media method of analysis. The second problem is to determine this permeability tensor from field tests. The third problem is to assign permeabilities to the volumes of rock that are not directly examined in the field. The macropermeability experiment at Stripa is an attempt to increase our understanding

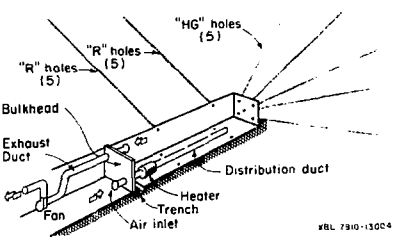

Fig. 1. Perspective section through the ventilation drift showing air flow pattern and hydrology instrumentation boreholes.

of the first two of these problems. The third is not discussed here.

As the volume of the fractured rock sample increases from zero, the average permeability will oscillate as either fractured or solid rock is added to the sample. When the volume of rock becomes sufficiently large that permeability is no longer sensitive to the effects of individual fractures, the oscillations will cease. An average permeability can then be assigned to that volume of rock which is called the representative elementary volume (REV). Theoretically, volumes of rock the size of the REV can be treated as porous media for regional groundwater flow analyses. Increasing the volume further may ultimately cause additional oscillations if a different realm of fracturing is encountered. When a single permeability measurement is made on an arbitrary volume of rock there is no way of knowing a priori whether or not the measured permeability lies on the oscillating portion of the curve. A series of measurements on different scales must be made to determine if there is a REV smaller than the rock mass itself and to determine the permeability associated with that volume.

In fractured rocks, where the discontinuities themselves may occupy areas on the order of 10^2 m^2, it is reasonable to expect REV's, if they exist, to be on the order of 10^4 or 10^5 m^3. The macropermeability experiment at Stripa will permit a measurement of the average permeability of 10^5 of rock. There is no assurance that this volume will be as large as the REV; however, the experiment, taken along with other small-scale tests performed at the same site, should provide strong indications of the size and existence of the REV.

The second problem is to determine the permeability of these large volumes from in situ tests. In high permeability soils or rocks, standard well tests can be run such that large volumes of the flow system are perturbed by the test in reasonable periods of time. However, in low permeability rocks, standard well tests may only affect the flow system within a few meters of the well. Determination of large-scale permeability values can therefore be attempted in two ways. The first way is to synthesize large scale values from a series of small-scale tests done in boreholes. The second way is to create a large scale sink (or source) which will perturb a large volume of the flow system, i.e., a macroscopic permeability test.

Small scale borehole tests will probably remain the mainstay of hydrologic investigations since boreholes are the only practical means of extensively exploring deeply buried rocks. Therefore, reliable methods for predicting macroscopic permeability from borehole data are needed. In order to perfect such methods they will have to be checked by performing large-scale in situ tests at the same site where the borehole data has been collected. The macroscopic permeability test at Stripa represents a large-scale measurement that will be used to check the analysis of an extensive series of small-scale borehole tests[3].

II. MEASURING MACROSCOPIC PERMEABILITY

Any measurement of permeability must be made on a flow system with specified boundaries. The potential distribution on these boundaries as a function of time and the flux through each boundary as a function of time must be inferred or measured. Then the effective permeability can be calculated using Darcy's law. Most in situ tests cannot be constructed such that all these conditions are exactly met. Some assumptions about boundary conditions are usually made in the analysis.

Theoretically, flow into the ventilation drift will approach steady conditions, but will never actually reach equilibrium. In order to use steady state analysis the experiment will continue for 3 to 6 months or until there is no discernible change in pressure and temperature. However, both the definition of boundary conditions and the measurement of flow into the drift are problems of some magnitude.

Theoretical Considerations in Pressure Measurement

The ventilation drift can be idealized as a long, but finite cylindrical sink. The inner boundaries of this flow system are well defined. The location of the boundary is the wall of the drift. The pressure on that boundary is essentially zero since the drift is kept dry.

The outer boundaries of the flow system are more difficult to characterize. Several possible approaches can be taken. One is to assume that at some distance from the drift the flow field is undisturbed and the hydraulic potential is constant. However, the hydrology of the region surrounding the drift is to a large extent dominated by the extensive Stripa mine workings. Piezometric profiles in the vicinity of the ventilation drift are irregular. An assumption of undisturbed conditions would not be valid.

Another method is to define a convenient boundary surface and measure the pressure distribution on this surface. Alternatively, pressure could be measured at an array of points in space such that an isopotential surface could be located in space. In an ideal, homogenous porous medium this method would present little problem. The open interval of the piezometer would intersect a large number of pores and grains and the pressure measured would be a physically averaged pressure. In a fractured system, however the piezometer interval may only intersect a few fractures. Since the direction of flow in these particular fractures is not necessarily in the direction of the average gradient as shown in Figure 2, the fractures sampled will not necessarily yield the average gradient. Without knowledge of the average gradient, the average or equivalent permeability cannot be calculated. The problem is equivalent to predicting the permeability of a porous medium from measurements of pressure in only a few pores.

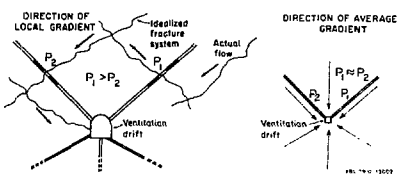

Fig. 2. Comparison of local and average gradients, P_i = pressure at point i.

As a partial solution to the above problem, piezometers can be installed parallel to the theoretical isopotential surfaces. These piezometers can then be open the whole width of the flow zone. In this case many fractures will intersect the piezometer and a physically averaged pressure will be recorded. Two problems are presented by this arrangement. The first is that long sections of open borehole may create a significant leakage paths and increase the flow into the drift. This will in turn increase the measured permeability. The closer the open borehole is to the drift the worse this problem is likely to be. Another problem is that this method of pressure measurement allows axial averaging but no circumferential averaging. The variability of pressure in the circumferential direction can be just as erratic as in the longitudinal direction.

The only way to ultimately insure a given set of boundary conditions is to create those conditions artificially. This can be accomplished by drilling a ring of closely spaced boreholes around the drift and maintaining them at constant hydraulic head. This method may be difficult and costly to construct, and it will not provide any information about anistropy.

Pressure Measurement at Stripa

At Stripa 15 boreholes 30 to 40 m long have been drilled from the ventilation drift into the surrounding rock (Figure 1). These boreholes are divided into 3 groups of 5 each. Two groups (the K-holes) are radial holes and one group (the HG holes) extend from the face of the drift. Each of these holes has been instrumented to monitor pressure. A total of 94 packers have been installed at approximately 5 m intervals. This prevents the boreholes from acting as drains into the drift and creates a 3-dimensional array of 94 zones, 90 of which are individually connected by tubing to pressure gages. Zones are numbered such that zone 1 in each hole is approximately 0 to 5 m from the drift; zone 2 in each hole is 5 to 10 m from the drift, and so on.

During the experiment air in the drift was kept at ambient temperature. Pressures in the boreholes and water flow into the drift are monitored until they are quasi-steady. In further experiments air temperature in the drift will be raised and the measurements repeated.

Between constant temperature experiments two further experiments will be conducted. The first will be small-scale permeability tests in which each zone in one or two boreholes will be drained. The flow rate from each zone will be monitored separately until approximately steady conditions are reached. By repeating this test after each constant temperature experiment it may be possible to detect local changes in permeability due to changes in temperature. These changes can then be correlated to changes in permeability detected for the whole macroscopic test.

The second test will be a pressure shunt test. At Stripa we will not be able to examine average pressures parallel to the theoretical average isopotentials. However, since the average gradient is not expected to be very large at the outer ends of the boreholes, we will be able to approximately examine the effect of zone length on pressure by hydraulically interconnecting adjacent zones through the pressure tubing and allowing the system to come to equilibrium. Head losses in the tubing will be known and the pressure in each of the interconnected zones can be calculated. Since flow rates between zones are in most cases expected to be quite low, the pressure in the zones should be nearly equal. The average of the pressures will be taken as an estimate of the pressure the zones would have if the packer between them were removed.

Theoretical Considerations in Flow Measurement

In most permeability tests, the water can be collected in a tube or pipe and the flow rate measured in a straight forward manner. However, in the low permeability rock of this experiment, the flow rate into the drift is so low and the surface area is so great that a significant proportion of the inflow would be lost to evaporation and the remainder would collect on the floor of the drift too slowly to measure in a reasonable amount of time. For example, inflow to the drift of Stripa is currently measured at 45 to 55 cm^3 per minute which is equivalent to collecting about 0.050 cm per day over the floor area of the drift.

One of the purposes of this experiment is to examine the utility of measuring these low flow rates by evaporating all the water into the ventilation air while measuring the change in water vapor content between the incoming and exhaust air streams. To operate successfully, the ventilation system should provide an air flow rate and temperature capable of vaporizing and carrying away all of the *influx water*[4]. In addition, all parameters must be steady enough to allow identification of the equilibrium conditions. Also, the differential relative humidity between the air entering and leaving the experiment area must be great enough to provide acceptable water vapor measurement accuracy. As a point of reference, .05 m^3/s (100 cfm) of air flowing at normal atmospheric pressure, 20°C, and 100% relative humidity will transport about 50 cm^3 of water vapor per minute.

For the macropermeability experiment it is necessary to measure: (1) the barometric pressure; (2) the air velocity in the exhaust duct; and (3) the wet and dry bulb temperatures of the incoming and exhaust air streams. These measurements allow us to calculate the incoming and exhaust mass flow rates of both the air and the water vapor associated with it. The difference between the incoming and exhaust water vapor flow rates is the amount of water which has evaporated from the surfaces of the drift. The floor of the drift and the surfaces of the walls can be observed to assure that all of the water is being evaporated as it arrives, without significant puddling.

To maximize the accuracy of water vapor transport calculations, one wishes to operate with the exit air stream as near to saturation as possible. Nomograms have been prepared for a variety of exit air temperatures to assist in the selection of air flow rates and heater power levels that will maintain an acceptable (± 20%) level of accuracy. One of these is shown in Figure 3.

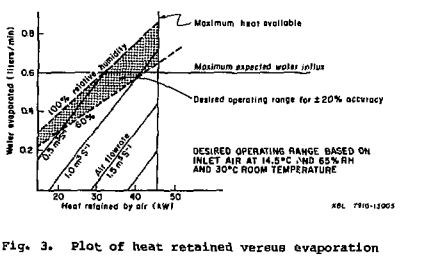

Fig. 3. Plot of heat retained versus evaporation rate.

Several months were required to establish near-equilibrium conditions in the rock temperature and water vapor flow regimes. The experiment was initiated with a room temperature control setting as near as possible to the preexisting ambient air

temperature. Some heat was added to assure that all available water is evaporated. Subsequently warmer equilibrium room temperatures will be established to investigate the impact of that temperature upon the water influx.

Flow Measurement at Stripa

A sketch of the experimental setup was shown in Figure 1. An air- and vapor-tight bulkhead seals off a 33 m length of the ventilation drift. This wall consists of a structural wooden frame covered with an 0.15mm thick sheet of PVC, as a vapor barrier, and fiberglass insulation to prevent condensation. The vapor barrier and the structure are keyed into a 20 mm deep notch on all four sides, with foamed plastic sealing in the notch to prevent the loss of water through the blast damaged surface rock. A frozen-food-locker type door provides access through the bulkhead.

The general mine ventilation system delivers about 1.4 m^3/s of fresh air to a point just outside the bulkhead. The experimental ventilation system admits a portion of this fresh air into the sealed room to pick up the water (as vapor) which flows into the sealed room through the surrounding rock. This secondary ventilation system is driven by a fan located in the exhaust duct so that a slightly negative pressure exists within the sealed room. Any air leaking through the bulkhead is into the room and it is the same air as that entering through the inlet duct. In this way, the inlet wet and dry bulb measurements are representative of both the intentionally admitted air and the leakage air. The flow measuring station as well as the exhaust wet and dry bulb sensors are in the exhaust duct. These sensors sense the total air flow including leakage.

The air entering the sealed room passes through an electric duct heater. It is then distributed through an insulated duct with multiple openings along the length of the room. The air issuing from these openings is directed preferentially onto any damp spots on the rock surface (most of the water arrives by seeping along discrete fractures). The walls of the drift are maintained in an almost-dry condition, with fans used where necessary to provide a high air velocity over particularly damp spots. The arrangement shown in Figure 1 will be modified for operation at higher room temperature. The air inlet duct will open directly into the room and a separate fan will recirculate room air through the heater and the distribution duct. This arrangement will separate the flow system for heating and circulating air within the room, where high air flow rates are desired, from the flow system for room ventilation (water vapor removal), where very low flow rates are required for accurate water vapor flow measurement.

The climatic conditions within the room are controlled by manually selecting a suitable air flow rate (by adjusting a damper on the fan exhaust) and then adjusting the heater power as required to maintain the desired air temperature in the room. The energy input from the heater is utilized in three ways: (1) the sensible heat of the exhaust air will be increased; (2) the heat of vaporization for the water will be provided; and (3) the rock will be heated. As equilibrium conditions are approached the third contribution would become negligible. The 45 kW heater is divided into six sections which are separately controlled. Five sections are under manual control and one is under automatic on-off control with feedback from a room-temperature sensor. The heater voltage is regulated to isolate it from the large voltage fluctuations observed in the mine power system.

A 75 mm-deep trench has been cut across the floor of the drift just inboard of the bulkhead. The trench and floor of drift are dry, therefore we conclude that lateral flow through fractures in the floor of the drift is negligible.

Preliminary Results from the Ambient Temperature Experiment

Instrumentation of the 15 boreholes was begun in June 1979 and completed in November 1979. Before fitting the holes with packers, the holes drained the surrounding rock into the drift. As such the upgrade holes were dry and the downgrade holes were filled with water under hydrostatic pressure. As each hole was fitted with packers the pressure in the hole began to rise. Example pressure records for RO7, HG2, HG1, and RO1 are shown in Figure 4, 5, 6, and 7 respectively.

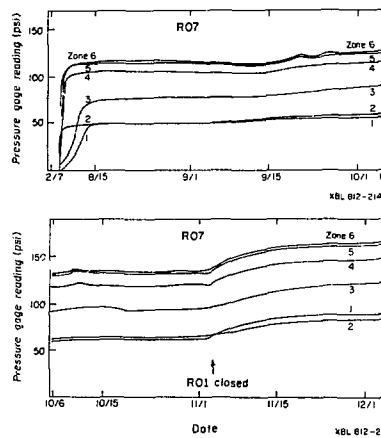

Figure 4. Example pressure gage readings for RO7.

Before instrumentation, when all the holes were draining freely, hole RO1 produced about as much water as all the other 14 holes combined. Earlier injection tests in RO1 resulted in pressure responses in many of the other holes in the drift. Consequently we instrumented RO1 last and monitored the response to pressure build-up in RO1 in all the other holes.

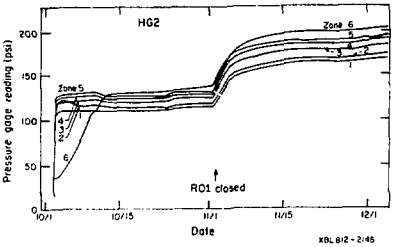

Figure 5. Example pressure gage readings for HG2.

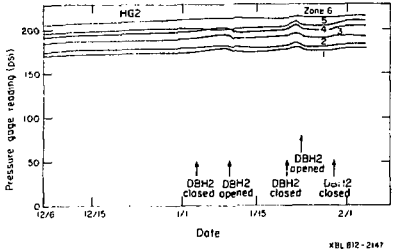

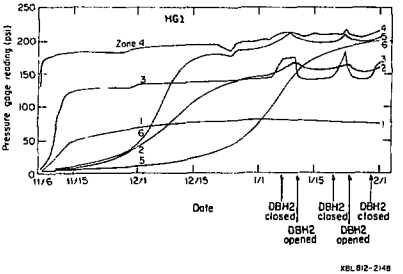

Figure 6. Example pressure gage readings for HG1.

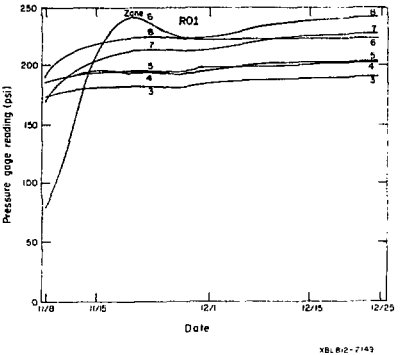

Figure 7. Example pressure gage readings for RO1

The effect of closing RO1 can be seen in the pressure records for RO7, HG2, and in Figures 8 and 9. Figures 8 and 9 illustrate the increase in pressure experienced in the R-holes and the HG-holes. The dashed lines represent pressures measured on October 30, 1978; the solid lines represent pressures measured on November 8, 1979. Instrumentation and pressurization of RO1 began October 31, 1979. The stippled area between the dashed and solid lines shows the initial pressure increase in each hole due to pressurization of RO1. No pressure increase is shown for R10 because it had been disassembled to fix a faulty packer. HG1 was instrumented just prior to RO1 and had not yet reached equilibrium when RO1 was installed. Pressure appears to decrease in zones HG33 (i.e., zone 3 in hole HG3) and RO54 because HG33 and RO54 had been bled during the period October 30 to November 8. The pressure declined in HG41, HG43, and HG44 without interference. All other zones throughout the drift increased in pressure. DSH2, a hole parallel to the drift was also instrumented. In December and January this hole was reinstrumented twice to

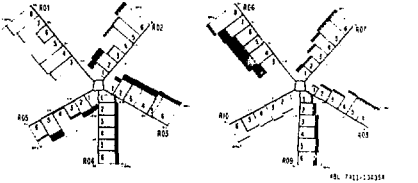

Figure 8. Pressure increase (stippled) in the R- holes due to instrumentation of RO1.

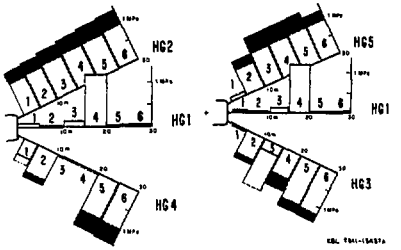

Figure 9. Pressure increase (stippled) in the HG- holes due to instrumentation of RO1.

repair packer leaks. The effects of these procedures can be seen in the pressure records for HG1 and HG2. The pressure record for RO1 shows the complex, dynamic buildup process in that hole. These dramatic hydraulic responses illustrate the complex nature of the fracture system at Stripa. The hydrology of this rock may well be dominated by a few high permeability fractures. Figures 10 and 11 show the pressure distributions at the end of the ambient test, March 20, 1980.

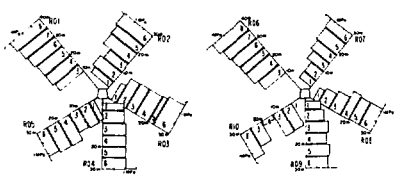

Figure 10. Pressures in the H- holes at the end of the ambient temperature run.

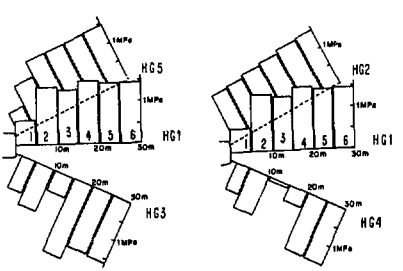

Figure 11. Pressures in the HG- holes at the end of the ambient temperature run.

Sealing the boreholes with packers decreased the flow into the drift from about 1000 cm^3/min to 20 to 30 cm^3/min. As the pressure in the holes built up the flow of water into the drift increased to 45-55 cm^3/min. (The 1000 cm^3/min represents cumulative flow from the open boreholes; after the boreholes were closed flow was measured with the ventilation system.) This decrease in flow is much greater than was expected. In order to maintain humidity of the exhaust air at 85% we have had to lower the air flow rate to 0.5 m^3/s. This air flow rate is at the lower end of the linear range of our airflow measurement system.

The record of flow rate is shown in Figure 12. Erratic variation at the beginning of the record is due to changes in operation of ventilation system and ongoing instrumentation of boreholes. However a gradual increasing trend can be discerned until late January when all the holes were instrumented. The most accurate data was recorded after February 26th when the room was consistently kept dry for almost a month.

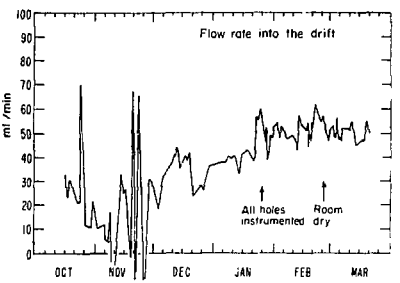

Figure 12. Inflow Record.

Figure 13 shows three separate values of conductivity that were calculated based on the assumption of steady state flow and using the pressure records in (1) all zone 4's, (2) all zone 5's, and (3) all zone 6's. Thus conductivity can be plotted against the volume of rock represented by the zones 4, 5, and 6, respectively. The calculated conductivity is fairly stable or about 6.5×10^{-11} m/s. This may be an indication that the volume of the REV is at least as small as 5×10^4 m^3, but further analysis may be needed.

Summary

The macropermeability experiment will provide: (i) a direct, in situ measurement of the permeability of 10^5 m^3 of rock on the order of 6.5×10^{-11} m/s; (ii) a potential method for confirming the analysis of a series of small scale permeability tests performed in surface and underground boreholes; (iii) a better understanding of the effect of open borehole zone length on pressure measurement; (iv) increased knowledge of the size and existence of a representative elementary volume in fractured rock; and (v) a basis for evaluating the

ventilation technique for flow measurements in large-scale testing of low-permeability rocks.

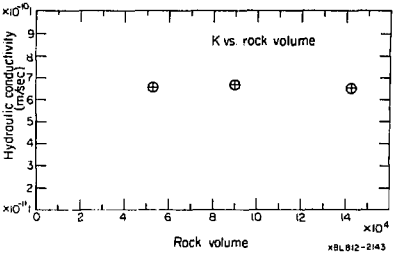

Figure 13. Permeability versus rock volume.

III. ACKNOWLEDGMENTS

This work was supported by the Assistant Secretary for Nuclear Energy, Office of Waste Isolation of the U. S. Department of Energy under Contract No. W-7405-ENG-48.

Funding for this project is administered by the Office of Nuclear Waste Isolation at Battelle Memorial Institute.

IV. REFERENCES

1. Witherspoon, P. A. and O. Degerman, 1978. Swedish-American Cooperative Program on Radioactive Waste Storage in Mined Caverns, Program Summary. LBL-7049, SAC-01, Lawrence Berkeley Laboratory, Berkeley, California 94720.

2. Witherspoon, P. A. et al, 1979. Rock mass characterization for storage of nuclear waste in granite. LBL-8570, SAC-18, Lawrence Berkeley Laboratory, Berkeley, California 94720.

3. Gale, J. E. and P. A. Witherspoon, 1979. An Approach to the fracture hydrology at Stripa: Preliminary results. LBL-7079, SAC-15, Lawrence Berkeley Laboratory, Berkeley, California 94720.

4. McPherson, M. J., 1979. Psychrometry: the measurement and study of moisture in air. Nottingham University Mining Magazine, University of Nottingham, United Kingdom.

IN SITU PERMEABILITY MEASUREMENTS FOR AN UNDERGROUND COMPRESSED AIR STORAGE PROJECT

M. Voegele, R. McCain, M. Gronseth, H. Pratt
Terra Tek, Inc., Salt Lake City, Utah

SUMMARY

Seven injection tests were conducted to determine permeability as part of a site investigation for a proposed compressed air energy storage/underground pumped hydro facility located in Maryland. The tests were conducted in a single NX borehole to depths of approximately 1000 meters in the Sykesville granitic gneiss formation. Four of the injection tests were single packer tests and were to determine the permeability of a large section of the hole. The tests were performed starting near the top of the hole and the packers were moved down the hole for each successive test. Three straddle packer tests were performed to determine the rock matrix permeability of an intact zone and the average permeability of two fractured zones. The interval tested during the straddle-packer tests was 28.2 meters long. From these tests, it appears that the rock matrix permeability is on the order of 10^{-15} cm^2 or less, and that the average permeability in the fractured zones tested is on the order of 10^{-12} cm^2.

INTRODUCTION

The typical load demand of a power generating facility tends to be cyclical with peak generation required only at certain times of the day. During off-peak hours the plants operate at a much reduced level of efficiency. To enable the generating plants to operate at a higher efficiency, load leveling techniques, which store the extra power generated during off-peak hours in an easily recoverable form, are currently under investigation. One technique, utilizing Compressed Air Energy Storage (CAES) together with an Underground Pumped-Hydro (UPH) scheme is presently being considered for implementation near Washington, D.C.

Compressed Air Energy Storage (CAES) has only recently become a technique for load leveling in the power industry. There has to date been no operating experience on water compensated hard rock cavern CAES plants, but considerable development work has taken place and a great deal of design experience has been gained in hydrocarbon storage and air storage for other applications. Water compensated CAES is a system in which the air storage caverns are connected to the surface by a water column, balanced by the air pressure in the storage cavern. The water column is then connected to a surface reservoir of sufficient volume to fill the underground reservoirs when the stored air is completely exhausted. One of the most important design parameters for a CAES/UPH facility is, of course, the rock mass permeability characteristics. The permeability coefficient of the host rock mass chosen for the site is the governing factor in determination of the air leakage potential at a given water compensated CAES site. In addition to permeability, in situ stress was measured at several depths using a hydraulic fracturing technique.

This paper presents a summary of the in situ permeability investigations at one CAES/UPH site. Included are discussions of the fluid injection equipment designed specifically for the project and the three distinct interpretative techniques utilized. Also included is a summary of the results obtained.

The underlying theme of this investigation was dictated by time constraint and monetary considerations. Accordingly, the field tests were performed in as short of a period of time as was consistent with the quality of data required. The assumptions required for the adopted interpretative techniques justified the use of relatively short data acquisition times for the permeability test data. However, it must be remembered that under these conditions, it is only realistic to calculate the permeabilities to within an order of magnitude. This level of calculation effort is also justified in light of the degree of confidence of the parameters which must be assumed in order to calculate the permeabilities.

Fluid Injection Equipment

An expected wide permeability range, together with very low permeabilities led to the design of a special equipment cart to handle the wide range of flow and pressure conditions. The two major design constraints were to be able to either maintain a constant injection rate or maintain a constant injection pressure and measure accurately very small flow rates.

Two air-driven intensifier-type pumps operate in tandem, with positive pressure on the input side of the pumps, to provide a maximum flow of approximately 1.8 gpm at 3000 psi. Pressure and flow on the high pressure side are regulated and most of the pump output is circulated back to the tank through the back pressure accumulator regulator. Fluid is drawn out of the circulation loop through an accumulator which provides a damping effect to pulsations in the circulation loop.

In the constant pressure injection mode, the fluid is routed directly through the flow meter and downhole, and the injection pressure is determined by the loop pressure setting. In the constant rate injection mode, fluid is routed through a metering valve and another back pressure regulator before being injected. Pressure is regulated to maintain a constant pressure drop across the metering valve regardless of downstream pressure.

The system is closed in the sense that the vent and bypass lines return to the supply tank. Cumulative flow can be obtained independently of the flow meter by measurement of the water level in the supply tank. Also, the amount of fluid returned when a test is vented can be determined. The equipment is capable of maintaining or measuring flows in the 0.005 to 0.3 gpm range with a resolution of 0.001 gpm at injection pressures as high as 6000 psi. The entire system is light and compact; it is easily portable on a small truck.

The straddle packer used for the tests was specially designed by Lynes for hydrogeological testing. Downhole pressures in the packed off interval were observed at the surface through the use of a Lynes quartz crystal conductor wireline probe (CWL). To determine if leakage had occurred around the lower packer element, a Lynes Digital Memory Recorder (DMR) was included in the tool string.

Interpretive Techniques

Injectivity tests were performed as part of the site investigation to provide order of magnitude estimations of the permeability of sections of the CAES/UPH test well located in the Sykesville Granite Gneiss Formation. Because the formation has relatively low permeability and porosity, injection tests using constant injection pressure formed the basis of the tests to determine the permeability.

Discussion of Assumptions. Several of the permeability coefficients were calculated on the basis of an assumed value of porosity. It must be emphasized that the equations used to interpret flow data are typically derived on the basis of a homogeneous medium and a radial flow regime. These boundary conditions are obviously unsatisfactory for a problem involving flow in a single fracture. One of the problems faced in this study was to determine whether or not fracture flow was the dominant mechanism observed at the CAES/UPH site. If it is clear that the flow is predominantly within the fractures, alternate interpretive equations must be found.

An examination of the core from the site suggests that the fracture frequency has a maximum of 1 fracture per foot. The fractures observed were all tight and, for illustration purposes, it will be assumed that the average fracture width was 0.1 mm. Using a fracture spacing of 1 ft., the fracture porosity is seen to be less than 1×10^{-4}. Allowing for a cumulative error equal to even an order of magnitude, the fracture porosity is still less than 10^{-3}.

The rock matrix porosity cannot be calculated easily and must be estimated on the basis of representative values. Several authors have tabulated values for crystalline rocks, (Krynine and Judd, 1957; Brace, 1965; or Farmer, 1968). Typical porosity values for gneissic rocks reported range between 1% and 2%. It is apparent that an assumed porosity value of 1.5% is reasonable for the rock in the CAES/UPH borehole.

The remaining question is, therefore, which value of porosity should be used in the permeability calculations. It should be obvious that the more permeable portion of the mass, be it the cracks or the inter-connected pore space, will allow the flow of fluid more easily than the less permeable portion of the mass. It therefore seems likely that the porosity value of 0.015 is justifiable and representative of the conditions encountered in the CAES/UPH boreholes.

The permeability values can easily be adjusted for a different value of porosity; for permeability in the 10^{-12} to 10^{-15} range, equation 3 is essentially linear. A porosity value of .5% thus would lead to a permeability coefficient one-third of that for a porosity value of 1.5%.

Finally, a comment regarding the validity of the interpretive techniques themselves is in order. Flow may be according to Darcy's Law, but the permeability may be so low such that the equations typically used do not apply. For example, the partial differential equation:

$$\frac{\partial^2 P}{\partial r^2} + \frac{1}{r}\left(\frac{\partial P}{\partial r}\right) + C\left(\frac{\partial P}{\partial r}\right)^2 = \frac{\phi \mu C}{K}\frac{\partial P}{\partial t}$$

is derived for radial flow from Darcy's law and conservation of mass. Typically the term $(\partial P/\partial r)^2$ is disregarded on the assumption that pressure gradients are everywhere small and the resulting equation is solved. For extremely low permeability, very large pressure gradients may exist, flow may be non-laminar, and the above simplification may not be valid.

At the present time there does not seem to be agreement within the literature upon how to assess this problem.

Steady State Conditions. During these tests, the borehole was rapidly pressurized to a given constant pressure, measured downhole, and the flow rate required to maintain that pressure was recorded.

If the test records indicated that conditions of relatively constant flow had been reached, an equation of the type presented by Snow (1968) was used to estimate the permeability.

$$K = 4.778 \times 10^{-8} \frac{q\mu \ln (24\ L/D_w)}{\Delta P L} \quad (1)$$

Where:

K = permeability, cm^2
q = flow rate, gpm
μ = viscosity, cp
ΔP = injection pressure, psi
L = interval length, ft.
D_w = hole diameter, in.

Curve Matching for Transient Conditions. For several of the tests it was not possible to reach and maintain steady flow or pressure conditions. In transient cases such as these, especially when the time of the test is short, the permeability coefficient is typically estimated using the type-curve matching technique developed by Jacob and

Lohman and reported in Earlougher (1977). This method was developed for a single well in an infinite system.

The permeability coefficient is determined by making a log-log plot of flow and time and comparing this plot with a dimensionless type-curve given in Earlougher (1977), until a match point is found. The coordinates of this match point are then used in Equation (2) to estimate the permeability.

$$K = \frac{4.183 \times 10^{-8}}{\Delta P L} \; B\mu \; \frac{q_m}{(q_o)_m} \qquad (2)$$

Where:
- K = permeability coefficient in cm^2
- B = formation volume factor, given the value 1.0
- μ = viscosity, cp
- ΔP = injection pressure, psi
- L = interval length, ft.
- q_m = flowrate at match point of type-curve matching, gpm
- $(q_o)_m$ = dimensionless flowrate at match point for type-curve matching

A relatively high degree of confidence in the accuracy of the fit of the data to the type curve was observed in one of the single packer tests and in two of the straddle packer tests.

Successive Approximations for Transient Conditions. While the injectivity tests were being run a second interpretive technique was used to analyze those tests which did not achieve steady state conditions. This technique involved an iterative approximation to the relationship developed by Jacob and Lohman. This relationship is given by equation (3).

$$P = 2.338 \times 10^{-8} \frac{q\mu}{KL} \; Ln \left(3.459 \times 10^{10} \frac{Kt}{\phi \mu C_f D_w^2}\right) \qquad (3)$$

Where:
- ΔP = injection pressure, psi
- q = flow rate, gpm
- μ = viscosity, cp
- K = permeability, cm^2
- L = interval length, ft.
- t = time hrs.
- ϕ = porosity, assigned the value of 0.015
- C_f = fluid compressibility, psi^{-1}, assigned the value of 3.3×10^{-6}
- D_w = borehole diameter, in.

This equation describes a curve, obtained by approximation, which matches with a high degree of accuracy, the type curves of Jacob and Lohman for low permeabilities. The idea behind the use of this equation was to continuously apply it and recalculate the permeability coefficient until a relatively constant value of the permeability coefficient had been obtained. To do this, an HP-67 calculator was programmed to solve the non-linear equation iteratively.

Shut In Tests. For those tests during which a relatively constant injection rate was maintained prior to shutting in the well, a standard shut-in analysis, such as that proposed by Horner (1967) was used to calculate the permeability coefficient. To use this method a plot of well pressure vs. log of a dimensionless time is used to determine a characteristic slope S.

$$S = \frac{\Delta P}{\Delta(\log \frac{t_o + t}{t})} \qquad (4a)$$

This slope is then used to determine the permeability:

$$K = 5.5 \times 10^{-8} \; \frac{q \mu}{S B L}$$

Where:
- ΔP = change in well pressure between time t_o and t
- t_o = time of well production, or in this case time since start of injection test to time of shut-in, hrs.
- t = time since shut-in
- q = flow rate in gpm
- μ = viscosity in centipoises
- S = slope of Horner plot (note that since this is build up following injection, slope used in calculation is actually the negative of that measured)
- B = formation volume factor, assumed = 1
- L = length of tested interval, ft.
- K = permeability in cm^2

Four of the injectivity tests, including two single packer tests and two straddle packer tests had data that was of sufficient quality to interpret by the Horner method. In fact the shut in data for one of the straddle packer tests was almost a textbook example.

Results

The results of the calculations to determine permeability coefficients are summarized in Table I and plotted in Figure 1 which also contains an abbreviated fracture log of the borehole based upon RQD and seismic velocities. The information summarized also includes test configuration and depth as well as the type of interpretive technique utilized.

These calculations indicate that the representative permeability coefficient for the fractured zones of the borehole could be as high as $10^{-12} cm^2$; that of the more intact sections of the rock mass is of the order 10^{-15} cm^2.

A comparison of the results obtained for all tests is illustrated in Figure 2; the calculated values of the permeability coefficients are separated according to the interpretive technique utilized. There are two pertinent observations to make concerning this figure: 1) there is remarkable agreement, considering a single test, for the values of the permeability coefficient as calculated by the steady state and curve matching methods; and 2) the permeability coefficients calculated by the shut-in method tended to be less, by approximately

an order of magnitude, than those calculated by the other methods. At these low permeabilities even this discrepancy is probably acceptable considering the assumptions and the length of the tests. The overall conclusion is that the data from the four interpretive techniques is acceptable and consistent.

The data base of in situ permeability coefficients for crystalline rocks is limited, but it is of interest to see how the results of this study compare with published data. Figure 3 illustrates a compilation of published data for in situ permeability tests in crystalline rocks. The only conclusion to be drawn is that the results of this study are in the expected range of 10^{-12} to 10^{-15} cm^2 seen at the Savannah River Laboratory and elsewhere for crystalline rocks at similar depths. Some investigators have proposed a decrease in permeability coefficient with depth in crystalline rocks (Snow, 1968). This may be true from the surface to a depth of approximately 100 meters. Below 100 meters there are little data and no trend can be quantitatively described (Figure 4). The available data indicate a general 10^{-12} - 10^{-15} cm^2 permeability for crystalline rocks to depths of up to 3000 meters. This study supports that proposition.

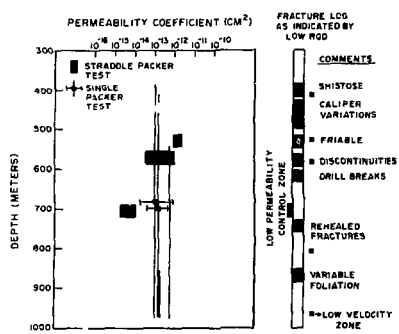

Figure 1

Compilation of permeability test results for Sykesville granite gneiss illustrating the relationship between permeability coefficient and degree of rock fracturing. Vertical lines indicate length of test interval while horizontal width indicates error bands on the data.

TABLE 1

Summary of Permeability Coefficients Determined in UPH/CAES Borehole Study, Sunshine, Maryland

Test 1: Hole Depth: 1279 to 3197 ft.
Single Packer Test
Length of Interval: 1918 ft.

Technique	Permeability
Steady state, ΔP = 70 psi	$9 \times 10^{-13} cm^2$
Curve Matching	$5 \times 10^{-13} cm^2$
Successive Approximations	$5 \times 10^{-13} cm^2$
Shut-in Analysis	$2 \times 10^{-14} cm^2$

Test 1B: Hole depth: 1343-3197 ft.
Single Packer Test
Length of Interval: 1854 ft.

Technique	Permeability
Successive Approximations	$5 \times 10^{-13} cm^2$
Shut-in Analysis	$4 \times 10^{-14} cm^2$

Test 2: Hole Depth: 1790 to 3197 ft.
Single Packer Test
Length of Interval: 1407 ft.

Technique	Permeability
Steady State, ΔP = 110 psi	$6 \times 10^{-13} cm^2$

Test 4: Hole depth: 2806 to 3197 ft.
Single Packer Test
Length of Interval: 391 ft.

Technique	Permeability
Steady State, ΔP = 945 psi	$2 \times 10^{-13} cm^2$

Test 5: Hole depth: 1691 to 1783.5 ft.
Straddle Packer Test
Length of interval: 92.5 ft.

Technique	Permeability
Steady State ΔP = 440 psi	$2 \times 10^{-12} cm^2$
Steady State, ΔP = 470 psi	$2 \times 10^{-12} cm^2$
Successive Approximations	$2 \times 10^{-12} cm^2$
Curve Matching	$1 \times 10^{-12} cm^2$

Test 6: Hole depth: 2267 to 2359.5 ft.
Straddle Packer Test
Length of interval: 92.5 ft.

Technique	Permeability
Steady State, ΔP = 945 psi	$4 \times 10^{-15} cm^2$
Successive Approximations	$2 \times 10^{-15} cm^2$
Shut-in Analysis	$1 \times 10^{-14} cm^2$

Test 7A: Hole depth: 1832 to 1924.5 ft.
Straddle Packer Test
Length of interval: 92.5 ft.

Technique	Permeability
Steady State, ΔP = 345 psi	$9 \times 10^{-13} cm^2$
Curve Matching	$1 \times 10^{-12} cm^2$
Successive Approximations	$8 \times 10^{-13} cm^2$
Shut-in Analysis	$4 \times 10^{-14} cm^2$

Note: for water at 20°C:
10^{-12} cm^2 = 10^{-6} Darcy = 10^{-7} cm/sec
10^{-15} cm^2 = 10^{-7} Darcy = 10^{-10} cm/sec

Summary

Seven injection tests to determine permeability coefficients were successfully completed as part of the site investigation for a proposed compressed air energy storage/underground pumped hydro facility located near Sunshine, Maryland. These tests were performed in a single deviated borehole in the Sykesville Granite Gneiss Formation.

Four of the injection tests were single packer tests and were to determine the permeability of a large section of the hole. The tests were performed starting near the top of the hole and the packers were moved down the hole for each successive test.

Three straddle-packer tests were performed to determine the rock matrix permeability of an intact zone and the average permeability of two fractured zones. The interval tested during the straddle-packer test was 92.5 ft. long.

From these tests, it appears that the rock matrix permeability is on the order of 10^{-15} cm^2 or less, and that the average permeability in the fractured zones tested is on the order of 10^{-12} cm^2. It is significant to note that all four of the interpretive techniques utilized gave results that agreed to within an order of magnitude for the calculated permeability.

Acknowledgements

The authors would like to express their gratitude to Acres American, Inc., the project managers and in particular, to Dr. A. S. Burgess, Acres Consulting Services, Ltd. for his constructive suggestions regarding interpretive techniques.

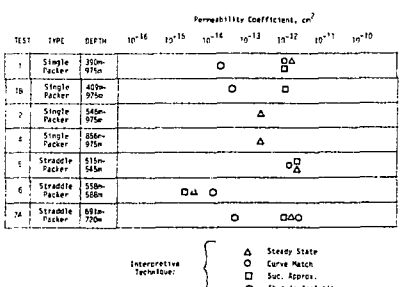

Figure 2

Permeability coefficients calculated for each of the seven injection tests by various interpretive techniques.

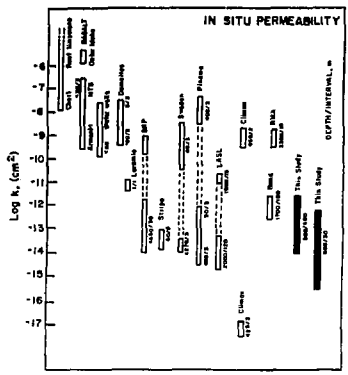

Figure 3

Compilation of in situ permeability test results for crystalline rocks (After Brace; 1980).

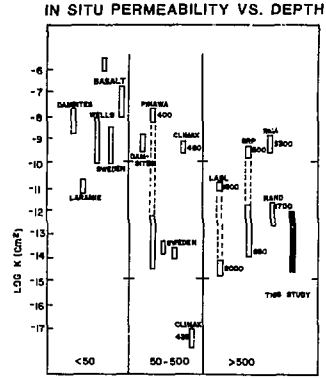

Figure 4

Compilation of in situ permeability test results for crystalline rocks grouped according to depth (After Brace, 1980).

References

1. Brace, W. F., "Some New Measurements of Linear Compressibility of Rocks", Journal of Geophysical Research, V. 70, n.2, p. 391-398, 1965.

2. Brace, W. F., "Permeability of Crystalline and Argillaceous Rocks: Status and Problems", Int'l. Journal of Rock Mechanics and Mineral Science, 1980 (in press).

3. Earlougher, R.C., "Advances in Well Test Analysis", SPE of AIME Monograph Series, V. 5, 1977.

4. Farmer, I.W., Engineering Properties of Rocks, Spon, London, 1968.

5. Horner, D. R., "Pressure Build-Up in Wells", in, SPE Reprint Series No. 9, Pressure Analysis Methods, 1967.

6. Jacob, C., and S. Lohman, "Nonsteady Flow to a Well of Constant Drawdown in an Extensive Aquifer", Trans A.G.U., V. 33, n. 4, August, 1952, pp. 559-569.

7. Krynine, D.P. and W.R. Judd, "Principles of Engineering Geology and Geo-Technigues", McGraw-Hill, 1957.

8. Snow, D.T., "Rock Fracture Spacing, Openings and Porosities", Journal Soil Mechanics and Foundation Engineering, ASCE 94:79-91, 1968.

CAPILLARY EFFECTS IN ROCKS OF THE EARTH; INFLUENCE ON WELL BEHAVIOR

Donald L. Katz
University of Michigan
Ann Arbor, Michigan

Water permeates the rocks of the earth. The capillary effects of water in water-gas systems in porous media frequently controls fluid movement. Oil recovery is thwarted in good part by capillary retention of oil. Caprocks in the main are sealed by capillary retention of water in the low permeability rocks. It seems that having a view of capillary effects is basic to understanding flow at wells in low permeability zones.

This paper sets forth concepts on capillary properties in the rocks of the earth which might be helpful in understanding the production of fluids from tight rocks. In underground gas storage, especially in aquifers, it became important to understand caprocks-the mechanism by which gas is held indefinitely in the earth. From studies of low permeability rocks, interest was developed in the fluid content of all rock layers of the earth. Capillary effects which are controlling in most caprocks are very significant in fluid flow in all low permeability rocks containing two phases.

What has been learned from threshold pressure studies for gas displacing water may be helpful in our considerations. Quite possible the most important aspect will be the relative permeability of the non-water phase in high capillary pressures rocks approaching caprocks.

Capillarity and Threshold Pressure

Important milestones in understanding capillary effects were the works of Schilthuis (1938), Leverett (1941) and Rose and Bruce (1949). The concept of threshold pressure of caprocks developed for gas storage in aquifers focused

on low permeability rocks; Thomas, Tek and Katz (1968) and Ibrahim, Tek and Katz (1970). A host of other papers and books cover the area generally as reviewed: Katz et al. (1959); Katz and Coats (1968).

Leverett presented his view of the distribution water and a gaseous phase within porous media in Figure 1.[2] A slightly revised concept to clearly portray the fact that inhibition does not give full saturation is shown in Figure 2.[5] The connate water content on Figure 2, point A, had been discussed by Schilthuis (1) earlier.

Capillary retention of liquids by cores was studied by Rose and Bruce (3), Figure 3. It may be seen that the 100% liquid saturation on drainage is in effect a threshold pressure for gas to enter a zone 100% saturated with water.

Thomas' thesis (4) took up the subject of threshold pressure for rocks of caprock quality and was able to show the relationship between his work and the earlier treatment by Rose and Bruce as well as other investigators, Figure 4(4).

Measurement of threshold pressures at higher pressure differentials were made using apparatus illustrated by Figure 5. It was shown that water saturated rock would hold gas at 1000 psi or greater differential by capillary forces. A much more extensive study by Ibrahim, Tek and Katz (1970) provided the relationship of threshold pressure with permeability, Figure 6.

What is Caprock

In the course of these studies, it seemed necessary to describe caprock. This was done by Figure 7. It is rock so low in permeability that gas below it will not penetrate the rock because the pressure differential across the interface is less than the capillary forces holding the water.

Now let us look at the spectrum of rocks, and their capillary qualities on Figure 8. The intercept at 100% water by drainage gives the capillary pressure equal to the threshold pressure. In our studies (5), a few non-porous rocks were found: anhydrite and dense limestone. They are represented by point S on Figure 8.

Scanning Nature of Interstices

At the conclusion of the AGA Studies (5), it became clear that displacement measurements in threshold studies should be made at the entrance to the core. Pandey (1973) at the University of Michigan took the measurements reported as Front-End Threshold Pressures (8). A limited supply of high pressure gas was admitted to the entrance to a water-saturated core and the pressure observed. In a pressure leveling technique as the interface movement stopped due to capillary forces, data of type of Figure 9 are taken.

Pandey working with Neilson Rudd (1973) at Geoengineering Laboratories developed a continuous scanning technique. Non-wetting fluid is forced through a water saturated core slowly with measured front-end pressures (9). Figure 10 shows the variable nature of the pore network.

A comment seems in order, the pore space is a network of channels of variable cross section and the threshold pressure reveals the largest channels through which fluids can flow. Using the formula: Pore radius = $\frac{2\sigma(\cos\theta)}{Fc}$ one can compute the pore radius. For the shale of Figure 9 with a threshold pressure of 1000 psi differential, the pore radius is computed:

$$\text{radius (cm)} = 2 \times 72 \frac{\text{dyne}}{\text{cm}} \times \frac{1.\ (\text{wetting}) \times 1.45 \times 10^{-5}}{1000\ \text{psi}} \quad \frac{\text{psi cm}^2}{\text{dyne}}$$

$$= 2.1 \times 10^{-6}\ \text{cm (0.02 Micron)}$$

It would seem that such a test might be adopted as a way of characterizing rocks.

Applications of Capillary and Threshold Pressure Information

Whenever two phases are encountered in the earth, i.e. water and gas, or oil and water, capillary effects may control flow. Production of gas to a well bore from a low permeability rock containing mobil water is influenced by the pressure difference between the gas phase in the well and the two phase system in the rock. With water bridging the fine interstices of the rock near the well bore added pressure drop occurs. When looking at the threshold pressure-permeability correlation and recognizing that the curve continues to higher permeabilities, pressure drops of 50-100 psi may occur at the well bore.

In fractured low permeability rocks, a similar pressure discontinuity can well occur at the matrix-fracture interface.

Consider a cavern in low permeability rock, containing fractures, with water saturated rock and gas phase in the cavern. At the matrix-cavern interface, pressure in the water phase can be 1000 psi or more higher than that of the gas phase in the cavern. The water in a rock at a hydraulic pressure less than the threshold pressure should not flow water into the cavern.

We know little about fracture behavior in this connection but it too would have a pressure discontinuity at the cavity wall, though much lower. It would be interesting to see threshold tests on insitu fractures described with some parameter like a permeability per unit area assigning some width to the fracture zone.

When fluids are stored in underground caverns, with fractures in the rock, the maximum storage pressure is generally set at the saturated rock hydraulic head.

Wells

Gas wells in low permeability rocks have difficulty in harvesting the gas. No first hand experience is available but water interference, reduction in permeability at the well bore as pressure drops, and the usual unsteady state effects of radial flow are involved.

Stripper oil wells in low permeability rocks are known to flow oil to a pumped well bore at low rates over decades. Fracturing is a well known technique for providing higher permeability channels to well bores, and is not considered here. However, the behavior of fluids at the interface of matrix rock and a fracture is akin to a well bore.

To make predictions of well behavior, it seems that relative permeability measurements would be very helpful when threshold pressures are used to characterize the rocks. A quick checking of the SPE literature revealed no relative permeability data below 1 millidarcy where the threshold effect begins to be consequential.

Reviewing Figure 8, drainage behavior, would not the step pressure occur at the well bore similar to the intercept at 100% water saturation? Surely, if water movement accompanies gas flow, would not water bridge the pores and be the equivalent of a dynamic threshold pressure restraint on flow?

Now a separate topic will be presented briefly, Where is the earth free of a moveable water phase?

Gypsum-Anhydrite Seal for Salt.

Michigan reef gas reservoirs have been shown to have no connate water in the upper main body of the reservoir. Dehydrated gas is injected in storage operations and remains dry upon removal. The only explanation found is that anhydrite within the reef rock has absorbed the liquid water.

The study of this phenomenon has led to an analysis of the seal for salt depositions. Salt deposits are believed to remain undissolved by a protective layer containing anhydrite which reacts with ground water to form a gypsum-anhydrite seal. My experiences indicate salt deposits and maybe possibly some limestone mines are the only rocks not containing water.

REFERENCES

1. Schilthuis, R.J. (1938) Connate Water in Oil and Gas Sands,Trans AIME Vol. 127, p 199.

2. Leverett, M.C. (1941) Capillary Behavior in Porous Solids,Trans AIME, Vol. 142, p 152.

3. Rose, Walter and W.A. Bruce (1949) Evaluation of the Capillary Character in Petroleum Reservoir Rock, Trans AIME, Vol. 186, p 127.

4. Thomas, L.K., D.L. Katz and M.R. Tek (1968) Threshold Pressure Phenomena in Porous Media,Trans AIME, 243, p. 174.

5. Ibrahim, M.A., M.R. Tek and D.L. Katz (1970) Threshold Pressure in Gas Storage,AGA Monograph.

6. Katz, D.L. et al. (1959) Handbook of Natural Gas Engineering, McGraw-Hill Book Co., New York.

7. Katz, D.L. and K.H. Coats (1968) Underground Storage of Fluids, Ulrich Books, Inc., Ann Arbor, Michigan.

8. Pandey, G.N., M.R. Tek and D.L. Katz (1973) Front End Threshold Pressure Measurements, Proc. AGA Transmission Conference. p 73-T-17.

9. Rudd, N. and G.N. Pandey (1973) Threshold Pressure Profiling by Continuous Injection,SPE Preprint 4597.

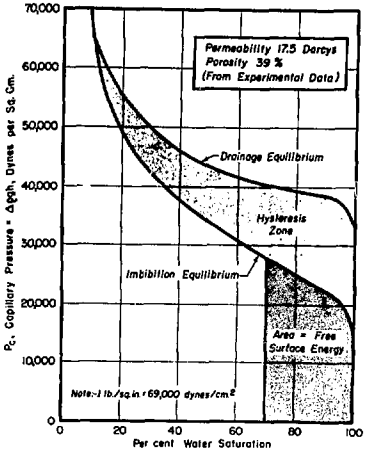

Figure 1 Capillary Distribution of Air and Water in Unconsolidated Sand (Leverett) (2).

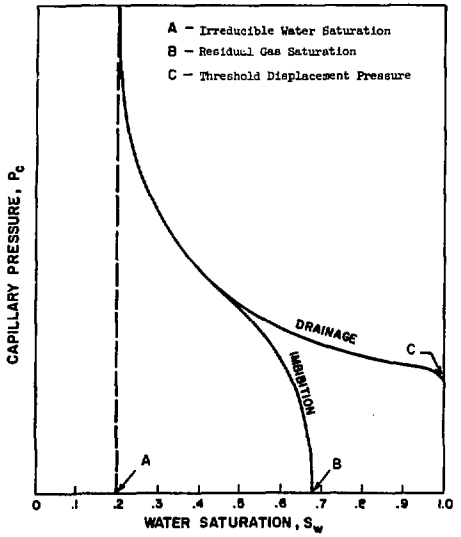

Figure 2. Inhibition and Drainage Capillary Pressure Curves (5).

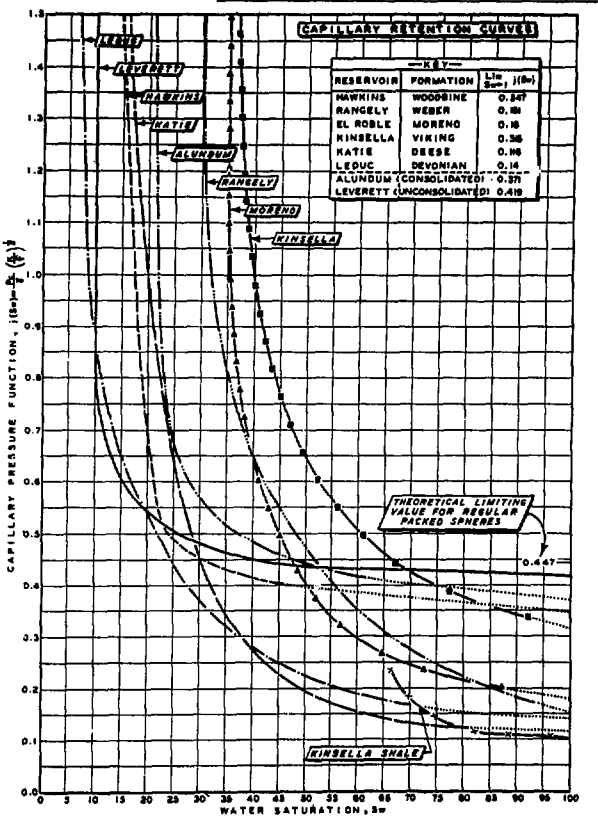

Figure 3 Capillary Retention Curves (Rose and Bruce) (3)

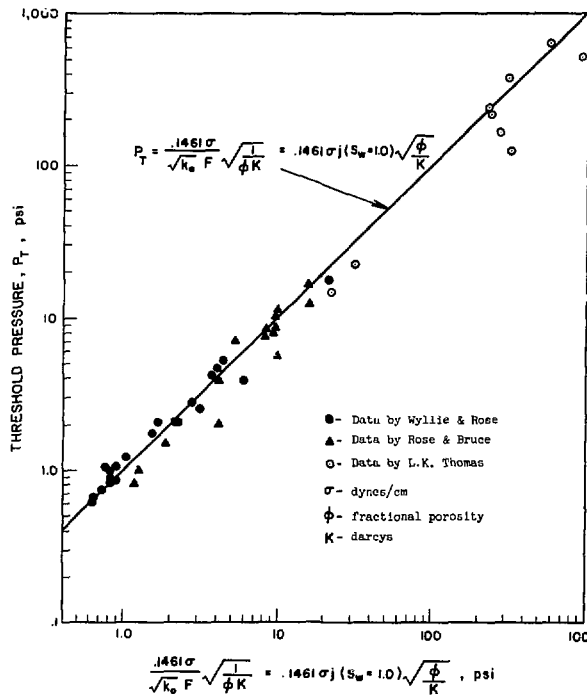

Figure 4 Correlation of Threshold Pressure with Other Properties of Porous Media (Thomas) (4)

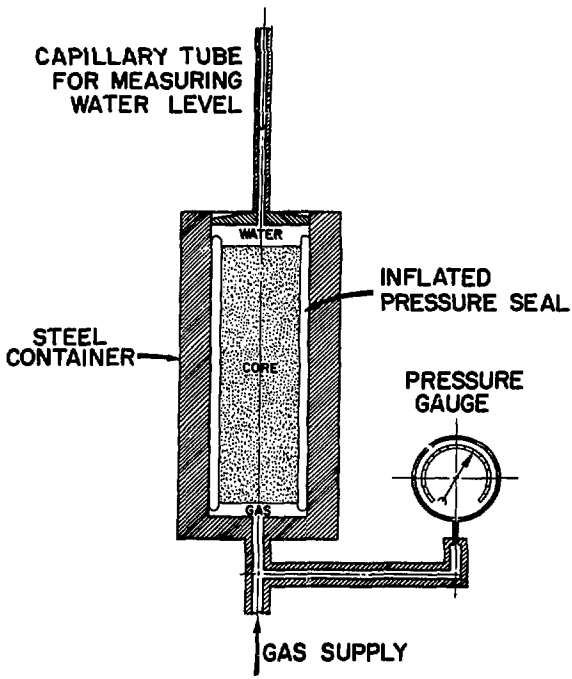

Figure 5 Diagram of High Pressure Core Holder for Threshold Displacement Tests (Thomas) (4)

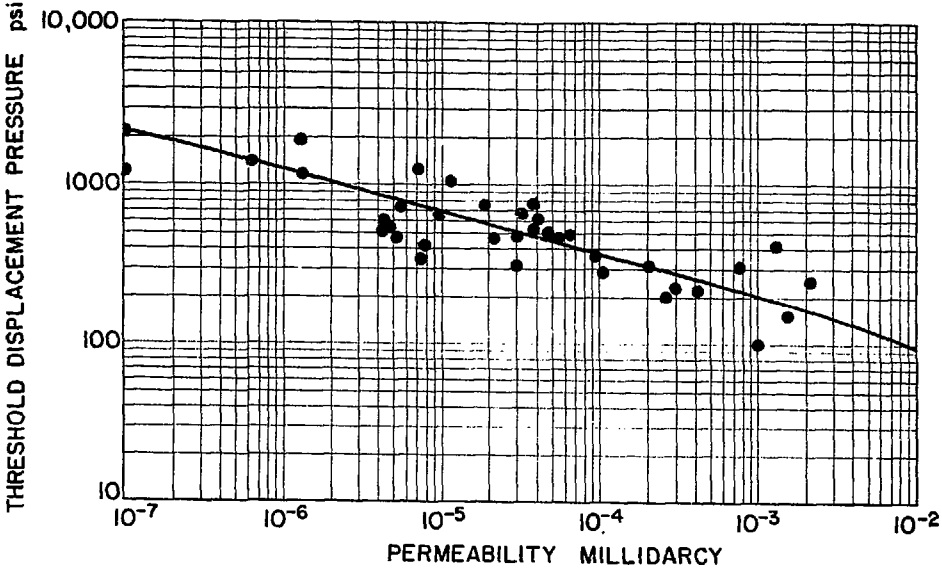

Figure 6 Threshold Pressure versus Permeability AGA Project (Ibrahim, Tek, Katz) (5)

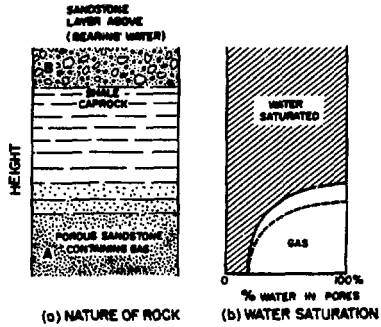

Figure 7. Nature of the Gas-Water Contact in the caprock (7).

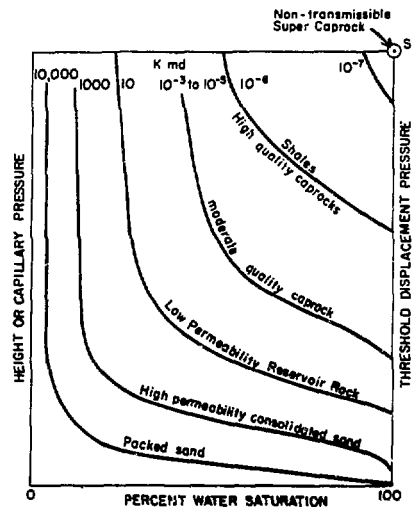

Figure 8. Variations in Capillary Pressure Behavior for Various Rocks (Ibrahim, T.-k, Katz) (5).

ABSTRACT

RADON AS AN INDICATOR OF WELLBORE INFILTRATION RATES IN URANIFEROUS IGNEOUS ROCK

P. H. Nelson and R. Rachiele
Lawrence Berkeley Laboratory
Berkeley, California

Granitic rock at an experimental site at Stripa, Sweden is unusually high in natural radioelements (~40ppm uranium), with even higher local concentrations occurring in thin chloritic zones and fractures. Gamma-ray logs made with a borehole probe demonstrate the background level and its uniformity throughout the rock mass; spectral gamma analysis of core samples provides a quantitative estimate of the radioelement content.

Groundwater seeping from these fractures into underground openings and boreholes is likewise highly anomalous in its radon content, with the groundwater activity ranging as high as one microcurie per liter. When gamma-ray logs are run in boreholes where the inflow is appreciable, the radon activity in the water, rather than the decay products in rock, dominates the gamma log. Where mixing occurs, the gamma-activity, which is proportional to the radon concentration, appears to vary in a linear fashion with the rate of water inflow. Hence, in high flow holes (above a few liters per day of inflow) the gamma ray log behaves as a crude flow log. Where mixing does not take place and where the inflow occurs at a discrete interval, a logarithmic decrease of activity along the hole is observed, caused by the gradual decay of radon as it migrates upward in the water column. This spatial decay can also be translated into an influx rate.

These observations indicate that the natural radioactivity in groundwater infiltrating into boreholes can be used as a method of measuring infiltration rates even where the infiltration rates are fairly low, on the order of a few liters per day, providing that the groundwater carries sufficient radon. The general applicability of

these observations will not be known until similar observations can be made in other igneous rocks. Both the abundance of uranium and its distribution along permeable fractures are critical in providing the natural radon tracer.

ABSTRACT

IN-SITU PERMEABILITY TESTING OF ROCK SALT

E. W. Peterson and P. L. Lagus
Systems, Science and Software
San Diego, California 92038

In-situ permeability tests have been conducted in the salt formation surrounding the AEC-7 borehole located at the WIPP site near Carlsbad, New Mexico. Injection tests were performed at depths of 1870 and 2270 feet using compressed air as the working fluid. Data were obtained using the Systems, Science and Software designed guarded straddle packer system capable of measuring permeabilities ≥.1 microdarcy. In each test a 100 foot length of borehole was isolated and the surrounding formation examined. The resulting data were interpreted in terms of formation permeabilities. These perr ability values were subsequently used in various repository design studies.

Complete descriptions of the instrumentation, measurement techniques, and test procedures are included herein. The analytical/numerical methods used for data analyses are presented and the implied permeability values discussed. Problems inherent in performing reliable reproducible quantitative microdarcy range permeabilities are identified and the resulting impact on data interpretation is discussed.

This work was performed for the Sandia Laboratory, Albuquerque as a part of their research and development activities in support of waste acceptance criteria for WIPP.

SOME CONSIDERATIONS FOR TRACER TESTS IN LOW PERMEABILITY FORMATIONS

Glenn Thompson
Department of Hydrology and Water Resources
University of Arizona
Tucson, Arizona 85721

Tracing experiments in low permeability formations are used primarily for measurement of porosity and dispersivity. In some cases they are used for measuring the direction and rate of water movement. Well layouts and test types are as variable as the situations in which they have been applied. In addition a correspondingly large variety of tracers have been used in the past eighty years to perform these tests. In order to provide some basic guidelines for performing tracer tests in low permeability formations, several conventional tracing techniques and a listing of the most commonly used tracers are given below.

TWO-WELL INJECTION-WITHDRAWAL TESTS

In this test type, water is pumped from one well and injected in a second well, thus developing the maximum possible gradient between the two wells. This is the most commonly applied technique and has the greatest chance of success in low permeability formations where wells are great distances apart or in circumstances where the probability of tracer interception would otherwise be very low. Figure 1 shows the typical [illegible]ing design with associated equipment [illegible] filters, flow meters) for a two we[illegible]gure 2 shows the theoretical flow pat[illegible]is established between the two wells after extended pumping. The measurement of porosity assumes that water is displaced through the indicated flow tubes.

The two well technique is most commonly used for measurements of effective porosity and dispersivity although it is relatively insensitive to the latter. Because the tracer can be added to the injection water for long periods of time, the overall effect of dilution can be reduced accordingly. Consequently, tracers that are detectable at extremely low concentrations are not necessary for this technique.

RADIAL FLOW

Radial flow techniques can only be used where a water supply is available for injection. This test requires water to be injected in a central well with regular sampling taking place at observation wells at various radial distances away from the injection well. Figures 3 and 4 show what may be considered a typical pattern of water movement away from the injection well. Water is usually displaced in a non-symmetrical or ameboid form around the injection well. Porosity and longitudinal dispersivity are obtainable from this test, although a large number of observation wells are needed to obtain a meaningful estimate of porosity due to the typically irregular shape of the displaced volume.

CONVERGENT-FLOW TESTS

In this test type, ground water is pumped from a single well creating a flow system in which the flow lines converge on a single point--the pumping well. This technique is useful for determining the same parameters as the previous methods. A typical well layout and the flow path of a tracer introduced into the system is shown in Figure 5. In this technique both the dispersion and porosity measurements are aided by the observation of tracer at points arranged in a line across the flow system, thus defining the width of the tracer plume. The principal difficulty associated with this method is dilution of the tracer. By comparison to the previous methods, only a small amount of tracer can be injected because it is normally added in a single instantaneous slug or pulse rather than being added continuously. Once injected, the tracer does not leave the well as a pulse, but is diluted out of the well at an exponentially decreasing rate. The tracer is further diluted at the pumping well when it mixes with unlabeled water converging there. This technique offers the advantage over radial flow techniques of not requiring a supply of injection water; in addition, it provides a more sensitive method of measuring dispersion than the two-well test.

POINT DILUTION METHOD

This technique utilizes the principle that the rate of solute dilution out of a well bore is a function of the flow velocity of water around the well. The technique may be useful for determining zones of high or low permeability in a well that is packed off accordingly. In high permeability formations the technique is useful for measuring groundwater velocity induced by the natural gradient. Figure 6 shows the results of a point dilution experiment conducted in the Conasauga Shale at Oak Ridge National Laboratory using a fluorocarbon tracer. The tracer concentration in the well is controlled by dilution effects down to a few parts per trillion, after which the concentration remains relatively constant due to the rate of desorption of tracer from the sides of the well bore. The equation for calculating the velocity is shown in the figure. The theoretical basis for the calculation is given by Drost.[1]

OTHER FACTORS

In addition to the factors influencing the choice of test type, other conditions will have a profound effect on the well layout. The scale of the dispersion parameters measured will be a function of the distance between the injection wells and the observation wells. However, as flux distance

increases, the time required to perform the test increases exponentially, tracer dilution problems increase, and for some tests the probability of *intercepting the tracer decreases rapidly.* Other more obvious factors that influence test design are: number of holes, funds for drilling, time available or required to run tests to completion, and manpower and equipment for pumping and monitoring.

SELECTION OF TRACER

Ideally, the first consideration in the selection of a tracer is the type of performance expected. In particular, one may be trying to model or trace the movement of the water itself or that of a solute species that is subject to some sorption. Although it is not possible to duplicate exactly the movement of water or most solute materials by means of tracer, some major pitfalls can be avoided by the use of the following basic guidelines for tracer selection.

In general, anions are the least sorbed solute species on natural silicate or carbonate aquifer materials. This is due largely to the fact that the minerals tend to have negatively charged surfaces, and since anions are also negatively charged, they tend to be repelled from the similarly charged mineral grain surfaces. Although anion exchange does take place on some clay mineral substrates, it appears to be of negligible importance in most ground water systems. Noncharged molecules (such as many organic species) tend to be sorbed more than anions as a function of their polarizability.[2] When exposed to a negative charge, a dipole may be induced on the otherwise symmetrical or neutral molecule. The positive pole created by the separation of charges makes the molecule susceptible to sorption on the negative mineral surface.

Cations, as one would expect, are the most sorbed solute species. These are also susceptible to cation exchange reactions on clays that are abundant in many aquifers. Figure 7 shows the results of a field tracing experiment which illustrates this point. Breakthrough curves of cationic, anionic and noncharged solutes are shown for an observation well 2 meters from the injection well. The experiment was conducted in the Ogallala Sand formation as part of an artificial recharge study performed by the U.S. Geological Survey.[3]

A variety of other factors may also influence the choice of tracer. The sensitivity and ease of detection are often the first considerations in selecting a tracer because the dilution requirements of a particular tracing experiment may be a primary limiting factor. Among the nonradioactive tracers, fluorocarbons offer the greatest dilution possibility having routine measurement capability in concentrations down to 1.0 part per trillion (1 pg/ml) or less. Fluorescent dyes probably rate second with rapid measurement capability down to 0.1 part per billion (1 ng/ml) if no background problems exist. Aromatic organic anions are rapidly measurable using liquid chromatographic techniques in concentrations down to a few ppb. Inorganic anions such as Cl^-, Br^- and I^-, are generally limited to about 1 ppm using selective ion electrodes.

Background problems also limit the utility of many tracers for field use. Anions such as Br^- and Cl^- which are otherwise excellent tracers often have backgrounds that limit their degree of dilution and their range of applicability. Slight variations in the background of a given tracer almost always lead to some confusion or ambiguity in the interpretation of the results.

A list of tracers and their important characteristics, organized according to their general class, is given in Tables 1A, 1B, and 1C. The list contains only representative examples although all of the most widely used conventional tracers are named.

Table 1. Common Groundwater Tracers

Tracer	Characteristics
A. Particulate Tracers	
Lycopodium spores	No chemical sorption, about 50 μm diameter, multiple tracers possible by dying spores different colors. Collected by trapping on plankton nets followed by microscope identification and counting. Used almost exclusively for tracing karst conduits.
Microorganisms yeasts coliform bacteria	Smaller than spores, 1 to 3 μm diameter, most useful for testing permeability of aquifer to transport of organisms. Movement primarily through fractures in sediment or rock. Organisms may sink or float in still water. Measured by filtration followed by incubation and counting colonies.
Viruses	0.02-0.05 μm. Many types sorbed on media due to positive charge on organism. Bacteriophage (virus infecting E. Coli) shows potential as good tracer due to negative charge on organism. Detection by culturing and colony counting.[4]
B. Nonionic Tracers	
Fluorocarbons CCl_2F_2 CBr_2F_2 $C_2Cl_3F_3$ $C_2Br_2F_4$ etc.	All fluoromethanes and fluoroethanes with chlorine and/or bromine substitutions. Slight to moderate sorption on silicate or carbonate material. Strong sorption by organic

Table 1. Common Groundwater Tracers - continued

Tracer	Characteristics
B. Nonionic Tracers - continued	
	materials such as coal and peat. Nondegradable, nontoxic, volatile, low solubility, difficult handling. Measurement by gas chromatography with electron capture detection. Most are detectable to 1 part per trillion.
Aldehydes and alcohols	Used in oil reservoir studies, degradable, detectable at ppm level with GC.
Tritium HTO, CH_3T	Radioisotope of hydrogen, low sorption on most aquifer materials, very restricted use in shallow aquifers due radiation hazard. Common use in oil reservoirs. $T_{1/2}$ = 12.3 yrs. Measurement by weak β radiation.
C. Ionic Tracers	
Halides	
Cl^-	No sorption, inexpensive, high background in groundwater, density problems when used in high concentrations, most useful in laboratory experiments, measured by titration methods or by electrical conductivity.
Br^-	Very slight sorption, low natural background in fresh water aquifers, best general purpose groundwater tracer, measurable using selective ion electrode, practical sensitivity about 0.5 ppm.
I^-	Moderate sorption, very low natural background, measured by selective ion electrode, 0.5 ppm.
^{131}I	Radioisotope $t_{1/2}$ = 8.2 days. Useful for short term tests, most common application in oil reservoir studies. β and γ emission.
Dyes	
Rhodamine WT	Red dye, moderate sorption, moderately stable, low background fluorescence, most frequently used in surface water

Table 1. Common Groundwater Tracers - continued

Tracer	Characteristics
C. Ionic Tracers - continued	
	and in karst tracing. Used in highly permeable sand and gravel aquifers. Detected by fluorimetry, 1 to 0.1 ppb.
Fluoroscein	Yellow dye, same as rhodamine WT but much stronger sorption on aquifer materials.
Chelates EDTA-^{51}Cr EDTA-IN	EDTA complexes with heavy metals, or radioisotopes detected by radiation or by post neutron activation. Some complexes unstable in presence of other cations in water. Numerous chelated tracers have been developed and tested with varying results, mostly in oil reservoir studies. Good sensitivity.
Thiocyanate SCN^-	Na, K or ammonium salts of thiocyanate, most commonly used chemical tracer of the oil industry. Low sorption, measured by colorimetry, detectable down to 0.1 ppm.
Organic anions sodium benzoate pentafluoro-benzoic acid	Unlimited variety of good tracers possible. Very low sorption, stability improved by fluorine substitution. Can be measured with high precision using HPLC. Detectable in low ppb range.

REFERENCES

1. Drost, W., D. Klotz, A. Koch, H. Moser, F. Neumaier, and W. Ravert, Point dilution methods of investigating ground-water flow by means of radioisotopes. Water Resources Research, V. 4, pp. 125-146, 1968.
2. Ciccioli, P., W. T. Cooper, P. M. Hammer and J. M. Hayes, Organic solute-mineral interactions: A new method for the determination of ground water velocities. Water Resources Research, V. 16, pp. 217-223, 1980.
3. Basett, R. and others, Preliminary data from a series of artificial recharge experiments at Stanton, Texas, U.S.G.S. Open file report P[illegible] (in preparation).
4. Gerba, C. P., personal communication, Baylor College of Medicine, Houston, Texas, 5/20/80.

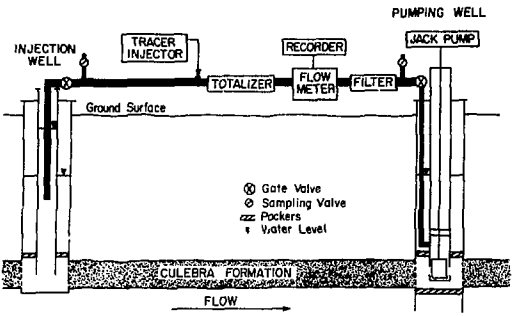

Fig. 1. Two well recirculating test.

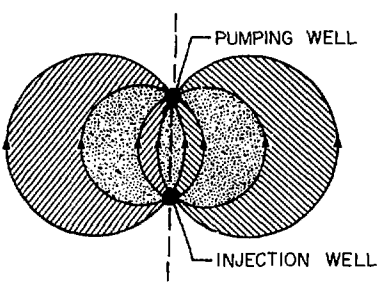

Fig. 2. Flow pattern for two-well injection-withdrawal in a homogeneous isotropic aquifer.

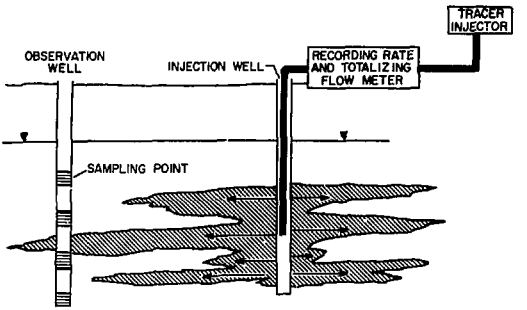

Fig. 3. Radial flow test.

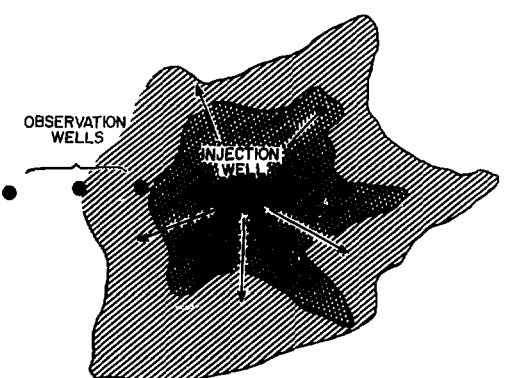

Fig. 4. Radial flow test.

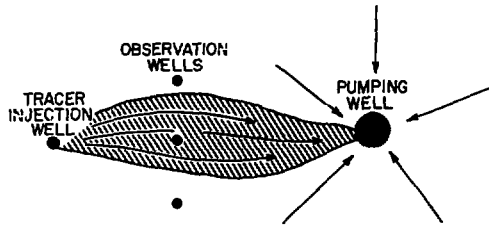

Fig. 5. Convergent flow test.

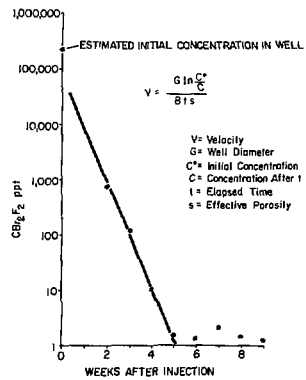

Fig. 6. Point dilution experiment in Conasauga shale at Oak Ridge National Laboratory, Oak Ridge, Tennessee.

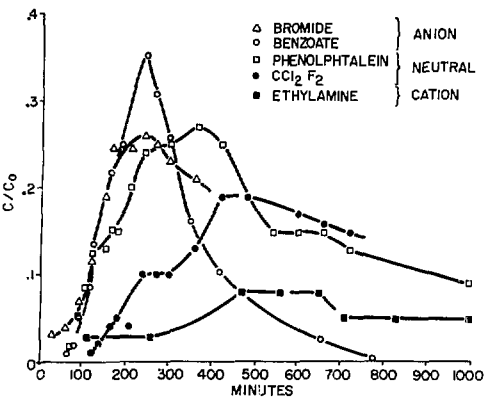

Fig. 7. Radial flow tracer experiment showing the behavior of selected anionic, neutral, and cationic compounds observed at a distance of 2 meters from the injection well in the Ogallala Sand Formation at Stanton, Texas.

INJECTION VERSUS PRESSURE PULSE BOREHOLE TESTS IN FRACTURED CRYSTALLINE ROCKS - OBSERVATIONS AND RECENT EXPERIENCES

C.B. Forster and J.E. Gale
Department of Earth Sciences
University of Waterloo
Waterloo, Ontario, N2L 3G1

Abstract

Previous workers have proposed the pressure pulse test as an alternative to steady-state determination of permeabilities in fractured crystalline rocks. A field and laboratory research program has been conducted to assist in developing techniques to analyze in-situ pressure pulse tests. Specifically this program was aimed at i) comparing steady-state conductivity determinations to pressure transient determinations, ii) assessing the effects of equipment compliance on pressure pulse test results and, iii) determining the radius of influence of a transient pressure pulse test in fractured crystalline rocks.

In the laboratory, transient pressure pulse tests and steady-state flow tests where performed on a sample of Stripa Granite core (11 cm long and 4.5 cm in diameter) containing a single natural fracture parallel to and centered on the core axis. The test configuration simulated a full scale borehole test cavity using borehole seals of various compliances in a 76 mm steel tube. Test results indicate a good correlation between steady-state and transient conductivity determinations. Packer compliance was found to cause underestimation of sample conductivity by up to a factor of 2. With decreasing sample permeability the significance of packer compliance was found to increase.

In the field, transient pressure pulse tests and steady-state flow tests were performed in an array of boreholes collared 338m below ground in a fractured crystalline rock mass. There is no apparent correlation between results of each test type. In order to determine the radius of influence of in-situ pressure pulse tests in low-permeability fractured rocks, the volume of water in the test cavity and the monitoring cavities must be the same order of magnitude as the volume of water in the rock mass influenced by the test.

Introduction

Analysis of contaminant movement through low permeability fractured crystalline rock must be based on an understanding of the physical hydrology of such rock masses. Fractured rock masses are generally characterized by narrow, relatively permeable zones within a low permeability framework. These zones are either discrete fractures, closely spaced groups of fracture or thin porous media zones. The matrix conductivities of most crystalline rocks generally range from 10^{-9} to 10^{-12} cm/sec. The hydraulic conductivity of the narrow, relatively permeable zones can be many orders of magnitude greater.

Measurement of rock mass conductivities in excess of 10^{-8}cm/sec. are commonly carried out using steady-state injection tests (Figure 1). Unfortunately, in lower conductivity rocks, an accurate flowrate measurement is difficult to achieve. Flowrates of fractions of millilitres per hour require long test times(hours to days), sensitive measurement equipment and long test intervals (tens of meters). Long test times increase the probability of flowrate measurement errors resulting from temperature and pressure variations during the test. Long test intervals reduce the capability of determining permeabilities of individual fractures or a small number of fractures. Thus, the transient pressure pulse test, as described by Brace et al(1968), has been proposed as an alternative to steady-state injection tests in fractured rocks.

Brace et al (1968) have described the use of the pressure pulse technique to perform permeability determinations in the laboratory. Figure 2 shows a schematic of the test configuration. A test is performed by placing a rock sample between two reservoirs of fixed volume (V_1 and V_2). If the pressure in the upstream reservoir (P_1) is raised instantaneously the rate of equalization of pressures P_1 and P_2 in the two reservoirs is related to the porosity and permeability of the rock sample. A confining pressure Pc is applied to the system to reproduce the state of stress expected at the point of sampling. Brace et al. analyzed the results of their tests by assuming that the laboratory system acts as an equivalent electrical circuit containing two capacitors (equivalent to V_1 and V_2) in series with an intervening resistor (rock sample). The upstream reservoir with applied pulse pressure $\Delta P = P_1 - P_2$ P_2 is represented by a capacitor fully charged at $t<0$ thus at $t = 0$ the capacitor discharges according to an exponential decay. Thus, the upstream reservoir pressure P_1 decreases while the downstream reservoir

pressure, P_2 increases until both reach the equalization pressure P_E. Following Brace et al (1968) the pressure volume relationships can be expressed in equation form by:

$$\frac{P_1 - P_E}{\Delta P} = \left(\frac{V_2}{V_1} + V_2\right) e^{-\alpha t} \quad (1)$$

$$\alpha = \left(\frac{kA}{\mu\beta^2}\right) \cdot \left(\frac{1}{V_1} + \frac{1}{V_2}\right) \quad (2)$$

where the parameter α is a function of, i) fluid visiosity, μ, and fluid compressibility, β, ii) sample permeability k and cross section area A and iii) reservoir volumes V_1 and V_2. This relationship requires that the parameter a^2 in the governing diffusivity equation

$$\frac{\partial^2 P}{\partial x^2} = a^2 \frac{\partial P}{\partial t} \quad (3)$$

be equal to zero. For a fractured sample, the parameter a^2 contains terms which include matrix fracture permeability, matrix and fracture porosity, fracture stiffness, rock compressibility and fluid compressibility. However, as a^2 is assumed to equal zero

$$\frac{\partial^2 P}{\partial x^2} = 0 \quad (4)$$

implying that the pressure gradient is linear at all times although varying in magnitude with time.

Lin (1977) used a more complete form of the same mathematical formulation, where a^2 was considered to be non zero, in a numerical simulation of a proposed laboratory testing program. Later, Lin (1979) used this same numerical technique to determine rock sample permeabilities from laboratory test data.

A pressure pulse test performed in the field uses the same borehole configuration as the injection test (Figure 1) and the pulse test principles described above. Once a borehole cavity is sealed, a pressure pulse is created within the test cavity by diplacement of several milliliters of water. The decay of the pressure pulse is monitored by a sensitive pressure transducer. The transient nature of the pressure pulse test produces a test time of minutes or hours which is much less than the hours or days required for injection testing of the same interval. Thus, analysis of pressure decay curves obtained from the relatively short pressure pulse tests in low permeability rocks are expected to yield more accurate rock mass conductivities than injection testing in fractured crystalline rock.

A method for analysis of in-situ pulse tests in fractured impermeable media has been proposed by Wang et al (1977) and investigated using a semi-analytical model based on solution of the diffusivity equation for different fracture configurations using appropriate rock and water properties and boundary conditions. However, this method is not yet amenable to analysis of the results of field tests. In order to assist in developing techniques to interpret results of in-situ pressure pulse tests, laboratory and field experiments have been performed to investigate the following:

i) comparison of conductivities determined by steady-state conductivity tests and transient pressure pulse tests,

ii) the radius of influence of a pressure pulse test performed in fractured crystalline rocks,

iii) the effect of variations in test cavity volume (due to equipment compliance) on pressure pulse test results.

Laboratory Experiments

The laboratory test program was designed to investigate; i) the comparison between transient annd steady-state conductivity tests and ii) the effects of packer compliance on pressure pulse tests performed in a simulated field configuration. A schematic of the test equipment is shown in Figure 3.

The test equipment consists of 3 main components; upstream reservoir, downstream reservoir and sample cell (Figure 3). A rock core (4.5 cm diameter and 11 cm long) containing a single fracture is held in the sample cell. This sample represents the dominant fracture controlling conductivity around the borehole with the sample cell exerting an hydrostatic stress on the sample which would be expected at depths of approximately 400 to 500 m. In this experiment the core is a sample of Stripa Granite containing a single natural fracture parallel to and centered on the core axis. The downstream reservoir is simply a steel water filled tank representing the porosity of the overall rock mass surrounding a test cavity. The upstream reservoir was designed to simulate the actual borehole cavity. A 7 metre length of steel tube with a 76 mm inside diameter was used to represent the borehole. Various borehole seals were

used to isolate a 3 metre section of the tube in order to represent varying degrees of packer compliance. Steel plugs were used to represent the least compliant case while standard air or water filled inflatable packers represent the more compliant field situations.

The test program was conducted after stressing the sample through three initial loading cycles (thus minimizing hysteretic effects of stress loading and unloading on fracture flow characteristics). During the fourth loading cycle the confining pressure was increased in a stepwise manner from zero to 3.4,6.9, and 13.9 MPa. At each step both steasy-state flow tests and pressure pulse tests were conducted with similar pressure gradients across the sample, (approx. 0.14 MPa). Also, at each step each different borehole seal was used in order to observe the effects of equipment compliance on the test results.

Steady-state flow tests were performed by applying a steady pressure gradient across the sample and monitoring the resulting flow of water through the sample. Once steady flow and pressure conditions were attained results were recorded and used in calculation of sample conductivity by standard techniques, (Forster and Gale, 1980).

Transient pressure pulse tests were performed by increasing the pressure in the upstream reservoir (by displacement of several millilitres of water) and monitoring the resulting pressure decay. The pressure time data was recorded and used in calculation of sample conductivity by Brace's semi-logarithmic straight line technique. Normalized pressure P_N was calculated by dividing the residual pressure decay (P_1-P_E) by the magnitude of the original pressure pulse (ΔP). A plot of the log of P_N against time for one portion of the test series is shown in Figure 4. This test series was run at the maximum confining pressure of P_c =13.8 MPa with pressure pulse ΔP=0.14 MPa (ΔP was 1% of P_c) and pore pressure P_p = 1.4 MPa (P_p was 10% of P_c).

An estimated value of a^2 for the sample tested is in the order of 10^{-5} s/cm^2 which is sufficiently close to zero for the purposes of our analysis. Thus using α, the slope of a plot of log P_N against time, permeability, k, can be calculated from equation 2. Using this approach transient conductivity values were calculated (Table 1). From Figure 4 and Table 1 it can be seen that the least compliant configuration, the steel plug seal, produces the steepest slope thus the highest conductivity value while the more compliant water and air filled packers yielded the shallowest slopes and lowest conductivity. From Table 1 it can also be seen that variations in packer compliance (by varying the borehole seals) causes a factor of 2 variation in conductivity. In addition, reasonable agreement was found between conductivities calculated from both steady-state and transient tests. However, our testing indicated that with decreasing conductivity the significance of compliance effects increases. It was also found that small variations in temperature ($\pm$ 0.01^{o} C), occurring during transient testing, can significantly affect the shape of the resulting pressure decay curves.

Field Experiments

The field test program was designed to investigate i) the comparison between steady-state and transient conductivity tests and ii) the radius of influence of a pressure pulse test in a fractured granite. The test program was carried out in an array of boreholes collared in a drift at the 338 metre level of the Stripa Mine, (Gale and Witherspoon, 1979; Forster and Gale, 1981). The drift extends into a fractured granite mass with the boreholes of interest extending beyond the end of the drift. The borehole array is shown in Figure 5 with the central HG-1 borehole oriented horizontally, HG-3 and HG-4 inclined downwards, HG-2 and HG-5 inclined upwards and DBH-2 oriented horizontally. Holes HG-1 through HG-5 are 30 m in length. DBH-2 is about 75 m in length but only a 30 m section was used. The dark cylinders shown in Figure 6 represent the borehole cavities isolated using standard inflatable packers. Twenty-five cavities were used in the test program, each approximately 7 litres in volume.

Both steady-state injection tests and transient pressure pulse tests were performed in the isolated cavities in order to compare the resulting conductivity determinations. Steady-state tests were performed by injecting water into the rock-mass under constant pressure while measuring the injection flow rate. Flow rate and pressure data obtained when steady-state flow conditions were reached was used to calculate the hydraulic conductivity of the rock around the test interval assuming a porous media approach. Pressure pulse transient tests were performed by displacing a small volume of water in a tube connected to the test interval while monitoring the resulting pressure increase and decay. In addition, pressures were monitored during each test both in the test cavity and in several observation cavities in order to observe the extent, or radius of influence, of both pressure pulse and steady-state tests.

Figures 7,8,9 and 10 show normalized pressure decay, P_N, plotted against log time for different test intervals. Steady-state conductivity values

(calculated from injection tests, assuming porous media conditions) are shown beside the corresponding pressure pulse decay curve for each interval. Also shown in Figures 7,8,and 9 are the fracture logs for each test interval, (Details on the fracture are given in Forster and Gale, 1981). Figure 10, without the fracture log, is a summary plot of the curves given in Figures 7,and 8. Tests performed in intervals HG1-1b, HG1-3b, HG3-4, HG3-5, HG5-2 and HG5-3 (Figures 7 and 8) show decay curves similar in shape but having a variety of decay times. Figure 9 shows that the pressure pulse curves obtained in intervals HG3-3, HG4-4 and HG4-5 have significantly extended decay times. These intervals also have correspondingly low steady-state conductivity values. One might expect that increasing decay times would correspond to decreasing steady-state conductivities. However, as shown in Figure 10 this trend does not appear. In fact there is a very poor correlation between decay time and steady state conductivity . This lack of correlation is expected to result from a combination of factors including, i) the complex nature of the fracture system, ii) nature of test equipment (packer compliance), iii) differences between the volume of rock mass tested by steady-state and transient tests (difference in radius of influence).

During each pressure pulse test up to seven adjacent borehole intervals were monitored to determine the radius of influence of a pressure pulse test. The minimum distance between cavities was 1.5 m ; however, throughout the test program no response was obtained in any observation cavity. Steady-state flow tests indicated a good connection between test cavities thus a response might have been expected. However comparison of the volume of the test cavity (7ℓ) to the volume of the pressure pulse displacement (several millilitres) suggests insufficient water was displaced in the test cavity to cause an observable response in the observation cavities.

Conclusion

In this paper the authors have described a laboratory and field program designed primarily to compare steady-state conductivity determinations to transient pressure pulse determinations.

Laboratory steady-state and transient tests were performed on a sample of Stripa Granite core (11 cm long and 4.5 cm diameter) containing a single natural fracture parallel to and centered on the core axis. Tests performed at three different confining pressures show a good correlation between steady-state and transient test results (Table 1). In addition, packer compliance was found to produce conductivity values which underestimate the non-compliant steel plug conductivities by up to a factor of 2. With increasing confining pressure (decreasing conductivity) the significance of packer compliance was found to increase. Significant compliance effects were also found to result from temperatures variations exceeding ± .01°C.

Field steady-state and transient tests were performed in an array of boreholes collared in a granite mass 338 m below ground, Transient conductivities have not been calculated; however steady-state conductivities have been calculated and compared qualitatively to the transient decay curves for each interval . There is no apparent correlation between the two types of test results. This lack of correlation is primarily attributed to the complex nature of the fracture system and differences between the radius of influence for each test type. Observation cavities did not respond to pressure pulses generated in test cavities despite hydraulic connection indicated by steady state testing. The minimum distance between cavities was 1.5 m. However, the large volume (7ℓ) of the observation cavities appears to preclude observation of any pressure response resulting from a displacement of only a few millilitres of water in the test cavity.

References

(1) Brace, W.F., Walsh, J.B., and Frangos, W.T., 1968. Permeability of granite under high pressure, J. Geophys. Res. Vol. 73, No. 6, pp. 2225-2236.

(2) Forster, C.B. and Gale, J.E., 1980. A laboratory assessment of the use of borehole pressure transients to measure permeability of fractured rock masses. Lawrence Berkeley Lab. Tech. Report 8674 University of California, Berkeley, California.

(3) Forster C., Gale J.E. 1981. A Field Assessment of the Use of Borehole Pressure Transients to Measure the Permeability of Fractured Rock Masses. Lawrence Berkeley Lab. Tech. Report 11829 University of California, Berkeley, California.

(4) Gale, J.E., and Witherspoon, P.A., 1979. An approach to the fracture hydrology at Stripa: preliminary results, Lawrence Berkeley Laboratory, University of California, Berkeley, California,USA.

(5) Lin,W., 1977. Compressible fluid flow through rocks of variable permeability, Lawrence Livermore Laboratory, University of California.

6) Lin, W., 1979. Measuring the permeability of Eleana Argillite from Area 17, Nevada Test Site, using the transient method. Lawrence Livermore Laboratory, Livermore, California, U.S.A.

7) Wang, J.S.Y., Narasimhan, J.N. Tsang, C.F. and Witherspoon, P.A., 1977. Transient flow in tight fractures, Proceedings of Invitational Well-Testing Symposium, October 1977, Berkeley, California.

Table I: Comparison of steady-state results and transient test results. Granite sample - Cycle #4

		Mean K_f (cm/sec)x10^3		Mean K_p (cm/sec)x10^7	
(MPa)	Borehole Seal	Steady State	Transient	Steady State	Transient
	Steel Plug		16		74
	Air Packers @ 3.4 MPa		16		54
		16		56	
3.4	Air Packers @ 5.5 MPa		14		46
	Water Packers @ 3.4 MPa		--		--
	Steel Plug		71		17
6.9	Air Packers @ 3.4 MPa	6.5	54	15	11
	Air Packers @ 5.5 MPa		55		11
	Water Packers @ 3.4 MPa		--		--
	Steel Plug		1.9		2.2
	Air Packers @ 3.4 MPa	2.2	1.7	2.9	1.9
13.8	Air Packers @ 5.5 MPa		1.4		1.5
	Water Packers @ 5.5 MPa		1.1		1.1

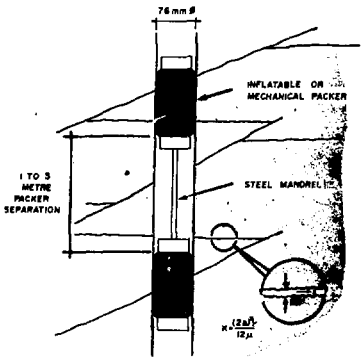

Fig. 1. Schematic of a saddle-packer system installed in a borehole.

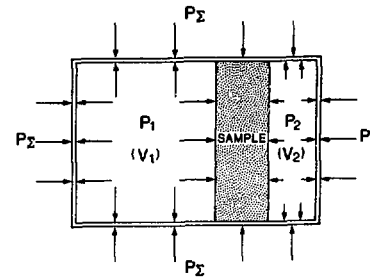

Fig. 2. Schematic of the test configuration used by Brace et al. (1968).

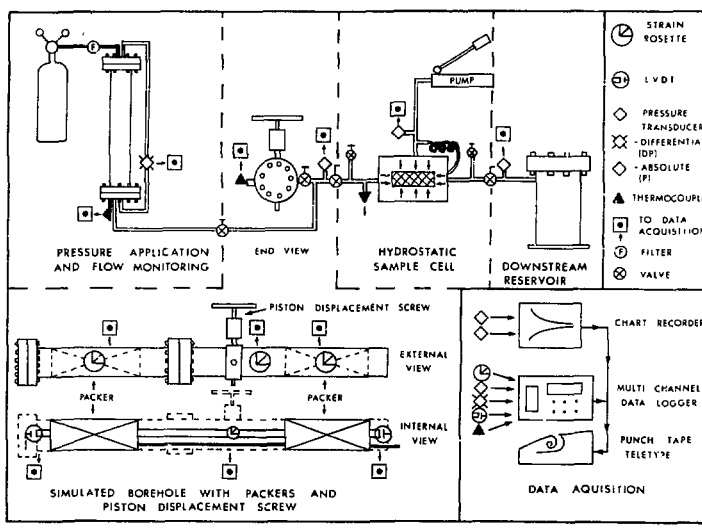

Fig. 3. Schematic of experimental apparatus.

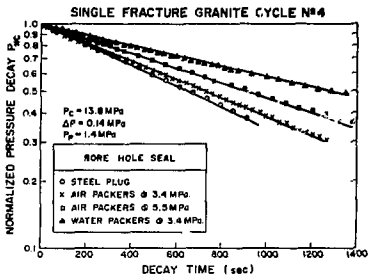

Fig. 4. Typical plot of log of normalized pressure decay against time for a granite sample containing a single fracture.

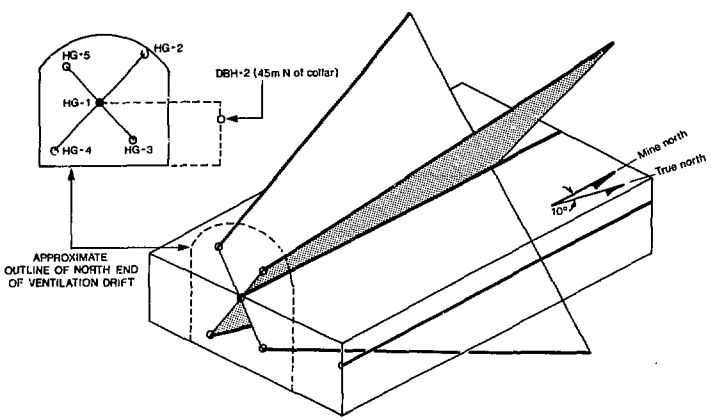

Fig. 5. Schematic perspective of boreholes north of the ventilation drift.

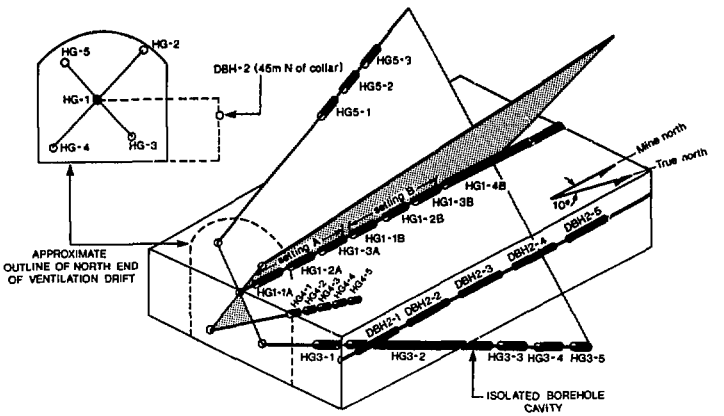

Fig. 6. Schematic perspective of borehole installation pattern.

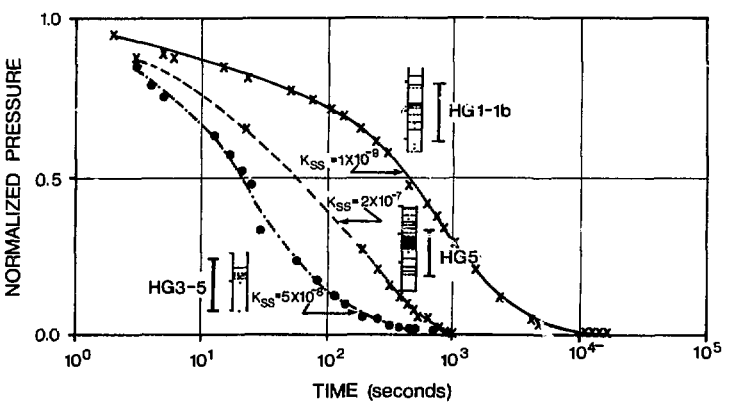

Fig. 7. Plot of normalized pressure against log time for pressure pulse tests in intervals HG3-5, HG5-3 and HG1-1b.

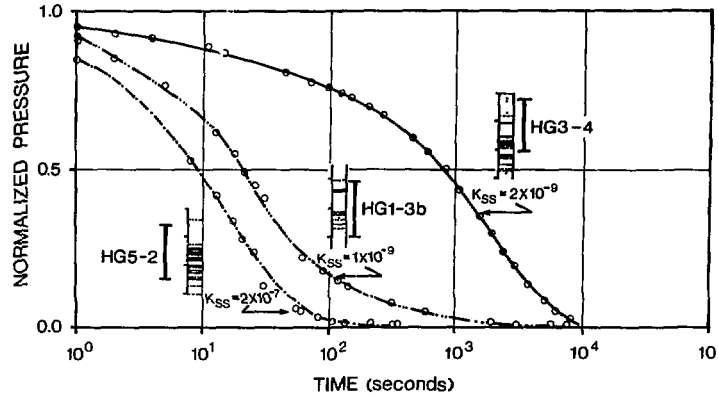

Fig. 8. Plot of normalized pressure against log time for pressure pulse tests in intervals HG5-2, GH1-30 and HG3-4.

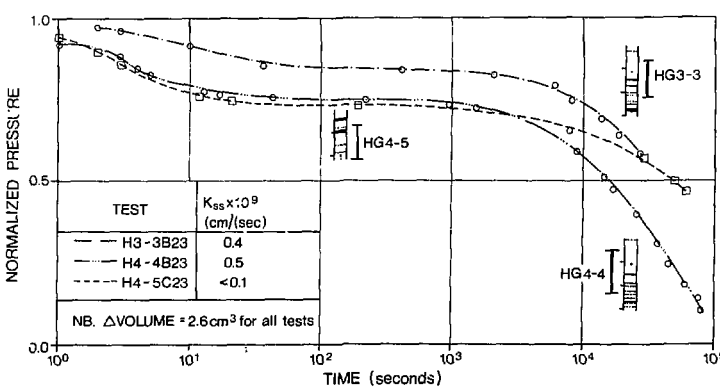

Fig. 9. Plot of normalized pressure against log time for selected pulse tests with extended decay characteristics.

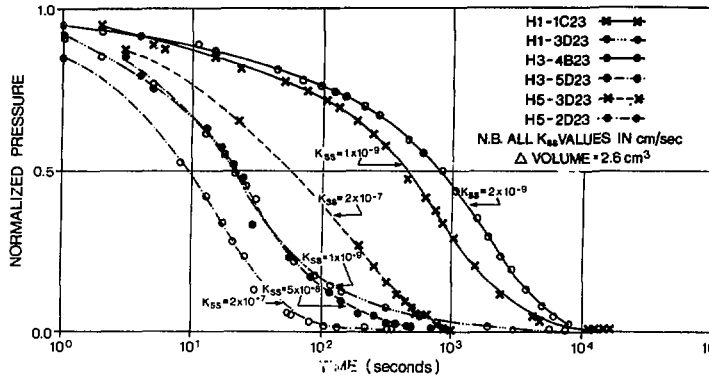

Fig. 10. Summary plot of normalized pressure against 14g time. Curves from figures 7 and 8.

ANALYSIS OF CONSTANT-HEAD WELL TESTS IN NONPOROUS FRACTURED ROCK

T. Doe and J. Remer
Lawrence Berkeley Laboratory
University of California
Berkeley, California 94720

The constant-head injection test, also known as the pressure test or packer test, has long been a standard permeability test in geological and civil engineering. Most of the published data on the permeability of nonporous fractured rock has been obtained by such tests. In general, the analysis of the data from constant-head tests has been made assuming steady radial flow by invoking a "radius of influence". If one compares the results of steady analyses and transient flowrate analyses, the error in assuming steady flow is less than an order of magnitude for reasonable values of storativity, and this error can be minimized through proper choice of radius of influence.

Although the steady flow assumptions do not result in large errors in the calculation of permeability, careful design of constant-head well tests can yield not only storativity, but also qualitative information on the areal extent of permeable zones or fractures tested.

Constant-head well tests have several major advantages over other well test techniques in low permeability rock. Unlike pump tests, wellbore storage effects are virtually nonexistant. Provided low-flow measurement apparatus is available, constant-level tests are far more rapid than slug tests and, unlike pulse tests, compliance of equipment is not a factor, since the system is maintained at constant pressure throughout the test.

Introduction

Low-permeability rocks (rocks with less than 10^{-5} cm/s permeability) are receiving considerable attention for both their energy resource potential and the isolation they can provide in waste disposal. Quantifying such permeabilities, however, is difficult as traditional well test techniques can require very long periods of time that make the costs of such tests prohibitive. For example, overcoming the wellbore storage effects above may require a week to pump-test rocks with transmissivities lower than 10^{-2} cm^2/S (Fig. 1, Wilson et al, 1979). Similarly slug tests can take a week for 75% decay for transmissivities lower than 10^{-5} $cm^2/5$. The only test techniques available which can test materials lower than about 10^{-4} $cm^2/5$ within reasonable test times are pulse tests and constant-head pump tests. Of the two, constant-head pump tests are applicable over a wider range of transmissivity values than pulse tests, yet with very-low-flow measurement instrumentation, constant-head tests are applicable to rock whose hydraulic conductivity is within two orders of magnitude of intact crystalline rocks.

In addition to the wide range of transmissivities over which constant head tests are applicable,

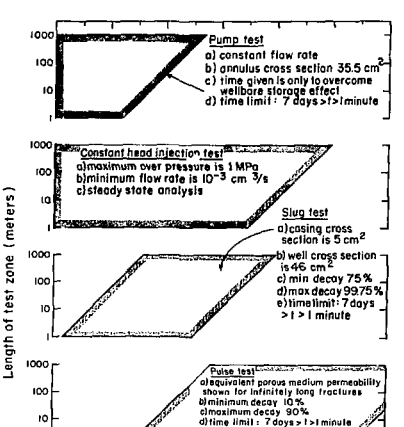

Fig. 1 Range of hydraulic conductivities over which common well test techniques are applicable (XBL 792-7379).

constant-head tests are free of wellbore storage effects. These effects include compliance or deformation of packers or other test equipment. Since all of the test is maintained at constant pressure, even very deformable components of the test system should not effect the test results.

The constant-head test has further significance in being the most widely applied well test for crystalline rock. The data compilations of Davis and Turk (1964) and Snow (1968) relied primarily on constant-head tests run by the U.S. Army Corp of Engineers. It should be noted, however, that most existing data from constant-head tests comes from civil and geologic engineering where the data have been interpreted using steady-flow techniques. Although much literature has been devoted to turbulence effects of fluid mechanics of constant head injection (Louis and Maini, 1970); Rissler, 1978) the steady flow assumptions are probably a more serious source of error in low permeability rocks. The purpose of this paper is to examine the constant-head tests in terms of steady versus transient flow, and analyze the

magnitude of error that can result from steady flow interpretation. Whereas the flow rate calculations depend on the storativity, the nature of storativity in crystalline rocks is discussed. Errors arising from the test equipment such as Dick's (1975) discussion of pressure losses in injection tubing are not discussed in this paper.

Description of the Constant-Head Test

Injection tests are the most common method of evaluating crystalline rock permeability for engineering purposes. Procedures are extensively discussed in Ziegler (1976), Snow (1966, 1968), Louis and Maini (1970), and Banks (1972).

The primary advantage of constant-head injection tests over the pump-test techniques standard in hydrogeology are, (1) they are applicable to small-diameter wells where pumps will not fit, (2) they are relatively rapid tests to conduct, and (3) they can easily isolate small sections of hole, thus determining structural features causing flow.

The basic test consists of injecting water to a section of a borehole isolated with inflatable packers (Fig. 2). The injection pressure is held constant, and when the water flowrate approaches a constant value, it is assumed that steady flow has been achieved. Two to eight progressively higher injection pressures are used in succession. Since the flowrate is a linear function of the injection pressure and flowrate can indicate departure from steady laminar flow assumptions. These deviations are shown in Figure 3 and can arise due to fracture deformation, packer leakage, or turbulent rather than laminar flow (Louis and Maini, 1970).

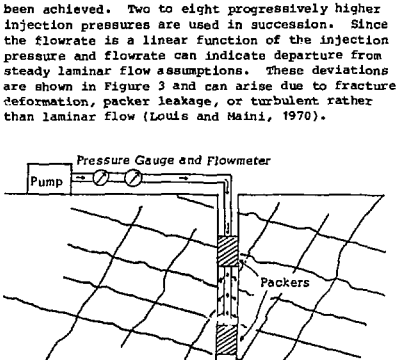

Fig. 2 Schematic of equipment used for constant head injection tests. (TBL 812-8187)

Constant-head tests were originally developed for damsite and other engineering investigations by the French engineer, Lugeon (Serafim, 1968). In Europe, hydraulic conductivity is often expressed in the Lugeon unit, which is equal to one liter per minute of flow per meter of hole length at an overpressure of 10 kg/cm^2. Such tests are commonly run by the Army Corps of Engineers, who have published two manuals of injection test procedure recommendations (Hvorslev, 1951; Ziegler, 1976).

Most literature on the permeability of crystalline rocks is based on constant-head tests, including Davis and Turk's (1964) study of permeability versus depth and Snow's (1965, 1968) work on fracture spacing and porosity. Constant-head injection tests can be run at any packer spacing; large spacings can be used for averaging the contributions of several fractures, while small spacings are used to isolate individual conduits such as single fracturse, faults, or shear zones.

Steady-Flow Analysis of Packer Test Data

The analysis of constant-head packer test data is most commonly done using steady-flow techniques. Generally the zone isolated is assumed to be a confined aquifer with full penetration by the well (Figure 3). The injection flowrate, Q, is given by

$$Q = 2\pi K (H_w - H_o) b (\ln r_o/r_w)^{-1}$$

Q = flow rate (cm^2/S)
K = hydraulic conductivity (cm^2/S)
b = straddle length (cm)
H = Head (cm)
r = radius (cm)
o = subscript for outer boundary
w = subscript for well boundary.

The radius of influence, r_o, is a result of a presumed open circular flow boundary.

Without an observation well it is difficult to determine very exactly the radius of influence, r_o; however, since r_o appears as a logarithmic term, large errors in the estimation of r_o only result in small errors in the calculation of either K from the injection test (Ziegler, 1976). For example, in a 7.6 cm diameter well, the $\log_e$ of the ratio of the radius of influence to the well radius only varies from 5.6 to 10.2 for r_o varying from 10m to 1000m.

To account for errors due to the flow not being perfectly confined and therefore not entirely radial, several "shape factors" have been used. Hydraulic conductivity determinsd from shape factors generally employs an equation of the form

$$K = \frac{Q}{bH} \times C \qquad (3\text{-}8)$$

where C is a dimensionless constant which varies depending on the assumed pattern of flow about the test zone. Such factors include (1) flow with potentials elliptical about the test zone (Hvorslev 1951), (2) radial flow near the well becoming spherical at r = b/2 (Moye, 1967), (3) empirical corrections based on electrical analogues of porous media (Sharp, 1970), and (4) radial flow with the radius of influence equal to the test zone length (Snow, 1968; Ziegler, 1976). For most normal test conditions, Ziegler (1976) notes that the variation between these correction factors is not greater than about 30%.

The importance of "shape factor" corrections in testing of fractured non-porous rock is questionable, unless the rock has a fracture spacing which is small relative to the length of the packer

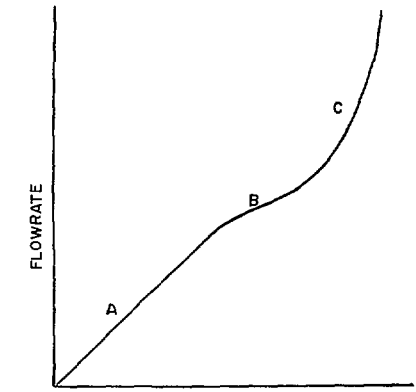

Fig. 3 Hypothetical pressure-flowrate curve for constant-head injection tests; A- laminar flow, B- turbulent flow, C- fracture deformation. (after Louis and Maini, 1970). (XBL 812-8194)

seal. For tests in rocks where the fracture spacing is large, only a few fractures will be contained in any given test interval, and of these only the fracture with the largest aperture will have any significance, due to the cubic relationship of aperture to flowrate. Flow will be confined to the planes of the large-aperture fractures unless they intersect other fractures of larger aperture close to the borehole. In either case, the equipotential lines about the test zone are unlikely to follow elliptical or spherical paths, and routine application of shape factors based on such assumptions may often be in error.

Transient Analysis of Constant Head Test Data

The steady-state procedure of analyzing constant-head injection test data requires several assumptions which may be difficult to quantify and unlikely to be met in nature. Among these assumptions are the existence of a radius of influence and the ability to determine the time required to reach steady flow conditions.

Although steady-flow equations were standard in the early days of hydrogeology and petroleum reservoir engineering, the recognition of the role of rock mass deformability (Theis, 1935) has made transient analysis the basis of pump and other well tests since the 1930's. Indeed, for infinite aquifers or fractures, steady conditions are never really achieved.

The major difference between pump tests and constant-head injection tests is that in pump tests the flowrate is held constant and the well test analysis is made on the basis of the transient change in pressure (or head) in the well. In packer tests, the wellbore pressure is held constant and the flowrate should be expected to be transient.

Constant-head well test solutions have not been as widely investigated in the hydrologic or petroleum literature as constant-rate tests. Nonetheless solutions for simple geometries have been available for some time. The first hydrologic applications were made by Jacob and Lohman (1952) who derived type curves for transient flow in infinite aquifers and applied the results to flowrate decline from flowing artesian wells. Hantush (1959) extended Jacob and Lohman's work to leaky aquifers, infinite aquifers, and aquifers with either closed or open outer boundaries. More recently, Jaiswal and Chauhan (1978) have investigated spherical flow under constant head conditions. Extensions of constant head solutions to include skin effects and pressure buildup after constant-head production have been made by Uraiet and Raghavan (1980) and Ehlig-Economides (1979), the former using finite differences, the latter by analytic solution.

Errors in Steady Flow Analysis of Constant Head Tests

A potential source of weakness in the practice of constant-head tests is the steady flow data analysis. First, steady flow analysis assumes an infinite conductivity material at the radius of influence; and, second, it ignores groundwater storage both due to water compressibility and to finite fracture or matrix stiffness.

Transient flowrate solutions overcome these objections. Time-variable radial flow under constant head can be described by

$$Q = 2\pi T\, G(\lambda)$$

where $$\lambda = \frac{Tt}{r_w^2 S}$$

$G(\lambda)$ = constant head well test function
q = dimensionless time
S = storage coefficient

Hantush (1959) gives solutions for both open and closed boundaries for infinite, open, and closed boundary type curves generated from Hantush's solutions are shown in Figure 4.

For a single fracture in a relatively impermeable rock, fracture aperture, e, determines flow by

$$T = (\rho g/\mu)\frac{e^2}{12}e = \frac{\rho g e^3}{12\mu} \quad .$$

ρ = fluid density
g = gravitational acceleration
μ = dynamic viscosity

The flow rate into a well injected at constant pressure should decrease rapidly upon application of the wellbore pressure and then decrease more gradually with increased time. If the aquifer or fracture is infinite, the flowrate should never

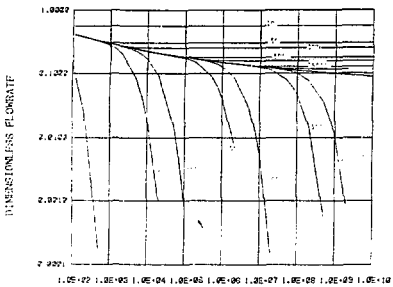

Fig. 4 Infinite, open, and closed boundary type curves for constant-head well tests, R_B/R_w is the ratio of boundary to well radius. (XBL 812-8188)

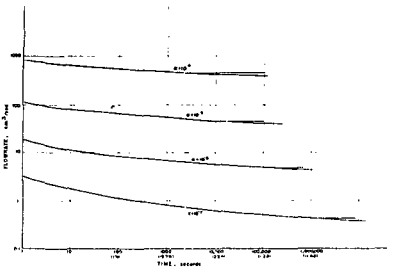

Fig. 5 Hypothetical transient flowrate curves for fifty-foot test zone in three-mile well; storage coefficient is 10^{-5}; hydraulic conductivity, K, is in cm/s. XBL 812-8199

reach a steady value. If the aquifer or fracture is leaky, or intersects a feature of much higher hydraulic conductivity, the flowrate should reach a steady value; and if the zone injected is finite, the flowrate should go to zero. In any case, the flowrate may not be the same as that predicted from steady-flow analysis for rock of the same hydraulic conductivity.

The error in using steady-flow analysis of well test data rather than the transient technique can be quantified by preparing flowrate versus time plots for the test geometry and a range of hydraulic conductivity values. The average flowrate over the period of time flowrate data were taken, Q_{av}, can be determined by integrating the flow over the period of time in question, i.e. taking the total volume of fluid injected and dividing by the time. w_{av} is the steady flowrate that would be recorded for use in steady-flow solutions. The difference between the hydraulic conductivity calculated using w_{av} in the steady analysis and the assumed hydraulic conductivity in the transient flowrate curve is the error in using the steady-flow analysis.

As an example of how the error in making steady-flow assumptions is calculated, consider a constant-head injection test on a 15.3 m (50 foot) section of an NX (r_w = 3.8 cm) borehole. First one can construct from the type curves a family of flowrate curves for various hydraulic conductivities assuming a value for the storage coefficient. (Fig. 5). In civil engineering practice the steady flowrate is measured at a time when the flow appears not to change appreciably with time (a highly subjective judgment). Assuming data is taken between one and five minutes of injection time, the volume of water injected can be taken from the area under the transient flowrate curve. Dividing by the total period of test time, t, gives the steady flowrate, w_{av} assumed by the test operator, or

$$w_{av} = \frac{1}{240} \int_{60}^{300} w(t)\, dt$$

Figure 6 shows the ratio of hydraulic conductivity calculated to actual hydraulic conductivity as a function of assumed radius of influence. Had the operator chosen a radius of influence comparable to the injection zone length, the use of steady-flow calculations would have resulted in overestimation of hydraulic conductivity by a factor of about two.

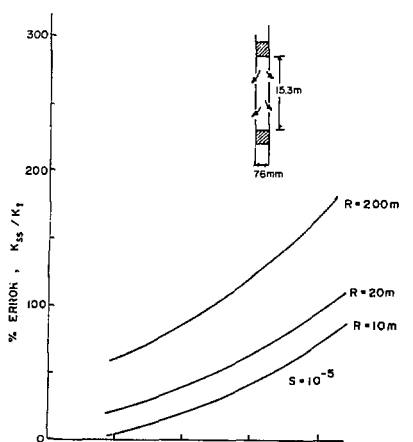

Fig. 6 Ratio of actual hydraulic conductivity to value calculated using steady-flow assumptions for test conditions in insert, 300-second test. (XBL 812-8190).

Selection of a smaller radius of influence could have resulted in less error. Figure 7 shows the radius of influence yielding no error for the case described above. Thus, by proper selection of radius of influence, the error in calculating hydraulic conductivities can be minimized.

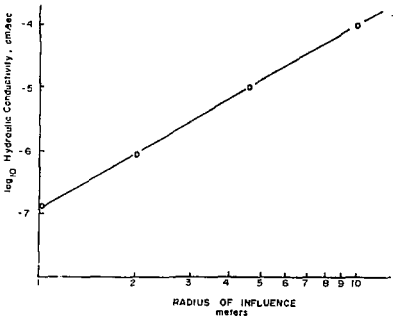

Fig. 7 Radius of influence yielding zero error in steady state calculation for a 300 second test and test conditions in Figure 6. (XBL 812-8191)

The error in use of steady flow assumptions increases with lower permeability, however, this can be compensated for either by using longer test times or smaller radii of influence. Figure 8 shows similar calculations of the error in steady flow calculations for two meter test zones over two hour periods. For the most extreme values of hydraulic conductivity and high values of storage, the error in calculating hydraulic conductivity is less than an order of magnitude and generally within about a factor of two or three.

Discussion

The calculation of the error in using assumptions of steady flowrate in constant head injection tests shows that the errors are small compared to the range of variability encountered in testing crystalline rock. Thus data which are reported in the literature for crystalline rock hydraulic conductivity based on steady flow analysis should be considered reliable so long as reasonable values of radius of influence have been used.

It is not advocated here that the steady flow assumption be used routinely in testing where it may be possible to obtain transient data. Transient analysis can be used for calculation of storage coefficients as well as to study boundary effects. For example, by knowing the time to deviation from the infinite layer type curve, one can determine the radial distances either to a boundary; or, if no deviation occurs, the radius over which the hydraulic properties are consistent. The dimensionless time (Tt/Sr_w^2) to deviation from the infinite layer type curve is shown in Figure 9 as a function of r_o/rw. By calculating T and S from the type curve match the radial distance affected by the test can readily be calculated.

Where steady flow assumptions might prove most useful in data analysis in very low permeability rocks. The lower limit of turbine flowmeter is about 4 ml/min, however flowrates can be measured by use of calibrated flowtanks which give the volume of water injected over a given period of time. For very low flowrates calibrated flowtanks may not have sufficiently rapid response to allow early time determination of the transient flow rate. For such uses, hydraulic conductivity can be calculated by use of average flowrate and steady flow assumptions provided care is exercised in choice of radius of influence.

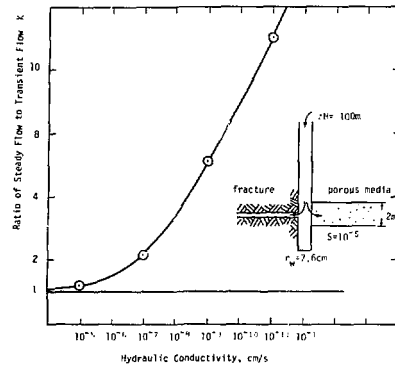

Fig. 8 Error in steady flow calculation in 2 meter test zone as a function of storage coefficient and hydraulic conductivity; 10^{-5} cm/s point is a 20m test, other points are for 2 hour tests. (XBL 812-8192)

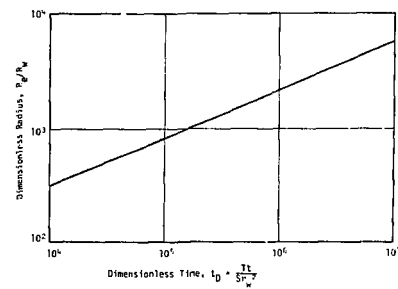

Fig. 9 Dimensionless time to deviation from infinite type curve as a function of distance open or closed to boundary. (XBL 812-8193)

REFERENCES

Banks, D.C., 1972 In situ measurements in basalt: Proc. symp. of percolation through fissured rocks, Int. Soc. Rock. Mech; Stuttgart.

Davis, S.N. and Turk, L., 1964, Optimum depth of wells in crystalline rocks, Groundwater 2:6-11.

Dick, R.C., In situ measurement of rock permeability - influence of calibration error on test results; Assn. Eng. Geol. Bull., 12:193-212.

Ehlig-Economides, C and Ramey, H. Jr., 1979, Transient rate decline for wells produced at constant pressure; Soc. Pet. Eng. paper 8377.

Hantush, M., Nonsteady flow to flowing wells in leaky aquifers; Jour. Geophys. Res. v 64 no. 8.

Hvorslev, M.J., 1951, Time lag and soil permeability in groundwater observations; U.S. Army Waterways Exp. Sta. Bulletin No. 36.

Jacob, C.E. and Lohman, S., Nonsteady flow to a well of constant drawdow. in an extensive aquifer: Trans. Am. Geophys. Union, v. 33 no. 4.

Jaisval, C.S. and Chauhan, H.S., 1978, Transient sperical flow to a nonpenetrating well with constant drawdown: groundwater, 16:432-436.

Louis, C. and Maini, T., 1970, Determination of in situ hydraulic properties in jointed rock; Proc. 2nd Cong. Int. Soc. Rock Mech., Belgrade v. 1, p. 235-245.

Moye, D.G., 1967, Diamond drilling for foundation exploration; Civil Eng. Transactions, Inst. Eng. Australia, v. CE9, p. 95-100.

Rissler, P. 1978, Determination of water permeability of jointed rock; Pub. Inst. of Fdn. Eng., Soil Mech., Rock Mech., and Waterways Construction, Auchen, Germany.

Serafim, J.L., 1968, Influence of interstitial water on the behavior of rock masses in Stagg, K and O. Zienkiewicz (ed) Rock Mechanics in Engineering Practice, Wiley, New York, p. 55-97.

Sharp, J.C., 1970, Fluid flow through fissured media; PhD thesis, Univ. of London, College.

Snow, D., 1965, A parallel plate model of fractured permeable media: PhD thesis Univ. Calif. - Berkeley.

_____, 1968 Fracture deformation and changes of permeability and storage upon changes in fluid pressure: Colo. Sil. Mines Quarterly, 63: 201-244.

_____, 1970, The frequency and apertures of fractures in rock; Int. Jour. Rock Mech., and Min. Sci.; v. 7, p. 23.

Theis, C.V., 1935, The relationship between the lowering of the piezometric surface and the rate and discharge of a well using groundwater storage: Trans. Am. Geophys. Union, v. 16, p. 519-524.

Uraiet, A.A. and Raghavan, R., 1980, Unsteady flow to a well producing at a constant pressure: Jour. Pet. Tech. (Oct) p. 1803-1812.

Wilson, C.R., Doe, T., Long, J. and Witherspoon, P., 1979, Permeability characterization of nearly impermeable rock masses for nuclear waste repository siting: in low flow, low permeability measurements in largely impermeable rocks, Proc. NEA IAEA workshop, OECD, p. 13-30.

Ziegler, T., 1976, Determination of rock mass permeability: U.S. Army Engineers Waterways Experiment Station, Tech. Report S-76-2, 85 p.

SOLUTE TRACER TESTS IN FRACTURED MEDIA

G.E. Grisak
Environment Canada
National Hydrology Research Institute
562 Booth Street, Ottawa, Ontario, K1A 0E7

SUMMARY

A single-well injection-withdrawal tracer test design with radial satellite instrumentation is used to illustrate design calculations for testing a single 100 μm fracture. Test durations of several days can conceivably provide tracer information over distances of tens of meters at realistic injection pressures. Calculations of the effect of matrix diffusion on the test results show that only in rocks with low (<0.01) matrix porosity would average solute velocities be obtained comparable to those based on the design injection conditions. Matrix diffusion in rocks with high matrix porosity would cause solute velocities to be much slower than the water velocity. It is considered that the primary function of a conservative (nonreactive) tracer is to provide verification of the average velocity in a fracture, usually calculated from hydraulic testing results. Reactive and nonreactive tracers used together can provide substantial information on in situ sorption properties if used in conjunction with radial instrumentation.

INTRODUCTION

Tracer testing techniques have occasionally been used in fractured media, generally with the assumption that porous media 'equivalent' parameters are applicable. (Webster, et al., 1970; Grove and Beetem, 1971; Kreft et al., 1974; Claassen and Cordes, 1975; Ivanovich and Smith, 1978; Landström et al., 1978). It is not certain however, that 'equivalent' parameters representative of a fractured media can be derived which adequately represent the transport processes or pathways in fractured systems. Grisak et al. (1980) derived 'representative' parameters for use in the analysis of a laboratory tracer test on a large, relatively undisturbed sample of fractured till. The 'representative' parameters were based on the concepts of flow in sets of planar fractures of simple geometry. The interconnectivity of the fracture sets was assumed to be represented by an *effective fracture spacing*, from which an *effective fracture aperture* was calculated. The effective aperture and spacing were then utilized in numerical simulations of the laboratory tracer effluent data. Simulations of this data using an analytical solution and parameters equivalent to those used in the numerical simulation showed good agreement (Grisak and Pickens, 1980a). The assumption of zero longitudinal dispersivity in the fracture, which is used in the development of the analytical solution, was shown to be suitable in fitting the laboratory tracer-effluent data.

One approach to evaluating solute transport through fractured media at the 'near-field' scale is to attempt to determine, with tracer tests, the transport processes in a single discreet fracture. Existing analytical techniques are suited to these tests, since the conceptual model on which most tracer testing techniques were developed is that of a single, permeable layer between parallel, relatively impermeable confining layers. There is a clear analogy to a single, continuous, planar fracture in relatively impermeable media. Analogies may also be possible between layered or stratified porous media systems and a set of subparallel fractures. An analysis of flow in layered porous media is given by Bear (1972, p.151-159) and Mercado (1967) discusses tracer spreading patterns in a permeability stratified porous media aquifer.

SINGLE FRACTURE

Single-well injection-withdrawal tracer techniques (diverging-converging flow) with satellite radial instrumentation can be used to illustrate test design and data analysis techniques in a single fracture. The type of data sought are similar to those presented by Pickens, Jackson and Inch (1980) in their dual tracer (reactive and nonreactive) test conducted in a confined porous media aquifer.

The hypothetical case of a single continuous planar fracture with an aperture width 2b of 100 μm is selected for illustration. Injection rates Q of 0.1 L/min are feasible at relatively low injection pressures of about 0.035 MPa (Davison, 1980) which should minimize the importance of any stress-opening of the fracture. If the porosity in the fracture is assumed equal to 1.0, the water velocity V at radial distances r, under steady state injection conditions, can be calculated (Figure 1) using equation [1]

$$V = \frac{Q}{2\pi r(2b)} \qquad [1]$$

The radial distance reached by injected water at any time t (Figure 2) can be calculated from equation [2]

$$r = [Qt_w/\pi(2b)]^{\frac{1}{2}} \qquad [2]$$

The transit time t_w, or time taken for water to move from the injection well to radial distances r, can be calculated by rearranging [2].

Table 1 lists transit times and radial distances from the injection well in a 100 μm fracture at injection pressures of 0.35 and 0.035 MPa. Also listed for comparison are calculations for a 10 μm fracture, although pressures as

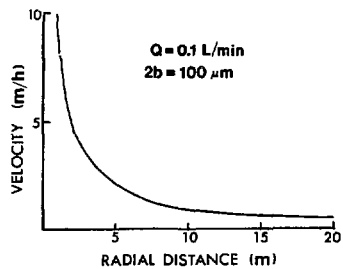

Figure 1 Water velocity in 100 μm fracture at radial distances r from injection well

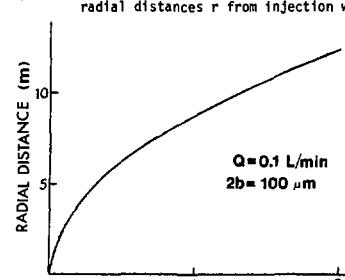

Figure 2 Graph of time taken for water from the injection well to reach radial distances r under steady injection conditions.

high as 0.35 MPa or greater may increase the width of the fracture aperture.

TABLE 1 Test design calculations for injection-tracer tests.

APERTURE (μm)		100	100	10
INJ. RATE (L/min)		1	0.1	0.01
RADIAL DISTANCE @ (m)	1 hr	14	4	1.4
	10 hr	44	14	4
TRANSIT TIME TO (h)	10 m	0.5	5.2	52
	20 m	2.1	21	210
INJ. PRESS. (MPa)		0.35	0.035	0.35

Matrix Diffusion

The diffusion of nonreactive and reactive solute from a fracture into the adjacent matrix can have a considerable effect on solute transport in even a low porosity matrix. A simple one dimensional analytical solution can be used to illustrate the effects that matrix diffusion can have on solute transport at the scale of a single fracture tracer test with the conditions illustrated in Figures 1 and 2. Analytical solutions to the radial case which describe injection/withdrawal tracer tests have not yet been developed. In order to illustrate the effect of matrix diffusion using a constant-velocity analytical solution, a term *transit velocity* V_t is defined as the ratio of the radius r to the water transit time t_w. The transit velocity is introduced to approximate a constant velocity system.

An analytical solution to one dimensional advective transport in a single fracture with matrix diffusion has been adapted by Grisak and Pickens (1980) from Carlsaw and Jaeger (1959) and Jost (1960). The solution for relative solute concentration (C/C_o) in the fracture ($C=C_f$) and in the matrix ($C=C_m$) is

$$\frac{C}{C_o} = \text{erfc}\left(\frac{\left(\frac{\theta_m D^*}{V_t b}\right)(x+y)}{2[D^*(t-\frac{x}{V_t})]^{\frac{1}{2}}}\right), \quad t>\frac{x}{V_t} \qquad [3]$$

$$= 0, \quad t<\frac{x}{V_t} \qquad [4]$$

with the boundary and initial conditions

$$C_f(x,y) = C_m(x,y) = 0, \quad t=0 \qquad [5]$$

$$C_f(0,0) = C_m(0,0) = C_o, \quad t>0 \qquad [6]$$

$$C_f(x,0) = C_m(x,0), \quad x>0,\ t>0 \qquad [7]$$

where x = distance in direction of flow
y = distance into the matrix perpendicular to flow
D^* = matrix diffusion coefficient
C_o = input concentration (1.0)

Using a transit velocity V_t of 1.9 m/hr and a matrix diffusion coefficient D^* of 10^{-6} cm^2/s, breakthrough curves calculated for a distance of 10 m are plotted on Figure 3. Matrix porosities (θ_m) of 0.3, 0.03 and 0.003 are used to illustrate porosities of shales and clays, welded tuffs (ignimbrites), and crystalline rocks, respectively. The calculations show that, with a porous matrix such as exists in shales, the average velocity ($C=0.5C_o$) at 10 m

distance from an injection well in a 100 μm fracture is reduced to less than 10% of the transit water velocity. The reduction in average velocity is due solely to solute diffusion from the fracture. The actual reduction may be somewhat less pronounced in a field injection situation since a constant velocity is used in the calculations. The effect of matrix diffusion in tracer tests can be reduced by 1) high water velocities or large fracture apertures, reducing the solute transported to solute stored ratio or 2) small matrix porosities.

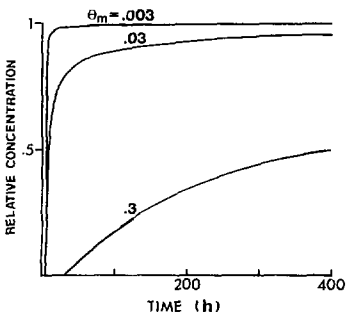

Figure 3 Breakthrough curves at 10 m from injection well approximated with the one dimensional analytical solution for fracture transport and matrix diffusion. θ_m = matrix porosity.

Dispersion in fractured media is a subject of considerable interest at present. It is not clear whether longitudinal dispersion in a single open fracture is an important process; however heterogeneity within a fracture plane can cause considerable uncertainty with respect to velocities and solute travel paths in any tracer test in a single fracture. Anisotropy within a fracture plane can be caused by a number of factors, such as fracture infilling and non-planarity, which can cause the aperture to vary in width and to range from totally open to totally closed. A discussion of dispersion processes in a single fracture and in fractured media is presented by Grisak and Pickens (1980b).

Given the uncertainties regarding the dispersion properties of a fracture, the primary function of a conservative tracer should be to provide verification of the average velocity rather than to quantify dispersion parameters. The velocity calculated from pressure testing results requires confirmation by direct measurement before it can be used in solute transport calculations. Results from radial instrumentation can be compared to velocities calculated from pressure testing results and further compared to injection withdrawal rates and withdrawal phase tracer data at the central well.

Reactive Tracers

Reactive and nonreactive tracers used simultaneously can provide substantial information regarding in situ sorption properties. The experiment presented by Pickens, Jackson and Inch (1980) illustrated that reactive tracers can yield in situ distribution coefficients (K_d's) which are similar to both laboratory column and 'batch' K_d's and K_d's calculated by chronological mapping, over the past 20 years, of a contaminant plume created by the experimental disposal of radioactive wastes in the same aquifer (Jackson and Inch, 1980).

The influence of sorption/desorption kinetics on the reactive tracer breakthrough data are difficult to overcome in tracer tests of relatively short duration. Sorption/desorption kinetics primarily cause increased spreading about the average velocity. For analysis of field tests, sorption kinetics may perhaps be adequately treated as a dispersive mechanism and its effect incorporated into the dispersion term.

REFERENCES

Bear, J., Dynamics of fluids in porous media. American Elsevier Inc., New York, 764 p., 1972.

Carslaw, H.S., and J.C. Jaeger, Conduction of Heat in Solids. 2nd Ed., Oxford University Press, London, 510 p., 1959.

Claassen, H.C., and E.H. Cordes, Two-well recirculating tracer test in fractured carbonate rock, Nevada. Hydrological Science Bull., XX(3), 367-382, 1975.

Grisak, G.E., and J.F. Pickens, An analytical solution for solute transport through fractured media with matrix diffusion. Submitted to Jour. Hydrology, 1980a.

Grisak, G.E., and J.F. Pickens, Solute transport through fractured media: 1. The effect of matrix diffusion. Water Resour. Res., In Press, 1980b.

Grisak, G.E., J.F. Pickens, and J.A. Cherry, Solute Transport through Fractured Media: 2. Column Study of Fractured Till. Water Resour. Res., In Press, 1980.

Grove, D.B., and Beetem, W.A., Porosity and dispersion constant calculations for a fractured carbonate aquifer using the two well tracer method. Water Resour. Res., 7, pp. 128-134, 1971.

Ivanovich, M., and D.B. Smith, Determination of Aquifer Parameters by a Two-Well Pulsed Method using Radioactive Tracers, Jour. Hydrology , 36, 35-45, 1978.

Jackson, R.E., and K.J. Inch, Hydrogeochemical processes affecting the migration of radionuclides in a fluvial sand aquifer at the Chalk River Nuclear Laboratories. National Hydrology Research Institute, Paper No. 7, Inland Waters Directorate Scientific Series No. 104, 58 p., 1980.

Jost, W., Diffusion in Solids, Liquids, Gases, Academic Press, New York, N.Y., Vol. 1 of Physical Chemistry: A Series of Monographs, 532 p., Revised Edition, 1960.

Kreft, A., A. Lenda, B. Turek, A. Zuber, and K. Czauderna, Determination of effective porosities by the two-well pulse method. In: Isotope Techniques in Groundwater Hydrology, IAEA-SM-182/46, pp. 295-312, 1974.

Landström, O., C.E. Klockars, K.E. Holmberg, and S. Westerberg, In situ experiments on nuclide migration in fractured crystalline rocks. Kärn-Bränsle-Sakerhet Teknisk Rapport 110, English Translation, 50 p., 1978.

Mercado, A, The spreading pattern of injected water in a permeability stratified aquifer. In: Int. Assoc. of Scientific Hydrology, Proc. Symp. of Haifa, Publ. No. 72, 23-36, 1967.

Pickens, J.F., R.E. Jackson, and K.J. Inch, Field measurement of distribution coefficients using a radial-injection tracer test. Prepared for submission to Water Resour. Res., July 1980.

ABSTRACT

TESTING LOW TO MODERATELY TRANSMISSIVE ZONES IN BASALT ROCKS

C. D. Updegraff, K. G. Kennedy, A. A. Bakr,
C. N. Culver and J. T. Kam
Science Applications, Inc.
Albuquerque, New Mexico

Nuclear waste disposal studies are providing unique opportunities for development and assessment of different types of borehole testing methods. Recently, we completed a six month field testing program directed at determining the hydrologic characteristics of basalt rock on part of the Hanford Reservation near Richland, Washington. Well testing was conducted principally using instantaneous (pulse or slug) withdrawal or injection, drill stem and airlift pumping tests. Testing in the low to moderately transmissive rocks required up to several days and in some instances weeks to provide a complete test record for adequate evaluation.

Pulse tests, where the response is shut-in, responded quickly to static conditions. They are preferred in zones with transmissivity less than about 10^{-8} ft^2/sec ($\approx 10^{-9} m^2/sec$.). The test's radius of influence is generally limited to a few wellbore diameters. At dual hole sites, no pressure responses were observed at wells 100 feet apart. Pulse tests can be analyzed by 'slug' type curves similar to those by Cooper et al. (1973) and Ramey et al. (1975). More rapid responses may necessitate generation of higher dimensionless storage coefficient curves than are currently published. Pulse test results can be anomalously high or low as wellbore damage can strongly influence these short tests. Testing in tight colonnade/entablature zones will require additional input regarding fracture distribution, orientation and matrix characteristics for proper hydrologic characterization. Slug tests, where fluid movement occurs in the tubing string as a result of flow from or into the formation, is generally non-responsive in formations with transmissivity less than about

10^{-7} ft ^{2}/sec ($\approx 10^{-8}$ m^2/sec). They are useful in moderately transmissive zones up to about 10^{-4} ft^2/sec ($\approx 10^{-3} m^2$/sec). For small storage coefficients, responses can be observed in observation wells and these data are analyzable using existing analytical solutions. Problems associated with these tests are wellbore inertial effects and permeability changes away from the wellbore.

Analysis of the recovery period of airlift, standard downhole pumping tests and drill stem-type tests data can provide the most complete and, in general, the best characterization when testing zones with transmissivities ranging from about 10^{-6} ft^2/sec ($\approx 10^{-7} m^2$/sec) to about 10^{-3} ft^2/sec ($\approx 10^{-4} m^2$/sec). The advantage of recovery tests is that the analysis can be performed adequately even if the wellbore is extensively damaged.

Drill stem-type tests can also be used in low permeability horizons but require extensive flow periods prior to their buildup period. The late time data is critical to these tests and accordingly the formation response should be allowed to return to initial or static conditions. The recovery and drill stem tests also allow evaluation of the wellbore storage effect and wellbore damage in the vicinity of the zone tested. The shape of the response curve also provides insight as to whether the media is responding as a fractured or equivalent porous media.

Tracer test results indicate I-131 can be effectively utilized in further assessment of basalt formation characteristics using a doublet well situation.

MEASUREMENT OF IN-SITU HYDRAULIC CONDUCTIVITY IN THE CRETACEOUS PIERRE SHALE

C. E. Neuzil and J. D. Bredehoeft
U.S. Geological Survey, Reston, Virginia 22092

SUMMARY

A recent study of the hydrology of the Cretaceous Pierre Shale utilized three techniques for measuring the hydraulic conductivity of "tight" materials. Regional hydraulic conductivity was obtained from a hydrodynamic model analysis of the aquifer-aquitard system which includes the Pierre Shale. Laboratory values were obtained from consolidation tests on core samples.

In-situ values of hydraulic conductivity were obtained by using a borehole slug test designed specifically for "tight" formations. The test is conducted by isolating a portion of the borehole with one or two packers, abruptly pressurizing the shut-in portion, and recording the pressure decay with time. The test utilizes the analytical solution for pressure decay as water flows into the surrounding formation. Consistent results were obtained using the test on three successively smaller portions of a borehole in the Pierre Shale.

The in-situ tests and laboratory tests yielded comparable values; the regional hydraulic conductivity was two to three orders of magnitude larger. This suggests that the lower values represent intergranular hydraulic conductivity of the intact shale and the regional values represent secondary permeability due to fractures. Calculations based on fracture flow theory demonstrate that small fractures could account for the observed differences.

INTRODUCTION

Because "tight" rocks such as shales may be used to confine hazardous waste and other materials stored underground, it is important to be able to measure their permeability. Very low permeabilities are difficult to measure and special techniques are required. For significant volumes of rock it is also necessary to consider the possible effects of discontinuities such as fractures which can significantly alter the gross permeability of "tight" rocks.

We have determined the hydraulic conductivity of the Pierre Shale in South Dakota utilizing three techniques. The values obtained are indicative of the hydraulic conductivity on three scales: regional, local, and small (laboratory) scale.

Values were obtained with special in-situ borehole tests at one site; these represent local or near borehole hydraulic conductivity. These tests gave consistent results for successively smaller portions of the borehole. Values for local hydraulic conductivity measured in this manner ranged from 10^{-11} m/s to 7×10^{-13} m/s.

The hydraulic conductivity of core samples retrieved from two boreholes was calculated by analyzing data from one dimensional consolidation tests. The hydraulic conductivity of the core samples measured in this manner depends on the effective stress and ranges from 5×10^{-12} m/s to 2×10^{-14} m/s.

Regional hydraulic conductivity of the Pierre Shale was estimated using a digital ground-water flow model of the aquifer aquitard system of which the Pierre Shale is a part. Regional values obtained in this manner range from about 10^{-11} m/s to 2×10^{-9} m/s.

The hydraulic conductivities measured in situ and in the laboratory are consistent and fall along a fairly distinct trend of decreasing conductivity with increasing effective stress, or depth. Regional conductivities plot distinctly apart from this trend and are some two to three orders of magnitude larger. We believe that the large regional conductivities reflect leakage through fractures or fracture zones in the shale which the boreholes did not penetrate.

Calculations based on fracture flow theory alone cannot indicate the size and spacing of the fractures. However, the range of combinations of fracture size and spacing which explain the conductivity difference can be shown.

In Situ Tests

A borehole located at site "B" in figure 1 was tested using the modified "slug" test of Bredehoeft and Papadopulos.[1] The borehole was drilled to 184 meters depth and approximately 13 centimeters diameter entirely in the Pierre Shale using an air drilling technique. No detectable water flowed into the borehole from the surrounding rock. Water was added to conduct the test.

The test utilizes the solution to the coupled equations of ground-water flow in the surrounding rock and storage in the wellbore. The "slug" is a nearly instantaneous change induced in a closed-in portion of the wellbore which is pressured by water. The volume of the closed-in wellbore is assumed to be constant and the change in storage and head in the wellbore is assumed to be due entirely to the compressibility of the water. This test is designed for low permeability formations.[1] After application of the "slug" the decline in head H in the wellbore is recorded with time and a plot of H/H_o (where H_o is the "slug") versus time is matched with a set of type curves of the solution.

The test set up is shown in figure 2. For redundancy, two separate transducers were used to record the pressure decay. A typical plot of H/H_o versus time matched to the type curve is shown in figure 3. The data for early time do not match the analytical solution well. This probably results from the fact that the "slug" was not truly instantaneous, usually taking approximately 100 seconds to apply.[2] For the purpose of plotting, t_o was chosen as the moment pressurization stopped; however, the flow into the shale commenced at the instant the pressure began to rise. Hence, the true t_o in the sense of an instantaneously applied "slug" is ambiguous, but it would be some time before pressurization ceased. As a result the data points are displaced ahead by the difference (t_o actual - t_o chosen). Because the time scale is logarithmic this effect is seen as a distortion of the data curve only in the early part of the plot.

Three tests were conducted in the borehole. A packer was set at 32 meters and the interval from the packer to the bottom of the hole was tested. Upon completion of the first test the packer was lowered and reset at 64 meters and a portion of the original section was retested. A third test was conducted in the same manner with the packer at 115 meters.

Since successively smaller portions of the original 184 meter section were tested, transmissivities of three separate portions of the borehole could then be calculated. The section of the borehole tested and the measured transmissivities are shown schematically in figure 4. The result is a fairly detailed picture of hydraulic conductivity with depth at this site as measured in situ with the modified "slug" test.

Discussion of In-Situ Tests

The modified "slug" tests are internally consistent; as successively smaller portions of the section were tested, successively smaller transmissivity values were obtained. In addition the calculated conductivity consistently decreases with depth.

The modified "slug" test is not without potential sources of error.[1] Very small volumes of water are pumped into the borehole and allowed to flow out, presumably into the rock. The possibility exists that sufficient leakage occurs through joints and connections in the test apparatus or past the packer to dominate the pressure decay. Leakage past the packer is particularly hard to rule out. However, if leakage occurs the computed conductivity will be higher than the true conductivity of the rock. In that sense the computed values can be viewed as maximum values.

There is evidence that leakage did occur in the system and the calculated conductivities are too high.[3] Inflation of the packer causes a small pressure rise which itself constitutes a "slug" test. In instances where the decay of these small pressure slugs was monitored, it can be seen that their relative decline (drop in H/H_0) is slower than that of the higher pressure slug. This suggests that the higher pressure differences associated with the full slug caused leakage around the packer. The actual conductivity of the rock may be lower than the values calculated.

Another limitation that should be recognized is the small volume of rock involved in the test. Using the solution of the ground-water equation for a semi-infinite strip with step change in head at the boundary an estimate can be gotten for the distance the disturbance will penetrate the rock.[4] For $K = 3 \times 10^{-13}$ m/s, $S_s = 3 \times 10^{-5}$ m^{-1} and $t = 12$ hours which are representative of these tests, discernable changes in pore pressure will have migrated less than one half foot into the rock from the well bore. The distance in the radial case will actually be smaller. Clearly, only a small annulus surrounding the borehole affects the test, and it includes the rock most likely to have been disturbed by drilling.

Laboratory Tests

Consolidation tests were conducted on samples of the core from boreholes at "B" and "C" in figure 1. The tests were conducted by the U.S. Army Corps of Engineers at their soil laboratory in Omaha, Nebraska.

The test consists of applying an instantaneous, uniaxial load to a laterally confined sample. Deformation is recorded as a function of time until the rate of deformation becomes small. The process is repeated with the load doubled for each repetition.

The deformation of the sample with time depends partly on the permeability of the sample.[5] A simple analysis of the time deformation curves from the consolidation tests can be made using Terzaghi's consolidation analysis from which the hydraulic conductivity can be extracted. More sophisticated analyses, such as the viscoelastic theory of Gibson and Lo may also be applied.[6] When the analysis of Gibson and Lo was applied to consolidation data for the Pierre Shale the hydraulic conductivity calculated differed from that calculated with Terzaghi's analysis by only a few percent. Therefore, the values obtained with the simpler theory of Terzaghi were used.

Since incremental loads are applied to the sample during testing it is possible to obtain values of hydraulic conductivity for a range of effective stress for each sample. The effective stress can be converted to an approximately equivalent depth by assuming near hydrostatic conditions. Hydraulic conductivity was calculated for effective stress loads ranging from 5×10^5 to 2.3×10^7 Pa which may be expected at depths of 50 to 2300 meters.

The hydraulic conductivities calculated in this manner define a fairly distinct trend decreasing with depth (see figure 7).

Hydraulic Conductivity of Shale Estimated with Regional Ground-Water Flow Model

The Pierre and other Cretaceous shales confine three major and several minor aquifers in South Dakota (figures 5 and 6). The aquifers and aquitards interact and together form a ground-water flow system. Primarily lateral flow takes place in the aquifers and vertical leakage through the confining beds.

Relatively complete data on hydraulic heads and transmissivity in aquifers, particularly the Dakota Sandstone, are available for South Dakota. By adjusting the vertical hydraulic conductivity in the confining layers, including the Pierre Shale, good agreement between calculated and observed hydraulic heads can be obtained.

For this study a numerical model of the major aquifers and based on earlier model studies was used.[7] A numerical model of the shales and minor aquifers above the Dakota Sandstone was also used.[7]

From these model simulations estimates of regional vertical conductivity in the confining layer above the Dakota Sandstone (here called the "Dakota confining layer") as a whole, and in each of the shales individually was obtained.

COMPARISON OF RESULTS

Results of the in-situ and laboratory tests and the model simulations are compared in figure 7. In figure 7 the abcissa represents the hydraulic conductivity and the ordinate represents depth or the equivalent effective stress. In-situ tests are plotted at the mean depth of the test section. Consolidation test results are plotted at the mean value of two successive load increments. The regional values are plotted at the arithmetic mean depth of the formation in the area modeled.

As seen in figure 7 the in-situ and laboratory tests fall along a single fairly well defined trend of decreasing conductivity with depth. The regional values for the shales also decrease with depth but at similar depths the regional conductivities are two to three orders of magnitude larger than the local conductivities.

These results lead to the conclusion that leakage through the shales on a regional scale occurs largely along pathways which are more conductive than the intact shale. It is hypothesized that the larger regional conductivities result from connecting fractures in the shales.

Fracture Leakage in the Shales

Throughgoing fractures can drastically affect the permeability of "tight" rocks. Fracture flow is usually approximated with the parallel plate analogy wherein flow is related to the fracture aperture as

$$Q_f = \frac{\gamma}{12\mu} Lb^3 J$$

where

- Q_f is the fracture flow (L^3/T)
- J is the hydraulic gradient (dimensionless)
- L is the length of the fracture normal to flow (L)
- μ is the dynamic voscosity (M/LT)
- γ is the specific weight of water (M^2/T^2L^2)
- b is the fracture aperture.

Although the parallel plate analogy only approximates the more complex flow in uneven walled fractures it can indicate the approximate range of fracture apertures and densities which can account for the observed differences in measured conductivity.[7]

If fractures in the shale are assumed to be vertical and parallel their average spacing as a function of aperture can be calculated for the Cretaceous shales based on the difference between the regional and local conductivity values. The results of these calculations are depicted in figure 8. From figure 8 it can be seen that small fractures, even relatively widely spaced, can cause the observed higher regional conductivities.

REFERENCES

1. Bredehoeft, J. D., and Papadopulos, S. S., 1980, A method for determining the hydraulic properties of tight formations: Water Resources Research, v. 16, p. 233-238.
2. Papadopulos, S. S., U.S. Geol. Survey, oral communication, 1979.
3. Papadopulos, S. S., U.S. Geol. Survey, oral communication, 1978.
4. Bredehoeft, J. D., and Hanshaw, B. B., 1968, On the maintenance of anomalous fluid pressures, I. Thick sedimentary sequences: Geol. Soc. America Bull., v. 79, p. 1097-1106.
5. Lambe, T. W., and Whitman, R. V., 1969, Soil Mechanics: New York, John Wiley, 553 p.
6. Gibson, R. E., and Lo, K. Y., 1961, A theory of consolidation for soils exhibiting secondary compression: Norwegian Geotechnical Institute, Publication No. 41.
7. Neuzil, C. E., 1980, Fracture leakage in the Cretaceous Pierre Shale and its significance for underground waste disposal: Ph.D. thesis, Johns Hopkins University, 150 p.

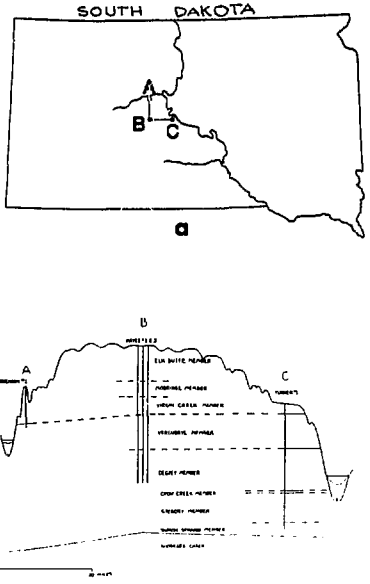

Figure 1. Boreholes drilled in the Pierre shale for this study. a) location map for borehole sites A, B, C. b) cross section showing boreholes in relation to topography and Pierre shale stratigraphy.

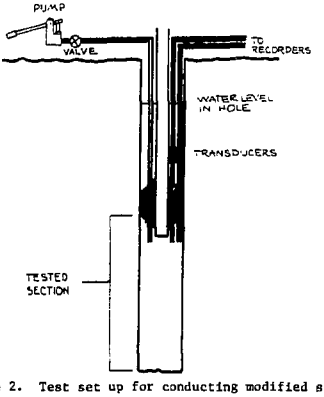

Figure 2. Test set up for conducting modified slug test.

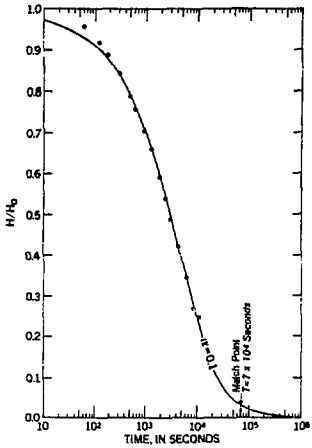

Figure 3. Pressure decay curve and type curve match for typical modified slug test in Pierre shale.

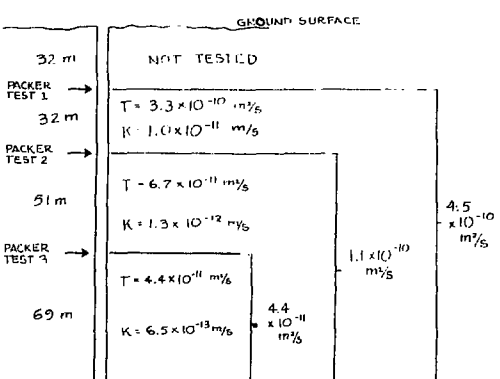

Figure 4. Results of modified slug tests in borehole at site "B."

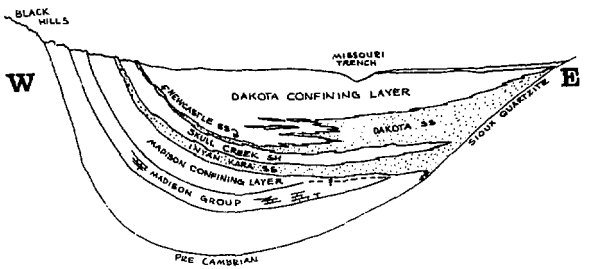

Figure 5. Schematic of major aquifers and aquitards in South Dakota (vertical dimension greatly exaggerated).

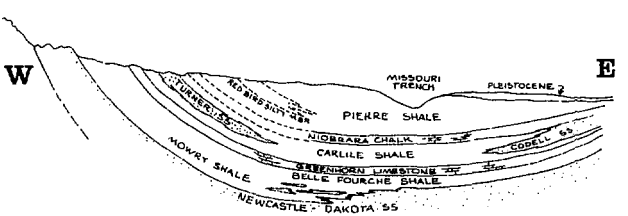

Figure 6. Schematic of aquifers and aquitards overlying the Dakota aquifer (vertical dimension greatly exaggerated).

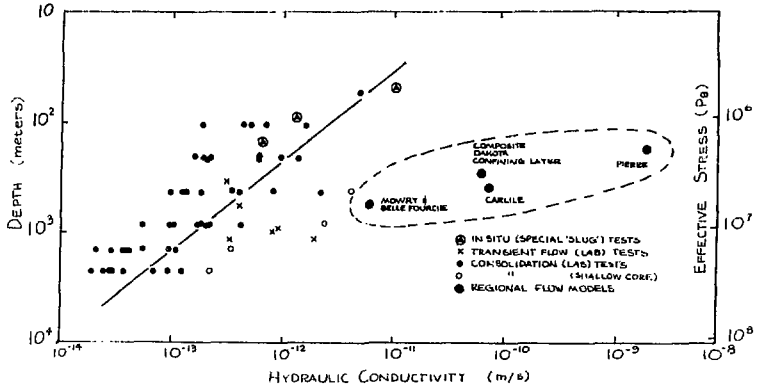

Figure 7. Comparison of regional, local, and laboratory hydraulic conductivities obtained in this study.

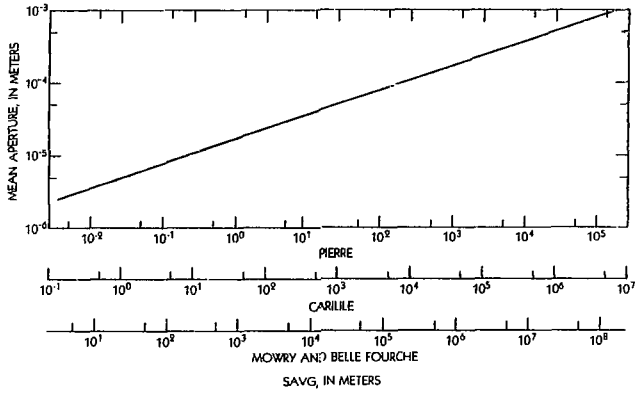

Figure 8. Range of S_{AVG} (average spacing), as a function of mean aperture of fractures for the shales of the Dakota confining layer.

ANALYSIS OF PUMPING TESTS PERFORMED IN A HORIZONTAL RECTANGULAR FRACTURE

D. THIERY
Bureau de Recherches Géologiques et Minières
Orléans - FRANCE

ABSTRACT

The analytical solution has been derived for a constant rate uniform flux pumping test in a single horizontal rectangular fracture. The solution is given for the drawdown at the pumped well and at an observation well inside or outside the fracture. A set of type curves which depend on two dimensionless parameters has been drawn. These type curves give the dimensionless drawdown at the pumped well versus the dimensionless time according to the shape factor of the fracture and the dimensionless aquifer thickness. Another set gives the average drawdown along the vertical at an observation well versus dimensionless time depending on the dimensionless distance and the shape factor.

For both the drawdown at the pumped well and at an observation well the solution has also been studied for early times and long times in order to derive approximative solutions which are compared to the well known solutions in isotropic aquifers.

1. INTRODUCTION

This paper presents results which have been obtained during the research contract n° 563-78 EGF for the Commission des Communautés Européennes. These results are described in detail , in French, in BERTRAND L., FEUGA B., NOYER M.L., THIERY D. 1980[1].

A review of the litterature has shown that analytical solutions have been derived to determine the unsteady state pressure distribution created by a well with a single flat fracture.

The available solutions are the following :

- a vertical finite length fracture (Gringarten et al, 1974)[2]
- a horizontal finite radius circular fracture (Gringarten et al,1974)[3]
- an inclined fracture (Cinco et al,1975)[4]
- a vertical fracture partial penetration (Raghavan et al,1976)[5]

For all these schemes (except the vertical fracture) only the pressure at the pumped well has been computed.

These schemes are interesting but they are not always adapted to real fractures mainly because of anisotropy of permeability in the horizontal directions.

A horizontal fracture is more likely to be elliptical than circular. In order to analyse drawdowns in such a fracture we derived analytical solutions for a pumping (or injection) test in a rectangular fracture which is a closer approximation to an elliptical fracture.

The drawdown has been calculated at the center of the fracture but also at an observation well.

2. DESCRIPTION OF THE SYSTEM

The geometry of the system is defined as follow :

the aquifer has an infinite lateral extension; its characteristics are :

- constant thickness h
- constant storage coefficient S

  (specific storage coefficient $S_s = S/h$)
- anisotropic permeability : Kx, Ky, Kz

The fracture , which is situated in the middle of the aquifer, has a rectangular shape with :

- a length 2 xf
- a width 2 yf
- a negligible thickness

3. BOUNDARY CONDITION INSIDE THE FRACTURE

Two types of boundary conditions may be set inside the fracture :

- an infinite conductivity fracture
- a uniform flux fracture.

a) An infinite conductivity fracture

It is a fracture which has an equivalent hydraulic conductivity (or permeability) much higher than the conductivity of the surrounding formation. As a matter of fact its transmissivity (K.h product) is much higher then the rock transmissivity This condition is usually met in thick fractures in a low permeability formation. The head gradient in an infinite conductivity fracture is equal to zero.

b) A uniform flux fracture

The discharge from the aquifer to the fracture is performed at a uniform rate per unit area of fracture.

This boundary condition is probably not exactly fulfilled but, as will be shown later, it is a close approximation of the infinite conductivity boundary condition.

The uniform flux boundary condition is very interesting because it makes it possible to compute the drawdowns analytically by the "source functions method" . This method has been described by(GRINGARTEN A.C. and RAMEY H.J. 1973)[6].

The source function associated to the rectangular fracture is obtained as the product of 3 elementary source functions as shown below.

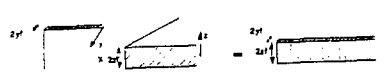

The product is then simplified considering that the thickness zf of the fracture is negligible compared to the thickness h of the aquifer.

c) Dimensionless notations

The following dimensionless variables are used :

- coordinates :

  $x_D = x/xf$

  $y_D = y/yf$

  $z_D = z/h$

- drawdown

  $s_D = 4\pi Ts/Q$ with $T = h\sqrt{KxKy}$ = transmissivity

- geometry factors

  $F = (xf/yf)\sqrt{K_y/K_x}$ (shape factor)

  $h_D = (h/\sqrt{x_f y_f}).\sqrt{K/Kz}$ (dimensionless thickness of the aquifer)

- time

  $t_{DF} = \pi Tt/x_f y_f S$ (relative to the fracture area)

  $t_{DX} = 4 K_x ht/x^2 S$ (relative to the distance to the center of the fracture).

Nota : All these notations are consistent with Theis's notations.

The shape factor F is the ratio of the length of the fracture to its width (corrected by the horizontal anisotropy factor)

For an horizontally isotropic aquifer :

F = 1 applies to a square fracture (it is the shape which is the closest to the circular fracture)

F = 10 applies to a rectangular fracture with a length equal to 10 times its width.

The dimensionless thickness h_D is the ratio of the aquifer width to the fracture extension (corrected by the vertical anisotropy factor) .The fracture extension is the geometrical mean of its length and its width.

For a fully isotropic aquifer :

$h_D = 0.1$ applies to a fracture with an extension equal to 10 times the thickness of the aquifer

$h_D = 10$ applies to an aquifer of thickness equal to 10 times the extension of the fracture.

4. DRAWDOWN AT THE CENTER OF THE FRACTURE

The drawdown at the center of the fracture is given by the following expressions which are easy to compute numerically :

$$s_D = \int_0^{t_{DF}} \operatorname{erf}\sqrt{\frac{\pi F}{4\tau}} \cdot \operatorname{erf}\sqrt{\frac{\pi}{4F\tau}}\, x \quad \ldots$$

$$\ldots \left[1+2\sum_{p=1}^{\infty} \exp\left(-\frac{4\pi p^2 \tau}{h_D^2}\right)\right] d\tau \qquad (1)$$

or :

$$s_D = \int_0^{t_{DF}} \operatorname{erf}\sqrt{\frac{\pi F}{4\tau}} \cdot \operatorname{erf}\sqrt{\frac{\pi}{4F\tau}} \cdot \frac{h_D}{2\sqrt{\tau}} * \ldots$$

$$\ldots \left[1+2\sum_{p=1}^{\infty} \exp\left(-\frac{\pi p^2 h_D^2}{4\tau}\right)\right] d\tau \qquad (2)$$

Expression (1) is easier to compute for late values of dimensionless time and expression (2) for early values.

The calculations have been performed for the following values of the geometry factors :

h_D = 0.1, 0.5, 1, 1.5, 2, 5, 10, 50.

and :

F = 1, 2, 5, 10, 50 which corresponds also to 1, 0.5, 0.2, 0.1, 0.02 .

Two kinds of type curves have been drawn :

- type curves for constant shape factor F (see graph 1)

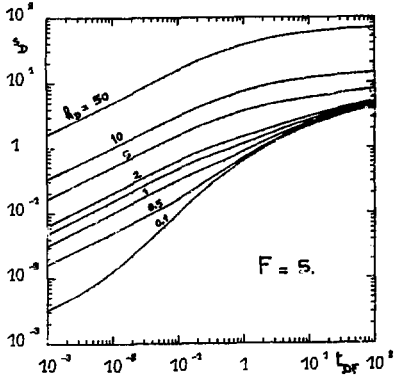

Graph 1 - Drawdown at the center of a horizontal rectangular fracture

- type curves for constant dimensionless thickness h_D (see graph 2)

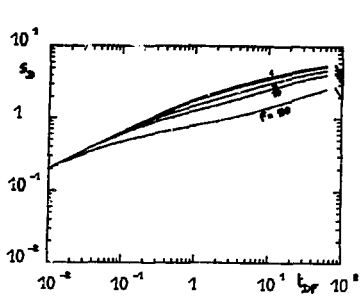

Graph 2 - Drawdown at the center of a horizontal rectangular fracture

For early dimensionless times the curves show a typical "one half slope" of equation :

$$s_D = h_D \sqrt{t_{DF}} \qquad (3)$$

This equation corresponds to a vertical flow from the formation to the fracture. It does not depend on the shape factor F because there is no flow in the horizontal directions.

For late dimensionless times the drawdown is a linear function of the logarithm of the time according to the following equation :

$$s_D = s_{DO} + L_n \frac{t_{DF}}{t_{DFO}} \qquad (4)$$

(s_{DO} is the drawdown at time t_{DFO})

This equation shows that, after a time t_{DFO} the variation of the drawdown does not depend on the geometrical factors F and h_D any more.

It is a radial flow which agrees with JACOB's approximation. The drawdown variation is plotted as a straight line on semi-logarithmic paper but Theis curve can not be recognized on log-log paper because of the constant s_{DO}

Equation (4) is valid after the following dimensionless times t_{DF} corresponding to a maximum error of 10% :

F \ h_D	0.1	1	10	100
1	5.2	5.2	23.8	2384
2	6.5	6.5	23.8	2384
5	13.6	13.6	23.8	2384
10	26.4	26.4	30	2384
50	131	131	131	2384

Equations (1) and (2) refer to the center of the fracture, but as a matter of fact, it is a close approximation of the drawdown at any location inside the fracture, because as it will be shown later the drawdown inside the fracture is nearly equal everywhere.

5. DRAWDOWN AT AN OBSERVATION WELL

A difficulty arises because the drawdown field is 3 dimensionnal : the drawdown is different at each altitude of an observation well. This difficulty has been solved considering a small diameter observation well with perforations along the whole aquifer thickness. The drawdown measured by such an observation well is the average of the drawdown along the vertical direction. This average , which has been computed analytically does not depend on the dimensionless thickness h_D.

The average drawdown at an observation well situated along the ox axis is given by the following expression :

$$s_D = \frac{3}{4} F x_D^2 \int_0^{t_{DX}} \frac{1}{2}\left[\operatorname{erf}\frac{\frac{1}{x_D}+1}{\sqrt{\tau}} + \operatorname{erf}\frac{\frac{1}{x_D}-1}{\sqrt{\tau}}\right] \cdot \operatorname{erf}\frac{1}{x_D F\sqrt{\tau}}\, d\tau \qquad 5)$$

The drawdown at an observation well situated along the oy axis is given by the same expression after replacing F by 1/F.

Expression (5) has been calculated numerically for the following values of the parameters :

x_D = 1, 1.1, 1.2, 1.3, 1.4, 1.5, 2, 3, 10

F = 0.1, 0.5, 1, 2, 5, 10, 50

Two examples of type curves are drawn on graph 3 and 4. They show that for $F \geq 1$ (observation wells situated along the ox axis), the curves are very close to Theis's solution ($x_D = \infty$) as soon as $x_D \geq 2$ even for early dimensionless times. For late dimensionless times the flow is radial and is described by equation (4) following JACOB'S approximation .

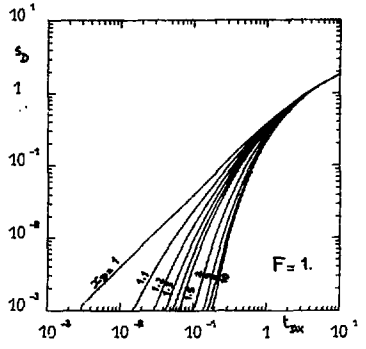

Graph 3 - Drawdown at an observation well (horizontal rectangular fracture)

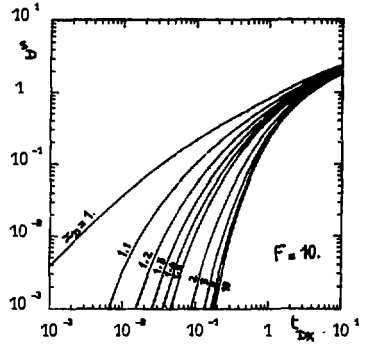

Graph 4 - Drawdown at an observation well (horizontal rectangular fracture)

Equation (4) is valid after the following dimensionless times corresponding to a maximum error of 10 %

x_D \ F	1	2	5	10
1	16.7	14.2	13.5	13.4
2	11.7	11.0	10.9	10.8
5	10.3	10.2	10.1	10.1
10	10.1	10.	10.	10.

It appears that JACOB'S approximation applies as soon as the dimensionless time is greater than about 10 (as in a pumping test without any fracture, excepted for $x_D = 1$, i.e., at the contact of the fracture, where this minimal time is increased to 13 to 17.

6. DRAWDOWN AT AN OBSERVATION WELL IN CONTACT WITH THE FRACTURE

The average of the drawdown along the vertical has been computed because it doesn't depend on h_D any more. The calculations have been performed for various dimensionless times.

For early dimensionless times the drawdown is given by the following equations :

$$\begin{cases} s_D = t_{DF} & D \ll x_D < 1 \\ s_D = \dfrac{t_{DF}}{2} & x_D = 1 \end{cases} \qquad (6) \quad (7)$$

The initial drawdown averaged along the vertical is linear with time ; it is represented by a straight line of slope 1 in log-log coordinates.

Equations (6) and (7) are valid, with a maximum error of 10% , before the following value of dimensionless time is reached :

$$t_{DF} < 1/F \qquad (8)$$

expression (8) shows that the linear drawdown is observed during a longer time when the shape factor is smaller i.e. when the shape of the fracture is closer to a square.

For late dimensionless times the variation of the drawdown is given by equation (4) . This equation , which describes JACOB's approximation, is valid as soon as the following dimensionless time is reached

F \ x_D	0	0.2	0.6	1
1	5.2	5.6	8.1	13.1
2	6.5	7.2	12.2	22.3
5	12.6	15.2	27.8	53
10	26.4	29.6	54.7	105
50	131	147	272	524

It appears that JACOB'S approximations is valid only after a long dimensionless time (greater than 100) for very rectangular fractures i.e. fractures with a large F shape factor. The drawdown inside the fracture has been drawn for different dimensionless times on graph 5. This graph shows that the drawdown is approximatively constant inside the fracture. It means that the equivalent transmissivity of the fracture is very high.

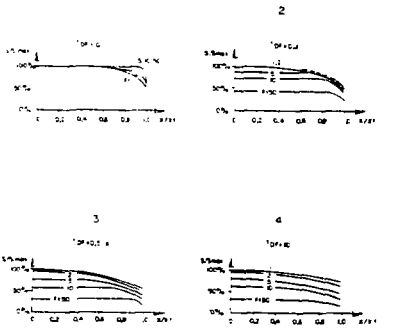

Graph 5 - Drawdown inside a horizontal rectangular fracture (average along the aquifer width)

The drawdown corresponding to a pumping test performed in a infinite transmissivity horizontal rectangular fracture is then closely approximated by the formula that we have derived for a uniform flux horizontal rectangular fracture.

7. CONCLUSION

A new scheme has been derived for pumping tests in fractured aquifers. This scheme is characterized by a single horizontal flat rectangular fracture.

The drawdown has been computed at the center of the fracture and also at an observation well situated along the principal directions. Types curves have been drawn which makes it possible to perform pumping test analysis or to compute the drawdown corresponding to a known rectangular fracture.

NOTATIONS

x, y, z } coordinates relative to the center of the fracture

x_D, y_D, z_D } Dimensionless coordinate

xf } Fracture half length

yf } half width

t = Time

τ = Dummy variable representing time

t_{DX}, t_{DF} } Dimensionless time

h = Aquifer thickness

h_D = Aquifer dimensionless thickness

Q = Pumped or injected discharge

s = Drawdown (or head difference)

s_D = Dimensionless drawdown

K_x, K_y, K_z } Permeability (hydraulic conductivity)

$K\sqrt{Kx\ Ky}$ = Horizontal permeability

T = Horizontal transmissivity (K.h product)

S = Storage coefficient

S_s = Specific storage coefficient = S/h

F = Fracture geometry factor

π = 3.14159 ...

erf= Error function

exp= Exponential function

REFERENCES

1. BERTRAND (L.), FEUGA (B.), NOYER (M.L.), THIERY (D.). - 1980 - Roches chaudes haute température ("Hot Dry Rocks") Contribution à la méthodologie de la détermination des caractéristiques hydrauliques des milieux rocheux fracturés naturellement ou artificiellement - Commission des Communautés Européennes - Contrat n° 563-78 EGF (rapport BRGM 80 SGN 029 GEG).

2. GRINGARTEN (A.C.), RAMEY (H.J.). 1974 - Unsteady state pressure distribution created by a well with a single infinite conductivity vertical fracture . - Soc. Pet. Eng. J. (Aug. 74)

3. GRINGARTEN (A.C.), RAMEY (H.J.). - 1974 - Unsteady state pressure distribution created by a well with a single horizontal fracture, partial penetration or restricted entry. - Society of petroleum engineers journal - (August 74)

4. CINCO, RAMEY (H.J.), MILLER . - 1975 - Unsteady state pressure distribution created by a well with an inclined fracture. Paper SPE 5591 presented at SPE AIME 50th. Annual fall technical conference and exhibition - (Dallas, Sept-Oct. 1975).

5. RAGHAVAN (R.), URAIET (A.), THOMAS (G.W.). 1976 Vertical fracture height effect on transient flow behavior. Paper SPE 6016 presented at the SPE AIME 51th. Annual fall technical conference and exhibition (New-Orléans, Oct. 1976).

6. GRINGARTEN (A.C.), RAMEY (H.J.). - 1973 - The use of source and Green's functions in solving unsteady flow problems in reservoirs - Soc. Pet. Eng. J. (Oct. 1973).

THERMAL EFFECTS IN WELLTESTS OF FRACTURED RESERVOIRS

G.S. Bodvarsson & C.F. Tsang
Lawrence Berkeley Laboratory
Berkeley, California

Introduction

Conventional well test analysis methods are usually based upon assumptions of isothermal fluid flow in homogeneous porous media reservoirs. Some solutions are also available for wells intercepted by single vertical or horizontal fractures (e.g., Cinco Ley et al.,(1978), Gringarten (1971), Streltsova-Adams (1978)) or by highly symmetrical fracture systems (e.g., Warren and Root (1963), Kazemi (1969)), but again they are limited to isothermal conditions. In geothermal reservoirs, considerable natural temperature gradients can occur and it is questionable if isothermal well test analysis techniques can be applied to such systems. Furthermore, reinjection of wastewater into geothermal reservoirs creates areal temperature distribution within the reservoir.

Injection testing of geothermal reservoirs is currently being used at a number of geothermal fields (e.g., Krafla, Iceland; Olkaria, Kenya; Los Azufres, Mexico; Wairakei, New Zealand), and a theoretical basis for the analysis of such non-isothermal tests is greatly needed.

In this paper, a numerical simulator is used to study two basic problems. The first problem involves the analysis of injection tests of homogeneous porous media geothermal reservoirs. Due to the dependence of viscosity and density of water on temperature, the pressure response at injection wells will be considerably different from the pressure transient resulting from a conventional (isothermal) pumping test.

The second part of this paper deals with the problem of wastewater injection into a fractured geothermal reservoir. It is commonly believed that when fractures are present, the injected cold water will rapidly advance along the fractures to wells in the production region. If true, this may cause a drastic reduction in the amount of energy which could be extracted from the geothermal resource. Using a simple reservoir model with a few major fractures,we have studied the movement of the thermal front in the fracture relative to its movement in the porous media during injection.

Numerical Model Used

For this study the 3-dimensional simulator CCC (Conduction-Convection-Consolidation), developed at Lawrence Berkeley Laboratory, was used. This computer code solves numerically the heat and mass flow equations for a fully saturated medium. It employs the Integrated Finite Difference Method (IFDM) in discretizing the saturated medium and for formulating the governing equations (Edwards, 1972, Narasimhan, 1975). The set of non-linear equations that arises at each timestep is solved by an iterative scheme and an efficient sparse solver (Duff, 1977). Details of the model are given by Lippmann et al., (1977), and Bodvarsson et al., (1979).

The numerical model has been extensively tested against analytical solutions for mass and heat flow. It has generally given results (Bodvarsson et al., 1980) that compare very well with values given by analytical solutions. Furthermore, the code has been validated against field experiments for underground storage of hot water (Tsang et al., 1979). In recent years the model has been used successfully in studies of problems in geothermal reservoir engineering, well testing, aquifer thermal energy storage, and radioactive waste isolation.

INJECTION TESTING OF WATER-DOMINATED POROUS-MEDIUM GEOTHERMAL RESERVOIRS

During injection tests, water of a lower temperature than the reservoir water is injected into the geothermal aquifer. A temperature variation will develop in the reservoir, with colder water close to the injection well and hotter reservoir water farther away. This in turn creates differences in density and viscosity of the fluid within the reservoir. In our numerical model the dependence of viscosity and density of the fluid on temperature is fully taken care of.

Problem and Approach

The problem considered is that of an injection well fully penetrating a horizontal homogeneous isotropic geothermal reservoir. The injected water is at a temperature of 100°C, but the reservoir contains single phase water at a temperature of 300°C. Actually, as will be seen later, the results obtained are valid for any temperature if appropriate correction factors are used.

In the numerical simulation a radial mesh (concentric circles) is used, with fine elements close to the well covering the region with temperature variations. Farther away from the well, the mesh is made to increase logarithmically. The reservoir is modeled as a single layer, and thus buoyancy forces are neglected. Figure 1 shows a schematic picture of the model used, and the parameters used in the simulation are given in Table 1.

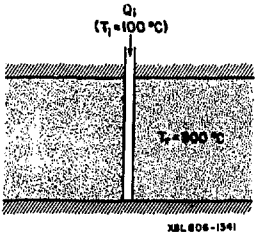

Figure 1. Model used in the study of injection into a porous media geothermal reservoir.

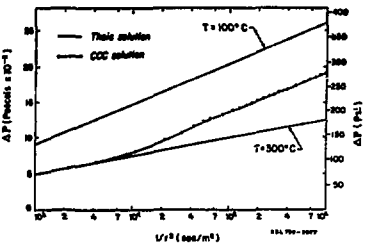

Figure 2. Pressure behavior at an observation well (r = 2.5 m) during cold water (100°C) injection into a 300°C geothermal reservoir.

Table 1. Parameters used in the study of injection testing of porous geothermal reservoirs.

Flow rate (kg/s):	.200
Reservoir thickness (m):	$1x10^{-3}$
Permeability (m^2):	$1x10^{-10}$
Thermal conductivity (Joules/m.sec.°C):	2.00
Density of solids (kg/m^3):	2650
Specific heat of solids (joules/kg.°C):	1000
Porosity (-):	.40
Specific heat of fluid (Joules/kg.°C):	4200
Injection temperature (°C)	100
Reservoir temperature (°C)	300

Injection Tests

When 100°C water is injected into a hot (300°C) porous reservoir, initially at equilibrium, the pressure behavior shown in Figure 2 will result. At early times the pressure at the injection well will follow the Theis solution for the hot reservoir (300°C), but at later times, following a transition period, the pressure will follow a line that is parallel to the Theis solution for 100°C water. This behavior is caused by the differences in density and viscosity of the injected water and the reservoir water. Tsang and Tsang (1978) solved this problem analytically using the Boltzmann transformation and by approximating the parameter k/μ as a Fermi-Dirac function of r^2/t. Mangold et al., (1979) used a numerical simulator to study the pressure behavior at a production well located in a hot spot; i.e., the well is completed in a localized geothermal hot region with colder water further away from the well.

Figure 3 shows how varying the permeability and the storativity of the rock matrix affects the pressure behavior at the injection well. When the transmissivity and the permeability of the rock matrix are kept constant but the storativity changed, the curves are just shifted along the time axis as predicted by the Theis solution. However, when the permeability is varied with the other two parameters kept constant, the time of deviation from the 300°C Theis curve changes. This is consistent with the results by Tsang and Tsang (1978) which found that the deviation time is dependent on the reservoir thickness (h) as well as other parameters such as the flowrate and the reservoir and fluid heat capacities.

Injection - Rest - Injection Test

Figure 4 shows the results when initially there is a circular region of cold water (cold spot) around the well. The type of presure response shown in Figure 4 should result when injection tests are performed soon after drilling is completed and the well has not been allowed to heat up. This kind of well test procedure is commonly used in geothermal fields (Krafla, Iceland; Olkaria, Kenya, etc.). The figure shows that at early times the pressure follows the 100°C Theis curve, and then after some time, which depends upon the radius of the cold spot, the pressure increases along a line parallel to the 300°C Theis curve. At still later time another transition occurs and the pressure again starts increasint at a rate corresponding to the 100°C Theis curve solution. These results indicate that using an injection-rest-injection well test procedure, the radius of the cold spot generated by the first injection may be determined. This may in turn allow the porosity to be approximated from equation 1, if the heat capacities of the reservoir solids and the water can be estimated.

$$\frac{v_T}{v_H} = \frac{\phi \rho_w C_w}{\rho_A C_A} \qquad (1)$$

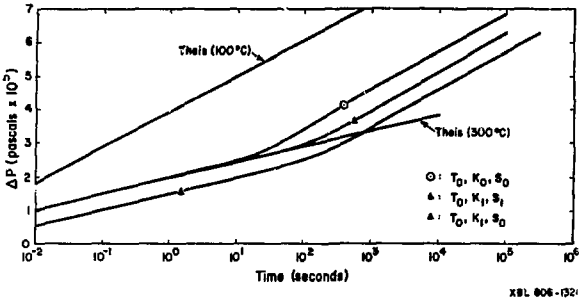

Figure 3. Transient injection pressure behavior, when 100°C water is injected into a 300°C reservoir, for different values of transmissivity and storativity of the reservoir.

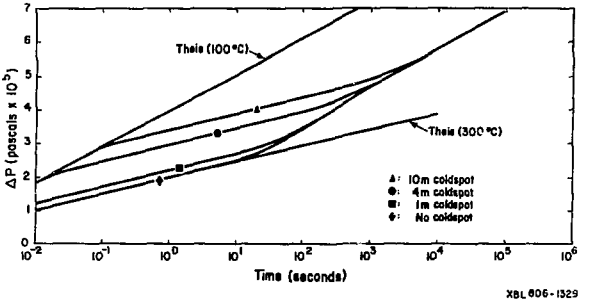

Figure 4. Injection pressure behavior, when 100°C water is injected into a well located in a cold-spot (lower temperature region).

In equation 1 the symbols used denote the following:

v_T : velocity of the thermal front

v_H : velocity of the hydrodynamic front

ϕ : porosity of the formation

ρ_w : density of the reservoir fluids

C_w : heat capacity of the reservoir fluids

$\rho_a C_a$: integrated reservoir mass heat capacity

where $\rho_a C_a = \phi \rho_w C_w + (1-\phi) \rho_s C_s$, and ρ_s is the density of the reservoir solids and C_s is the heat capacity of the reservoir solids.

Injection - Falloff Test

At the time when injection has just been terminated there is a pressure as well as a temperature gradient within the geothermal reservoir (Figure 5). If at this time a falloff test is performed, the pressure response shown in Figure 6 would result. The pressure will initially decline

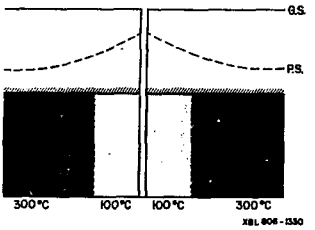

Figure 5. Schematic diagram showing reservoir conditions immediately after injection.

at a rate corresponding to the 100°C Theis solution, but later a change in slope will occur and the 300°C Theis curve will be followed. These results are consistent with those obtained by Mangold et al., (1979).

Injection - Production Test

A case was studied where production immediately followed an injection period (that is, with reservoir initial conditions as shown in Figure 5). The calculated pressure behavior in the well is shown in Figure 7. It is characterized by three distinct straight lines. At first the pressure decreases at a rate that corresponds to twice the rate given by the Theis solution for 100°C water. Later on the pressure decrease follows a slope that equals two times the slope given by Theis solution for 300°C water. The obvious reason for the doubled pressure decrease in comparison with the Theis solution is that two independent forces control the drawdown: the constant withdrawal rate and the initial pressure falloff condition in the reservoir.

After the two double slopes, a transition occurs, after which the pressure starts declining at a rate corresponding to the Theis solution for 300°C water. During the transition, the pressure in the well actually increases, probably because of rapid changes in the viscosity of the water. As shown in Figure 7, the temperature of the produced water changes from 100°C to 300°C during the transition implying a more than threefold decrease in the viscosity of the water.

Discussion

Data from injection tests of porous media geothermal reservoirs show several linear segments in a pressure-log time plot. This behavior is due to the dependence of fluid density and viscosity on temperature. Our results indicate that when an injection-rest-injection procedure is employed, the radius of the cold spot resulting from the first injection period may be determined. Consequently an estimate of the effective porosity of the reservoir can be obtained.

An injection - production test may be advantageous because larger pressure changes can be observed (2 times the rate predicted by the Theis solution). An observation of three different linear segments in the data may also lead to a better determination of the reservoir parameters. It must be noted, however, that other factors may cause a

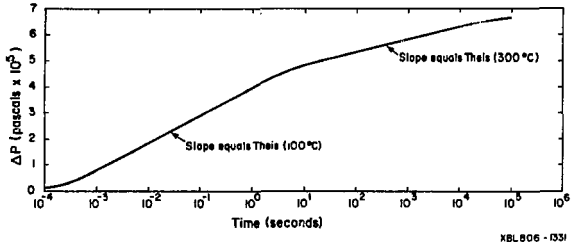

Figure 6. Pressure falloff after 1.2 days of injection.

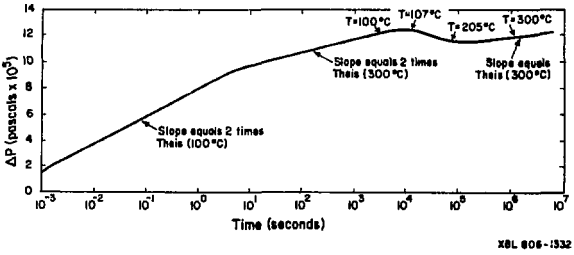

Figure 7. Pressure transient behavior during a production test, immediately following 1.2 days of injection.

similar break in the slope in the data shown in Figures 2-7; e.g., boundaries, as well as permeability variation within the reservoir. One must therefore be quite careful when analyzing injection test data. Accurate knowledge of the temperature of the injected water and the reservoir fluids is essential for accurate determination of the reservoir hydraulic parameters.

INJECTION INTO A FRACTURED GEOTHERMAL RESERVOIR

The objective of the following sections of this paper is to study the movement of the thermal front in horizontal fractures relative to its movement through the porous media matrix when cold water is injected into a fractured water-dominated geothermal reservoir. To date, little work has focused on problems involving non-isothermal flow through fractured media, although some initial studies have been done, including Romm 1966; Bodvarsson, 1969; Kasameyer and Schroeder, 1976; and O'Neill, 1978. Our present calculations can be considered as a first step to model and study the influence of fractures on the time of cold water breakthrough at the production region, when reinjection is used.

Problem and Approach

The problem considered involves an injection well fully penetrating a reservoir with a number of evenly spaced infinite horizontal fractures (Figure 8). The temperature of the injected water is 100°C, while the temperature of the reservoir water is 300°C. Again, we assume gravity effects to be negligible, and therefore due to symmetry only half of the basic section shown in Figure 8 needs to be modeled. This section consists of half of the fracture and half of the rock matrix associated with each fracture (note that the fractures are assumed evenly spaced).

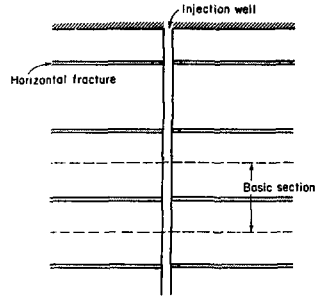

Figure 8. Model used in study of injection into a fractured geothermal reservoir.

The mesh used for this study consists of 144 elements in the horizontal direction, with elements that are fine close to the well and logarithmically increasing in size away from the well. In the vertical direction, 6 layers are used, with fine elements close to the fracture but larger elements away from the fracture. In the study an 8 in. diameter well is used, and two alternative fracture spacings of 5 or 10 meters. Values of other parameters used in the numerical simulations are given in Table 2.

The cases studied can be subdivided into 3 basic categories as shown below:

1. Injection into a fracture in an impermeable formation
2. Injection into a fracture in a permeable formation
3. Injection into a well connected to both the fracture and permeable formation

The following section will describe each of these cases and the primary results obtained.

Injection into a Fracture in an Impermeable Formation

Water at 100°C is injected into the fracture (Figure 9) and the effect of heat conduction on the movement of the thermal front is studied. Figure 10 shows the importance of thermal conduction between the fracture and the rock matrix in relation to the movement of the thermal front within the fracture. After only 1.2 days of injection the thermal front has advanced over 80 meters when no conduction is allowed between the fracture and the rock matrix, but only about 8 meters when a thermal conductivity of .1 Joules/m.sec.°C is used. On the average the thermal conductivity of rock-water mixtures is about 2.0 Joules/m.sec.°C. In this simulation a thermal conductivity of .65 Joules/m.sec.°C is used for the fracture elements, and this causes the diffusion of the thermal front shown in Figure 10.

Table 2. Parameters used in the study of injection into a fractured geothermal reservoir.

Rock Matrix		Fracture
Thermal conductivity (J/m.sec.°C):	.1-5.0	0.65
Heat capacity of fluid (J/kg.°C):	4200	4200
Heat capacity of solids (J/kg.°C):	1000	1000
Density of solids (kg/m^3):	2650	2650
Permeability (m^2):	$0-1x10^{-13}$	$1x10^{-10}$
Specific storage (m^{-1}):	$5x10^{-5}$	$5x10^{-6}$
Porosity (-):	0.01	0.40
Fracture aperture (m):	$5x10^{-4}$	
Fracture spacing (m):	5.0-10.0	
Injection temperature (°C):	100.0	
Reservoir temperature (°C):	300.0	

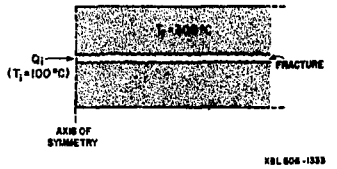

Figure 9. Cold water injection into a fracture in a porous reservoir.

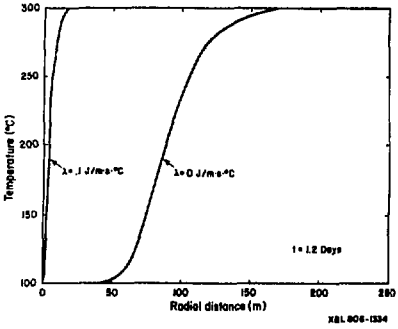

Figure 10. Effect of heat conduction on the movement of the thermal front in the fracture: temperature versus radial distance.

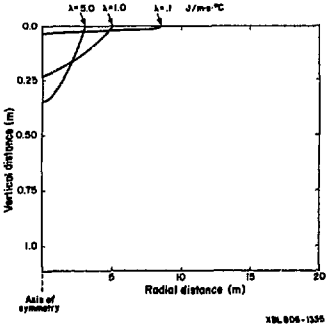

Figure 11. Effect of heat conduction on the movement of the thermal front: 200°C temperature contour in r-z plane.

Increasing the coefficient of thermal conduction between the fracture and the rock matrix further retards the movement of the thermal front along the fracture. Figure 11 shows the location of the thermal front after 1.2 days of injection for three cases using different values of the coefficient of thermal conduction (λ = .1, 1.0, 5.0 Joules/m.sec.°C). The figure also shows how increasing the thermal conductivity increases the penetration of the thermal front into the surrounding formation.

When the cumulative areal velocity of the thermal front is plotted against the coefficient of thermal conduction, the curves in Figure 12 result. The cumulative areal velocity is calculated based upon the radial distance of the thermal front (200°C isotherm) from the injection well at a given time. The curves show a rapid decrease in the cumulative areal velocity of the thermal front for low values of thermal conductivity, but they level off for higher values. The shape of the curves suggests that an exponential relstionship may exist between the thermal conductivity and the cumulative areal velocity of the thermal front.

Another point of interest shown in Figure 11 is that the cumulative velocity of the thermal front is time dependent, but not constsnt, as in the case of a homogeneous porous reservoir of constant thickness. This behavior can be explained when one considers that during injection the thermal front is moving radially away from the well, and the effective surface area for conductive heat transfer between the fracture and the rock matrix is rapidly increasing. The energy flow into the fracture rapidly increases and consequently retards the advancement of the thermal front. O'Neill (1978) found similar retardation of the thermal front in the linesr case, but of course this phenomenon is much more significant in the radial case.

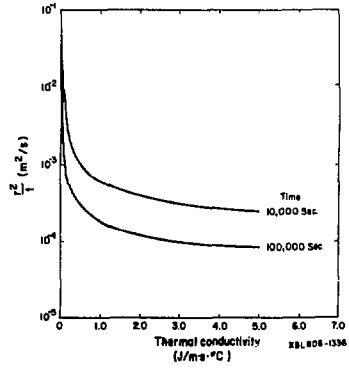

Figure 12. Thermal front movement in the fracture: cumulative areal velocity as a function of thermal conductivity.

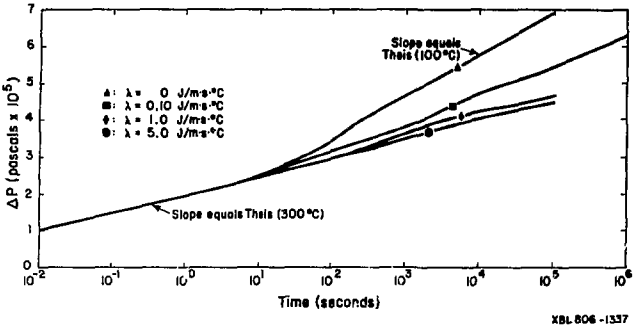

Figure 13. Injection pressure behavior during injection into the fracture in a porous reservoir, for different values of thermal conductivity.

Figure 13 shows the pressure behavior at the injection element, during cold water injection into the fracture. When there is no conduction, similar pressure behavior is observed, as in the case of a homogeneous porous reservoir (see last section), with two distinct linear segments having slopes corresponding to Theis solution for the two temperatures. (In the model we assume that Darcy's law can be used to calculate fluid flow within the fracture). However, conduction between the fracture and the rock matrix retards the movement of the front and consequently the latter linear segment is not observed during the simulation, although it may show up at larger times. When a large coefficient of thermal conduction is used (λ = 5.0 Joules/M-sec.$^{\circ}$C), the linear segment corresponding to the 300°C Theis continues at all times during the computer simulation.

Injection into a Fracture in a Permeable Formation

A few computations were made in order to study the movement of the thermal front when cold water was injected into a horizontal fracture in a permeable medium. The thermal conductivity of the rock matrix was fixed at 2.0 Joules/m.sec.$^{\circ}$C, but the thermal conductivity of the fracture remained at .65 Joules/m.sec.$^{\circ}$C. A fracture permeability of 1 x 10^{-10} m^2 or 100 darcies was used for all of the cases, but the permeability of the rock matrix varied.

Figure 14 shows the temperature contours in the fracture and the rock matrix after 1.2 days of injection. In this run the permeability ratio between the fracture and the rock matrix (k_D) is fixed at 10^4 (the permeability of the rock is 10^{-14} or 10 md). As the figure shows, the permeable rock allows penetration by the injected water, and consequently the cold water front (the 200°C isotherm) penetrates the rock considerably. Most of the heat transfer between the rock and the fracture is by convection. However, if the permeability ratio (k_D) is increased to 10^7, the conductive heat transfer is still very significant (Figure 15). A comparison of two computer runs with thermal conductivities of 5.0 and 2.0 Joules/m.sec.$^{\circ}$C, and all other parameters remaining the same, shows that the thermal front has advanced 3 and 4 meters respectively, after 1.2 days of injection.

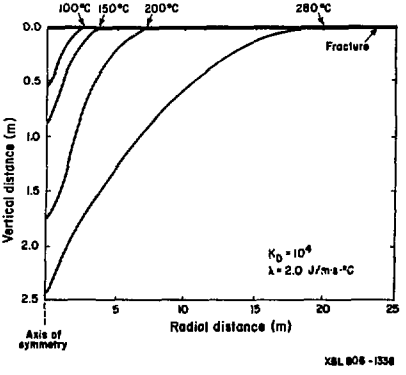

Figure 14. Isotherms after 1.2 days of injection into a fracture in a porous reservoir.

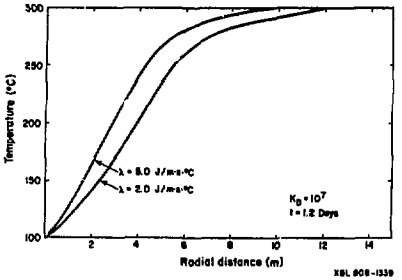

Figure 15. Effects of thermal conduction on the temperature distribution within the fracture.

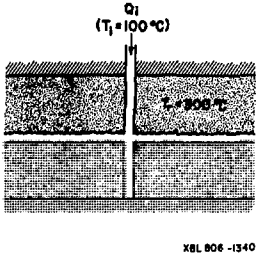

Figure 16. Model used for injection study of geothermal reservoirs containing horizontal fractures.

Injection into a Well Connected to Both the Fracture and the Permeable Formation

In this case the fluid is injected both into the fracture and the permeable formation directly through the injection well (Figure 16). Thus the thermal front moves radially away from the well both in the fracture and in the rock, although not necessarily at the same rate. Two cases are studied: in the first one a permeability ratio (K_D) of 10^4 and fracture spacing of 10 meters is used; in the second, the permeability ratio is fixed at 10^3 and the fracture spacing at 5 meters. In both cases, a fracture permeability of 10^{-10} m^2 or 10 md and a thermal conductivity of 2 Joules/m.sec.°C is used.

Figure 17 shows temperature contours after 1.2 days of injection for the first case. At this time the thermal front (200°C temperature contour) has advanced considerably farther in the fracture than in the porous media, over 5 m in the fracture, compared to 1.5 meters in the formation.

Figure 18 shows a plot of the cumulative areal velocity of the thermal front versus time for the first case. The lack of data for the thermal front in the rock at early times is due to the space discretization used in the study. We have defined the thermal front as the 200°C isotherm, and at early times the first rock elements have not cooled down sufficiently to allow accurate determination of the location of the thermal front. The figure shows that at early times the cumulative areal velocity of the thermal front is more than an order of magnitude higher in the fracture than in the formation. One must bear in mind that for a homogeneous porous radial system and a constant injection rate, the areal velocity of the thermal front should be constant. As the injection continues the cumulative areal velocity of the thermal front decreases rapidly, almost linearly at first, then gradually levels off. The cumulative areal velocity of the thermal front in the rock increases with time until it coincides with the velocity of the thermal front in the fracture, after which the fronts advance together. The two curves for the rock shown in Figure 18 represent observation points at different distances from the fracture. At the end of the simulation the thermal front in the rock close to the fracture is advancing at the same rate as the thermal front in the fracture, but in the rock farther away from the fracture the thermal front still lags somewhat behind.

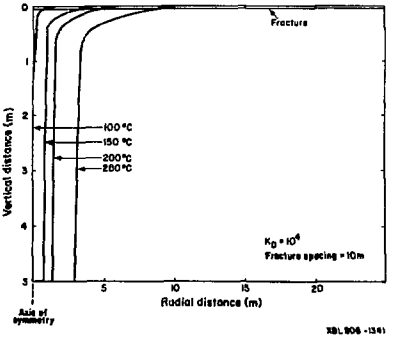

Figure 17. Isotherms after 1.2 days of injection into a well connected to both fracture and the porous formation.

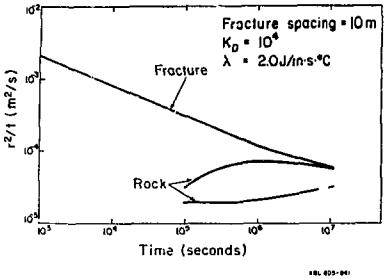

Figure 18. Cumulative areal velocity of the thermal front during injection. The observation points in the rock matrix are .10 and 3.3 meters from the fracture.

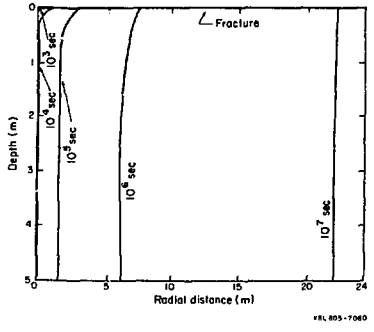

Figure 19. Isotherms after 115 days of injection.

The rapid decrease in the cumulative areal velocity of the thermal front in the fracture with time is due to the continuously increasing surface area, through which conductive and convective heat transfer between the fracture and the formation can occur. The increase in the cumulative areal velocity in the rock is probably due to cooling effects from the fracture.

Another calculation was made using K_D equal to 10^3 and fracture spacing of 5 meters. Similar results to those shown in Figure 18 were obtained, although the cumulative areal velocity of the thermal front in the fracture is less in this case at all times, due to the increased permeability of the rock and consequently relatively less water entering the fracture from the well. Figure 19 shows the location of the thermal front at different times during the simulation. The figure shows that at early times the thermal front in the fracture is well ahead of the thermal front in the rock. Later on, however, the thermal front in the rock starts to catch up with the thermal front in the fracture and after only 10^7 seconds (about 115 days) the two fronts almost coincide. It is of interest to note that after only 23 meters from the injection well the two fronts advance practically side by side.

Summary and Discussion

The studies described in the last few sections can be considered as a first step to answer the key question of how fractures affect the breakthrough time of cold water from injection wells into the production region in a geothermal field. Our results indicate that when cold water is injected into horizontal fractures in impermeable rocks, heat transfer by thermal conduction between the fracture and the rock matrix retards the movement of the thermal front in the fracture considerably. Of course, the higher the coefficient of thermal conduction, the more the thermal front gets retarded, and our results indicate that there may be an exponential relationship between the areal velocity of the front and the thermal conductivity of the rock matrix.

When cold water is injected into a horizontal fracture in a permeable hot reservoir, the heat transfer between the fracture and the formation may become dominated by convection, depending upon the permeability ratio (k_p) between the fracture and the rock matrix and the thermal conductivity of the rock. The permeable rock allows flow of cold water from the fracture into the formation and consequently the cooling effects extend deep into the surrounding rock.

We also studied the case of cold water injection directly from the well into both the fracture and the formation. Our results indicate that although the thermal front advances much more rapidly in the fracture than the rock at early times, the thermal front in the rock eventually catches up with the one in the fracture, after which time they will advance at the same rate. The distance from the injection well to the point where the fronts will coincide depends on many factors, such as the permeability ratio between the fracture and the rock matrix, the spacing and aperture of the fractures, and the thermal conductivity of the surrounding rock.

Although the results presented in this paper are quite preliminary and require further investigation, they imply that in geothermal formations dominated by horizontal fractures, rapid movement of the injected water shooting through the fractures may not accelerate the cooling of the reservoir much. Thus, in such formations injection may safely be used to maximize the energy recovery of the geothermal system, if the spacing between the injection and the production wells is appropriately selected.

Acknowledgment

The authors wish to express their gratitude to Dr. Marcelo Lippmann for critically reviewing this manuscript. They would also like to acknowledge Eden Wang for plotting the data, and Mary Bodvarsson and Becky Sterbentz for drafting the figures. This work was performed under the auspices of the U.S. Department of Energy, Division of Geothermal Energy, under Contract Number W-7405-ENG-48.

References

Bodvarsson, G. (1969), "On the Temperature of Water Flowing through Fractures," Journal of Geophysical Research, vol. 74, No. 8, p. 1987-1992.

Bodvarsson, G.S., and Lippmann, M.J., (1979), "Recent Modifications of the Numerical Code CCC," in The Annual Report of the Earth Science Division, Lawrence Berkeley Laboratory, LBL-10795.

Bodvarsson, G.S., and Lippmann, M.J., (1980), "The Numerical Simulator CCC," paper presented at the Fracture Hydrology Modeling Workshop at Lawrence Berkeley Laboratory, Feb. 19-20, paper to be published in the proceedings of the workshop.

Cinco-Ley, H., Samaniego, V.F., and Dominguez, A.N., "Transient pressure behavior for a well with a finite conductivity vertical fracture," Soc. Pet. Eng. J., Aug. 1978, 253-264.

Duff, E.S., MA28 - "A set of Fortran subroutines for sparse unsymmetric linear equations," Report AERE-R8730, Harwell/Oxfordshire, Great Britain.

Edwards, A.L., "TRUMP: A computer program for transient and steady-state temperature distributions in multidimensional systems," Lawrence Radiation Laboratory, Livermore, Report UCRL-14754, Rev. 1, 1968.

Gringarten, A.C., "Unsteady state pressure distribution created by a well with a single horizontal fracture, partial penetration, or restricted entry," Ph.D. Dissertation, Stanford, 1971, 110 p.

Kasameyer, P.W., and Schroeder, R.C. (1976), "Thermal Depletion of Geothermal Reservoir with both Fracture and Pore Permeability," Lawrence Livermore Laboratory report UCRL-77323.

Kazemi, H., "Pressure transient analysis of naturally fractured reservoirs with uniform fracture distribution," Soc. Petr. Eng., vol. 9, 1969, p. 451-462.

Lippmann, M.J., Tsang, C.F., and Witherspoon, P.A., (1977), "Analysis of the Response of Geothermal Reservoirs under Injection and Production Procedures," SPE-6537, presented at the 47th Annual California Regional Meeting SPE-AIME, Bakersfield, California, April 1977.

Mangold, D.C., Tsang, C.F., Lippmann, M.J., and Witherspoon, P.A., (1979), "A Study of Thermal Effects in Well Test Analysis," SPE-8232, presented at the 54th Annual Fall Technical Conference SPE-AIME, Las Vegas, Nevada, September 1979, Lawrence Berkeley Laboratory, LBL-9769.

Narasimhan, T.N., and Witherspoon, P.A. (1978), "An integrated finite difference method for analyzing fluid flow in porous media," Water Resources Res., vol. 14, no. 2, p. 255-261.

O'Neill, K. (1978), "The Transient Three-dimensional Transport of Liquid and Heat in Fractured Porous Media," Ph.D. Thesis, Princeton University.

Romm, E.S., (1966), "On One Case of Heat Transfer in Fractured Rock," All-Union Institute for Scientific Research and Geological Exploration for Petroleum, U.S.S.R., Preprint.

Streltsova-Adams, T.D., (1978), "Well Hydraulics in Heterogeneous Aquifer Formations," in Advances in Hydroscience, vol. 11, Academic Press, Inc., p. 357-423.

Tsang, Y.W., and Tsang, C.F., (1978), "An Analytic Study of Geothermal Reservoir Pressure Response to Cold Water Reinjection," in The Proceedings of the 4th Workshop in Geothermal Reservoir Engineering, Stanford University, p. 322-331.

Tsang, C.F., Buscheck, T., and Doughty, C., (1979), "Aquifer Thermal Energy Storage; a Numerical Simulation of Auburn University Field Experiments," Submitted to Water Resources Research.

Warren, J.E., and Root, P.J., (1963), "The Behavior of Naturally Fractured Reservoirs," J. SPE no. 3, September 1963, pp. 245-255.

AQUIFER RESPONSE TO EARTH TIDES

B. Y. Kanehiro and T. N. Narasimhan
Earth Sciences Division, Lawrence Berkeley Laboratory
University of California
Berkeley, California 94720

INTRODUCTION

The earth is, theoretically, within the gravitational fields of all other celestial bodies and as such is subject to tidal forces. The sun and moon, however, because of their respective sizes and proximity account for virtually all the tidal forces experienced by the earth. While all of the earth is subject to tidal forces, the ocean tides of the hydrosphere provide by far the most dramatic evidence of these forces at work. These same tidal forces also act on the atmosphere and the lithosphere and generate atmospheric and solid earth tides. These tides are of small magnitude, however, and are more difficult to measure accurately.

The response of groundwater aquifers to ocean tides has been observed since the time of the Greeks and has been widely documented and studied. Aquifer response to the atmospheric or barometric tide exists but is difficult to study. The response is very small and the barometric tide itself is masked by pressure variation due to nontidal forces such as those associated with atmospheric circulation and the daily heating and cooling of the atmosphere. Aquifer response to earth tides has been known for some time. Unfortunately, the small magnitude of the response has greatly impeded efforts at quantitative investigation.

The magnitude of the water-level fluctuations resulting from aquifer response to earth tides is on the order of one centimeter over a 12-hour period. The present generation of extremely sensitive pressure transducers which use quartz crystal sensors have made it possible to obtain good measurements of this fluctuation. This in turn has led to renewed interest in the reservoir mechanics related to earth tides.

HISTORY

Perhaps the earliest suggestion of the response of groundwater levels to earth tides was made by Grablovitz in reference to periodic water-level fluctuations in a flooded coal mine in the landlocked country of Czechoslovakia reported by Klonne in 1880. Since 1880 there have been many reports of fluctuations of a tidal nature in wells that may be attributable to aquifer response to earth tides. Young (1913) reported on tidal fluctuations in a well near Cradock, South Africa. In 1939, Robinson published hydrographs of several wells in New Mexico and Iowa showing tidal fluctuations attributable to earth tides. More recently, George and Romberg (1951) reported on water-level fluctuations showing aquifer response to earth tides in a well at Fort Stockton, Texas. Tidal fluctuations have even been reported in a well drilled in a water table aquifer by Richardson in Oakridge, Tennessee. More extensive work on both earth tides and the response of aquifers to earth tides has been done by Melchior (1956, 1960, 1964). He reported on tidal fluctuations in deep wells in Turnhout, Belgium, and a hot spring at Kiabukwa, Belgium Congo.

Early discussions of the theoretical analysis of the response of aquifers to earth tides were presented by Theis (1939) and Pekeris (1940). In 1964 Melchior presented an analysis for a spherical cavity. A good general discussion and an analysis based on expected dilatation was presented by Bredhoeft in 1967. In 1970, Bodvarsson presented an analysis assuming a spherical cavity. Recently, Morland (1977) presented an analysis assuming either plane or axial symmetric flow and a time-dependent overburden. And most recently (Ardity, et al, 1978) an analysis for a radially symmetric flow to a well has been presented.

EARTH TIDES

As will be seen in examining this problem, the physical phenomena associated with aquifer response to earth tides are somewhat unusual when compared with more common reservoir engineering problems. For this reason it is necessary to carefully consider the physical situation before attempting to apply the standard equations of fluid flow through porous media.

The earth tides themselves are often described as either a change in tidal potential or as a change in gravitational acceleration at a given point.

It is often convenient and sufficient to represent the tidal forces in terms of the tidal potential W given by

$$W_2 = \frac{Ga^2}{2}\left[\frac{M_s(3\cos^2\theta_s - 1)}{R_s^3} + \frac{M_m(3\cos^2\theta_m - 1)}{R_m^3}\right] \qquad (1)$$

where G is the universal gravitational constant; a is the mean radius of the earth: M_s is the mass of the sun: M_m is the mass of the moon and θ_s, θ_m, R_s, and R_m are shown in Figure 1. (Rinehart 1975)

The change in acceleration due to gravity is then

$$\Delta g = \nabla W_2 \qquad (2)$$

The radial or vertical component is

$$\Delta g_r = -\frac{\partial W_2}{\partial r} \qquad (3)$$

and the tangential or horizontal component is

$$ag_y = -\frac{1}{a}\frac{\partial W_2}{\partial \theta} \qquad (4)$$

If a is assumed to be much smaller than R_m or R_s, higher order terms can be neglected and

$$ag_z = GA\left[\frac{M_s(3\cos^2\theta_s - 1)}{R_s^3} + \frac{M_m(3\cos^2\theta_m - 1)}{R_m^3}\right] \qquad (5)$$

and

$$ag_y = \frac{3}{2}GA\left[\frac{M_s \sin 2\theta_s}{R_s^3} + \frac{M_m \sin 2\theta_m}{R_m^3}\right] \qquad (6)$$

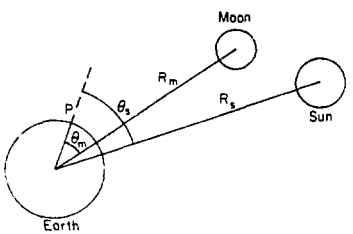

XBL 756-7537

Figure 1. Relation of the sun and moon to a point, P, on the surface of the earth

Before discussing the effects of the earth tides on a reservoir the complex time-dependent nature of the tides should be considered. While the relative movements of the sun, moon and earth are indeed complicated they are to a high degree of precision periodic. For this reason the complex time-dependent nature of the gravitational tidal potential can be dealt with by using either Fourier analysis or a filtering scheme and invoking superposition. While this can become an involved process, it will be assumed for the present that the tidal potential and the signal at the well can be decomposed into discrete sinusoidal components.

From the above, it might seem reasonable to assume that the change in acceleration due to gravity accompanying the change in tidal potential implies a change in weight of the overburden of the reservoir. This changing overburden stress may then cause the observed change in pore fluid pressure seen in the aquifer. This simplistic model, however, cannot account for the magnitude of the change in pore fluid pressure seen in even moderately deep reservoirs.

The measured amplitude of the change in gravitational acceleration due to earth tides is generally on the order of 100 microgals. An overburden of 1,000 meters with a density of 2,650 kg/m^3 would therefore imply a change in stress of only 2.65 Pa (2.7×10^{-4} m of water). This is obviously a relatively small effect that is at or beyond the range of accuracy of even a quartz crystal pressure transducer.

DEFORMATION OF THE EARTH

While it was not pointed out in the previous discussion of the change in acceleration due to gravity, the earth is not a rigid body. Indeed it is in part, the deformation of the earth that causes the change in acceleration due to gravity to be so complex. It is also this deformation that causes the change in pressure in the reservoir.

In a gross sense this deformation may be viewed as a bulging of the earth resulting from the gravitational attraction of the moon and/or sun on the one side and centrifugal force on the other. Unfortunately the description of the mechanics of the situation is very complicated. In a general sense, however, it can be said that the magnitude of the dilatation at a point is determined by the change in gravitational potential that can be calculated from the positions of the sun, moon and earth and a semitheoretical model of the earth or empirically determined coefficients.

The original theory of Love (1911) assumes that a spherical harmonic of second order can be used to approximate the perturbing potential. It is further assumed that the deformation of the earth induced by this perturbing potential may be expressed as the product of the harmonic and some numerical coefficient. These coefficients are related to the distribution of densities and moduli of rigidity in the semitheoretical earth model or can be empirically estimated. Historically, they came to be called Love numbers and are used singularly or in simple algebraic combinations.

While a considerable amount of interesting work has been done on the estimation of Love numbers and the deformation of the earth, it is sufficient to limit the scope of this paper to the estimate of the total dilatation presented by Takeuchi.

$$\Delta = 0.5\,\frac{W_2}{ag} \qquad (7)$$

From this it may be seen that the perturbing potential may be calculated with some accuracy because the motions of the earth, sun, and moon are reasonably well understood. The deformation resulting from the perturbing potential, however, is not easily determined because an earth model and Love numbers must be estimated. For this reason it must be understood that any estimations of reservoir or aquifer characteristics based on response to earth tides will of necessity have certain unavoidable uncertainties associated with them.

There remains of course, at least in theory, the possibility of literally measuring the strain induced in the earth by earth tides. What would be required is a very accurate measurement of strain in six directions over a relatively large area. Since the radial component is relatively small with respect to the horizontal components, however, it may be possible to use only the horizontal components. Given such a strain

measuring network at the site of a reservoir, a very interesting analysis may be possible.

THE PROBLEM CONSIDERED

Two types of models are considered in this analysis of the response of the reservoir to the earth tides described above. The first is that of a confined aquifer with a single packed-off well, and the second is a confined aquifer with a well open to the atmosphere where the water level is allowed to fluctuate. The first case will be considered in some detail followed by field examples. The second case will be briefly considered in a later section. Because good data was not available, only hypothetical cases are covered in the section dealing with the second model.

COMPRESSIBILITIES AND THE STORAGE TERM

From the physical situation of the first case it is apparent that the properities that may be estimated from the aquifer's response to the earth tides are related to compressibilities. In the fields of hydrology and petroleum engineering, however, it is more common to deal with some type of storage term rather then compressibilities directly. The storage term encompasses the compressibilities but is more convenient to use when working with equations dealing with flow. This is because the majority of problems in hydrology and petroleum engineering are related to the addition or removal of fluid from the aquifer or reservoir. Such a situation can be termed a drained problem where the addition or removal of fluid acts as the driving force. In contrast to this is the undrained problem where fluid is not being injected or withdrawn. Rather, the driving force or load on the system is in the form of an externally applied stress.

Historically, the first storage term to be defined in hydrology was the storage coefficient now also known as the storativity. It is currently defined as the volume of water which an aquifer releases from or takes into storage per unit surface area of aquifer per unit change in the component of head normal to the surface (Ferris, 1962). Earlier definitions of the storage coefficient expressed the same idea, but were more restrictive in that they were formulated in terms of aquifer thickness. The other common storage term used in hydrology is the specific storage storativity. It is the storativity normalized with respect to the thickness of the aquifer. In petroleum engineering the storage term is generally expressed as ϕcH. The relationship between ϕcH and specific storativity is,

$$\phi cH = \frac{S_s}{\rho_f g} H \tag{8}$$

where

c = total compressibility of the aquifer

ϕ = porosity of the aquifer

S_s = specific storage

ρ_f = density of the fluid

H = thickness of the aquifer

Since the storage term is defined with respect to the addition or removal of fluid from the reservoir, its relationship to compressibilities and changes in pressure are not immediately obvious. To circumvent this problem for the present situation, the following definition for the storage term is adopted.

$$S_s = \rho_f g \left[\phi c_f + (1 - \phi) a_v\right]$$

(Jacob, 1940). Or similarly,

$$\phi cH = H\left[\phi c_f + (1 - \phi) a_v\right]$$

where

$$c_f = -\frac{\Delta V_f / V_f}{\Delta P_f} \tag{9}$$

where V_f = volume of fluid and P_f = fluid pressure. and a_v, defined as

$$a_v = -\frac{V_v / V_s}{d\sigma'}$$

where V_s = volume of the solid grains and

σ' = effective stress, i.e., the total stress less a percentage of the pore fluid pressure.

The above relationship, unlike the original definition, does not make direct reference to the drained or undrained nature of the problem. By adopting this relationship in place of the original definition it is possible to consider the undrained problem. In this case the magnitude of the change in pore fluid pressure resulting from a load is not the same as the magnitude of the change in the effective stress. The total quantity of fluid in the aquifer or reservoir, however, must remain the same.

From the definitions of the fluid compressibility, the coefficient of compressibility, and since

$$\frac{V_v}{V_s} = \frac{\phi}{1 - \phi} \tag{10}$$

then

$$a_v = -\frac{\phi}{1 - \phi} \frac{dV_v / V_v}{d\sigma'} \tag{11}$$

Since fluid is not being added to or removed from the reservoir and the medium remains saturated, the change in fluid volume is equal to the change in void volume. Hence,

$$a_v = -\frac{\phi}{1 - \phi} \frac{dV_f / V_f}{dp_f} \frac{dp_f}{d\sigma'} \tag{12}$$

From the definition of fluid compressibility

$$c_f dp_f = a_v \left(\frac{1-\varphi}{\varphi}\right) d\sigma' \tag{13}$$

From the effective stress law,

$$\sigma' = \sigma - np_f \tag{14}$$

$$a_v = c_f \left(\frac{\varphi}{1-\varphi}\right) \frac{dp_f}{d\sigma - ndp_f} \tag{15}$$

The specific storage may then be written as

$$S_s = \rho_f g \left[\varphi c_f + (1-\varphi)\frac{\varphi}{1-\varphi} c_f \frac{dp_f}{d\sigma'}\right]$$

$$= \rho_f g \varphi c_f \left[1 + \frac{dp_f}{d\sigma - ndp_f}\right] \tag{16}$$

Similarly,

$$\varphi cH = \varphi c_f H \left[1 + \frac{dp_f}{d\sigma - ndp_f}\right] \tag{17}$$

The specific storage is now written in terms of the change in pore fluid pressure which can be measured, the change in total stress, the porosity, and other coefficients which can be easily estimated. Recall, however, that the calculations based on the change in gravitational potential allow only for the estimation of the change in dilatation. Since this problem only deals with changes in volume, any deviatoric portion of the stress tensor need not be considered. The deviatoric portion only gives rise to a change in shape (Chierici, et al. 1967). This implies that the octanedral stress, σ_O, defined as

$$\sigma_O = \frac{\sigma_{rr} + \sigma_{\varphi\varphi} + \sigma_{\theta\theta}}{3} \tag{18}$$

may be used. Since

$$\sigma_{rr} = \lambda\omega + 2\mu\varepsilon_{rr} \tag{19}$$

$$\sigma_{\theta\theta} = \lambda\omega + 2\mu\varepsilon_{\theta\theta} \tag{20}$$

$$\sigma_{\varphi\varphi} = \lambda\omega + 2\mu\varepsilon_{\varphi\varphi} \tag{21}$$

and

$$\lambda = K - \frac{2}{3}\mu \tag{22}$$

$$d\sigma_O = K\omega \tag{23}$$

where K = the bulk modulus.

Thus the σ required to evaluate the specific storativity or φcH may be estimated from the dilatation if the magnitude of the bulk modulus is realistically known. The next section deals with how a value for the bulk modulus can be reasonably deduced from available data.

ESTIMATING THE BULK MODULUS

The question of deciding what value should be used for the bulk modulus is not a simple one. It becomes a question of trying to decide what the bulk modulus used should represent. Should the bulk modulus reflect the rocks making up the aquifer or should it simply be taken as the value obtained from the earth model that the tidal potential is applied to? The answer appears to be somewhere in between. The real earth is not concentrically homogeneous like the earth model. On the other hand the rocks making up the aquifer probably have a lower bulk modulus than the majority of the other rocks at a given depth and this might imply that the representative value of the bulk modulus in or near the aquifer might be somewhat lower than the value that might be expected from a global point of view or from the point of view of the earth model.

The point is that there does not appear to be any physical way to clearly determine what value should be used for the bulk modulus. In fact, given the heterogeneities in the system, it appears that for practical purposes it is not feasible to consider trying to determine explicitly what the representative bulk modulus is, even by using such powerful methods as numerical analysis capable of handling the arbitrary geometries. While the problem of picking a representative value for the bulk modulus is a difficult one, it should be noted that other similarly difficult problems are encountered in doing the more common tests for the determination of the hydraulic characteristics of aquifers such as pump tests. Since there is much more experience in dealing with these more common types of test, however, the required assumptions that must be made are often made in a matter of fact fashion and not subjected to much question. For example, in many pump tests it is virtually certain that the field conditions do not conform to the boundary or heterogeneity conditions of the analysis being used, but experience has shown that the analysis may still be applied to arrive at satisfactory results. The reason that the results of the analysis appear to be satisfactory in many cases may be because the assumptions are indeed reasonable, but in other cases it may be because there is really no way to independently arrive at a better estimate and thereby bring the assumptions into question. That this is sometimes true may be seen in the extremely large differences in values determined at the same well by a longer term and a shorter term pump test. Of course, in the present problem a numerical quantity must be estimated and since it is easy to change a numerical quantity without radically changing the analysis as would be required in the case of a change in geometry there is a tendency to expect the "right" number to be chosen for each problem. Given that there is justification for making some estimate for the representative bulk modulus the question of how this estimate is to be made arises. The best estimate for the bulk modulus from the earth model of Takeuchi (1950) based on the values of elastic moduli presented by Bredehoeft (1967) is 1×10^{11} Pa. This is a rather high value being approximately that of the ultrabasic rock, dunite. Since aquifers are in the upper part of the crust and hence usually in areas of somewhat lower bulk

modulus it is reasonable to take the value of 1 x 10^{11} Pa as an upper limit. Further, since the area being considered includes the aquifer it is reasonable to assume that the representative value for the area would be less than this value. Values for the bulk moduli of sandstones and other common rocks are presented in table 1. As can be seen these values are almost all substantially below 1 x 10^{11} Pa. As previously stated, however, the deformation being considered is on a large scale and the relatively low bulk modulus of the aquifer would be expected to affect, but not totally govern the system. The best value for the representative bulk modulus is then somewhere between these values. Since the highest values for bulk moduli of common continental rocks at depths of relatively deep aquifers is on the order of 2 x 10^{10} Pa to 7.5 x 10^{10} Pa and since the aquifer is not really at a depth where rocks approaching dunite are found it is assumed that a best estimate for the value of the representative bulk modulus is 5 x 10^{10} Pa.

Table 1 Representative bulk moduli of a few rock types

Rock type	Bulk modulus
Basalt[1]	7.5 x 10^{10} Pa
Dunite [1]	1.0 x 10^{11} Pa
Granite[1]	5.5 x 10^{10} Pa
Sandstone	1.7 x 10^{10} Pa
Iron (solid)[1]	1.6 x 10^{11} Pa

[1]Stacey, 1969

FIELD APPLICATIONS

Data from two different wells were analyzed. These wells are located in East Mesa, California and Marysville, Montana. Since the overall quality of the record from the well in Montana is considerably better than the records from the other well it will be considered first and used for illustrative purposes.

A. WELL AT MARYSVILLE, MONTANA

The Marysville well is located approximately 30 kilometers northwest of Helena, Montana. It is 2,000 meters deep with an uncased portion 0.20 meter in diameter in a fractured granite-like, quartz porphyry. While the well is not a packed off well the diameter is relatively small and as a first approximation the packed off analysis was used.

As can be seen in Figure 2 the well record shows periodic fluctuations that appear to correspond with those of the earth tide shown in Figure 3. Fourier analysis was applied to both records to produce the spectrum of the well record shown in Figure 4 and the spectrum of the earth tide shown in Figure 5. In these figures the harmonic number is equal to the record length (28 days) divided by the period of the component.

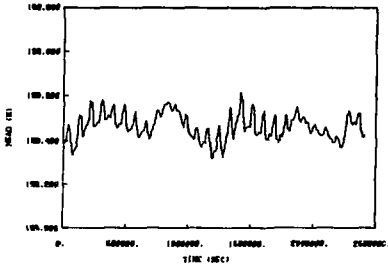

Fig. 2 Well record of the well at Marysville, Montana (XBL 811-7715)

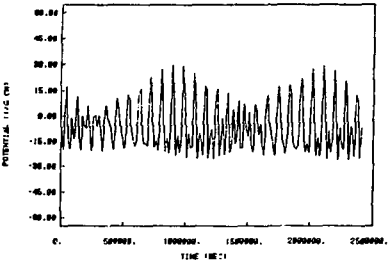

Fig. 3 Earth tide at the site of the well at Marysville, Montana (XBL 811-7716)

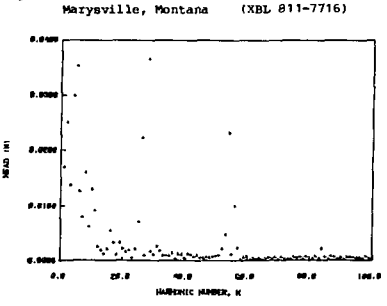

Fig. 4 Spectrum of the well record from the well at Marysville, Montana (XBL 811-7717)

By assuming a fluid density of 1,000 kg/m^3 and a fluid compressibility of 4.6 x 10^{-10} 1/Pa (1/Pascal), the analysis described above may be applied to the amplitudes of the tidal components of the well record and the tide. The results of this analysis based on a representative bulk modulus of 5 x 10^{10} Pa are shown in table 2. It can

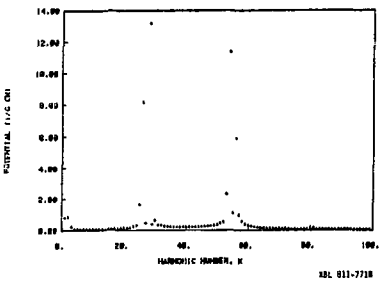

Fig. 5 Spectrum of the earth tide at the site of the well at Marysville, Montana (XBL 811-7718)

be seen that the calculated value of specific storativity over porosity is at least a reasonable one, implying that the application of the packed off analysis is at least not grossly erroneous.

Table 2. Results of the analysis of the record from the well at Marysville, Montana (bulk modulus of 5×10^{10} Pa assumed for the region around the aquifer)

TIDAL COMPONENT	ΔW_2 (x 1/gm)	Δp_f (Pa)	$S_{s/\phi}$ (1/m)
O1	8.126×10^{-2}	2.176×10^{2}	1.485×10^{-5}
P1, K1	1.318×10^{-2}	3.581×10^{2}	1.535×10^{-5}
N2	2.315×10^{-2}	4.600×10	9.351×10^{-6}
M2	1.133×10^{-1}	2.260×10^{2}	9.366×10^{-6}
S2	5.863×10^{-2}	9.782×10	7.962×10^{-6}

$S_{s/\phi}$ (mean) = 1.14×10^{-5} 1/m

Standard Deviation = 3.45×10^{-6} 1/m

Well At East Mesa, California

Data from two geothermal wells at East Mesa, California were studied. The first of the two wells is located about 30 kilometers east of El Centro, California in the Imperial Valley. Lawrence Berkeley Laboratories conducted interference well tests in the area in the past few years in conjunction with the U.S. Bureau of Reclamation's investigation and an evaluation of the site as a geothermal resource (Witherspoon, et al, 1976; Narasimhan, et al, 1977a; Narasimhan, et al, 1977b).

The Imperial Valley is part of a large sediment filled depression known as the Salton Trough that forms the landward continuation of the East Pacific Rise and the Gulf of California (Swanberg, 1975). The field itself is situated in essentially flat lying poorly consolidated late Pliocene to late Pleistocene sandstones, siltstones and clays derived from the Colorado River (Narasimhan, et al, 1977b). The reservoir itself appears to be confined between crystalline basement rocks below and a sequence of rocks that are predominantly clay and about 2,000 feet thick on the top. The well is approximately 2,000 meters deep with a slotted section of about 250 meters. It is shut-in and monitored with a Paroscientific quartz crystal type pressure transducer.

Aside from any problems related to the quality of the well record, there are two questions that arise in this area. The first question is related to the abnormally high temperature that is found in all the sites studied. Since temperature changes the viscosity of the fluid much more than the density, however, the effects on a quasi-static problem like the one being considered will be much less than one where flow is taking place. Further, since the object of the analysis is to determine physical properties for the aquifer or reservoir under naturally occurring conditions one would not really be too concerned about correcting for a lower temperature unless the interest lay in considering what would happen to the reservoir if the temperature was lowered, say because of overproduction. This, however, would be a totally different case and would require a new set of data and analysis much like new pump tests are required if the conditions of the reservoir change.

A second question of some concern in this area has to do with the question of possible ocean loading. The field in question is approximately 100 kilometers from the Salton Sea and 130 kilometers from the Pacific Ocean. This might imply yet another possible source of error in the prediction of the earth tides. In light of the other assumptions that are already made, however, this is not likely to significantly affect the results.

In a manner exactly the same as described for the Montana well the well record from the East Mesa was submitted to Fourier analysis and compared with the predicted earth tide. The results of the analysis are summarized in table 3. As can be seen in the tables the best value of the specific storativity over porosity for the East Mesa aquifer based on the aquifer's response to the earth tides and a bulk modulus of 5×10^{10} Pa is 5.1×10^{-6} 1/m.

Pumping tests conducted at the East Mesa field suggest ϕcH values of 2.0×10^{-8} m/Pa to 1.1×10^{-7} m/Pa. This implies a storage coefficient or storativity of 2.0×10^{-4} to 1.0×10^{-3}. If a value near the center of this range is assumed, the most probable value based on pumping test is approximately 6.2×10^{-4}.

The comparison of specific storativity over porosity as determined from the analysis based on the aquifer response to the earth tides and the storativity as determined from the pumping tests requires that the porosity and thickness of the aquifer be known or estimated. Since in this case an estimate of the thickness of the aquifer based

on the geology is available the porosity can be estimated and the specific storativity over porosity compared with the pump tests' value of storativity. Alternatively, the porosity can be calculated. A geologically based estimate of the aquifer thickness of 1,000 meters (Narasimhan, et al, 1977b) implies a porosity of twelve percent using the specific storativity over porosity estimate based on the bulk modulus of 5×10^{10} Pa. The reasonable estimate of twelve percent for the porosity of the aquifer indicates that the analysis of the well record based on this theory of the aquifer's response to the earth tides gives credible results in this case.

Table 3. Results of the analysis of the record from the well at east mesa, California (bulk modulus of 5×10^{10} Pa assumed for the region around the aquifer)

TIDAL COMPONENT	ΔW_2 (x 1/gm)	Δp_f (Pa)	S_s/φ (1/m)
O1	7.060×10^{-2}	2.924x10	5.052×10^{-6}
P1, K1	7.362×10^{-2}	4.745x10	5.416×10^{-6}
N2	3.754×10^{-2}	1.102x10	4.881×10^{-6}
M2	1.704×10^{-1}	5.526x10	4.923×10^{-6}
S2	9.234×10^{-2}	3.717x10	5.035×10^{-6}

S_s/γ (mean) = 1.14×10^{-5} 1/m

Standard deviation = 2.11×10^{-7} 1/m

THE INFLUENCE OF FLOW TO AN OPEN WELL ON MEASURED AQUIFER RESPONSE

The original intent of this study did not include the consideration of an open well and its associated complexities. Because of the potentially large number of applications in the field, however, it was decided that some work in this direction should be done. Since there was no readily available data for a large open well with good independent pump test results it was decided that only hypothetical cases would be studied. Before discussing the problem of flow to a well open to the atmosphere it is useful to consider what might indicate that appreciable flow is indeed taking place and must be considered. Basically two things would be expected. First, there would be a phase lag between the signal seen in the well and the earth tide. Second, there would be an attentuation of the signal when compared to the signal of a packed off flow where no flow takes place. Since the magnitude of the phase lag and attenuation is function of the properties of the aquifer it is reasonable to attempt to use the response of the aquifer to the earth tides to determine these properties. The approach taken, in this somewhat preliminary study, is to explore the possibility of using a numerical model to deal with the inverse problem.

THE PROBLEM CONSIDERED

As previously discussed, the quantity most readily calculated from the earth tide is the change in dilatation and from this the change in total stress experienced by the aquifer. The fluctuating water level in the open well indicates a small though finite volume of flow. In a sense the problem may be viewed as one of well bore storage imposed on the earth tide esponse problem. Before attempting to treat this problem as a simple drained problem with sinusoidal boundary conditions, however, two points should be made. While it is true that in the region near the well the magnitude of the change in effective stress resulting from the change in total stress is equal to the magnitude of the change in pore fluid pressure, there is some question as to the extent of this area. Further, even if some kind of effective radius is hypothesized, the problem will not be as simple as a pumping test problem because the entire aquifer, and not just the portion inside the fictitious boundary, is being affected by the driving force. While some effort was made to study the possibility of an analytic solution, a complete solution was not attempted. The purpose of this study is aimed at two things. First, it is directed toward looking at the possible implications and the relative sizes of the effects of flow to an open well. Second, it is aimed at showing the possibility of dealing with particular field situations on a case by case basis.

The model actually used for this study is based on an integrated finite difference scheme. The code, TERZAGI, written by T.N. Narasimhan, 1975, and based on a heat transfer code by A. Edwards, 1969. Since this code has been verified under many diverse situations (Narasimhan, 1975) there was no need for further verification of the basic code.

In view of the physical situation an axisymmetric mesh with nodes logaritmically increasing in size away from the well is used. The node representing the well is given a finite size and a sinusoidal pressure generation is introduced throughout the mesh. The well bore storage in the well is handled by assigning an appropriate storage capacity to the node representing the well (see Narasimhan, 1975).

The mesh and configuration used for this problem were checked in two ways. The first was with a slug test problem. In the slug test a finite volume of fluid is "instantaneously" introduced into the well and the decline of fluid in the well is monitored. The results of the simulation were compared to an analytic solution presented by Cooper et al, 1973 with excellent matching. The second check was made by packing the well off. This was done by assigning the material properties of the fluid alone to the well element. The results showed that the pressure in the well was the same as that throughout the aquifer as would be expected.

Before discussing the numerical solution it should be noted that while some parameters such as the permeability and the specific storativity of the aquifer are chosen to reflect

typical field situations, other parameters such as the size of the well and the magnitude of the driving force are chosen to show the effect of relatively large flow to the well. The results of this study of a hypothetical problem should therefore not be taken to a necessarily indicative of the effects that might be seen in a real field situation. In fact the effects of flow to an open well shown in this study are likely to be larger than that seen in the average real world field situation.

Three parameters were considered in this study. They are the period of the tidal component, the permeability of the aquifer and the storativity of aquifer. While this study is of a relatively preliminary nature it does show the possibility of treating a real field situation as an inverse problem and some initial attempts are made at systematizing the inverse problem into a type curve scheme.

Because of space limitations only a very brief summary of the results are presented below. Further, since most of the numerical simulations are similar in appearance, only one sample example is shown in figure 6. This example clearly shows the phase lag and damping for a 24 hour tidal component in an aquifer with a permeability of 5×10^{-14} m^2 and specific storativity of 1×10^{-4} $1/m$.

When the period of the tidal component was varied the phase lag and damping increase with a decrease of period. This is a function of the system having more time to equilibrate for the longer period components. The possibility of using several components for a phase lag analysis and a very long period component to approximate a packed off well therefore arises. These possibilities are considered in the type curve study presented below. The magnitude of this increase however, is not very large unless a relatively large diameter well is considered.

As would be expected decreasing the permeability of the aquifer increases the phase lag and the damping. The magnitude of this increase however, is not very large unless a relatively large diameter well is considered.

Also as might be expected, a smaller specific storativity implies a more damping and phase lag. In terms of inverse problems it may be possible to estimate the storativity from the very long period component response and then only deal with the permeability problem.

THE POSSIBILITY OF GENERATING AND USING A TYPE CURVE

While the possibility of generating and using some form of type curve is always attractive in a situation where field application is envisioned, there are a number of complicating factors in this case. The primary problem is the large number of unknown variables.

While the objective of this study is not to generate type curves, a few attempts were made to survey the possibilities. Because of economic and time considerations only a limited number of simulation runs were made.

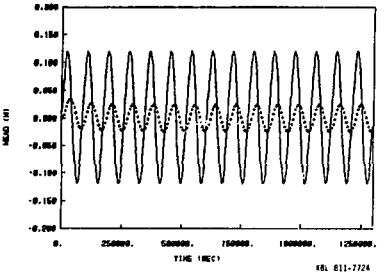

Fig. 6 Pressure fluctuation in the well element (points) and an element distant from the well element (line) in the case of a well open to the atmosphere. The period of the sinusoidal generation term is 86,400 seconds (24 hours). (XBL 811-7724).

The combinations of variables that are plotted to generate the type curve are,

$$\log\left[\frac{T}{r_w^2}\,\varepsilon_p\right]$$

where T = the transmissivity (hydraulic conductivity times the thickness of the aquifer), r_w = the radius of the well, ε_p = the phase lag, and

$$\frac{po - p}{po}$$

where p = the amplitude of the pressure signal at the well, po = the amplitude of the pressure signal at an infinite distance from the well.

A sample curve for a well of 0.2 meter radius in an aquifer ten meters thick is shown in Figure 7. The discrete points represent actual simulations that were run to generate this curve. The smooth curve is based on interpolation and extrapolation.

It might be noted that there is at least a possibility of using this approach in the field if fortnightly unusually good data are available so that phase lag can be determined for the semidiurnal, diurnal and yearly tidal components. If the record is good enough and sufficiently long so as to determine the bimonthly tidal component it can probably be assumed that the well equilibrates over this period. In that case the porosity and the thickness of the aquifer might be estimated and the storativity determined from the relationship presented in the first part of this paper. Alternatively, the well could be packed off to get a better estimate. This narrows the possible

curves down to those corresponding to that storativity.

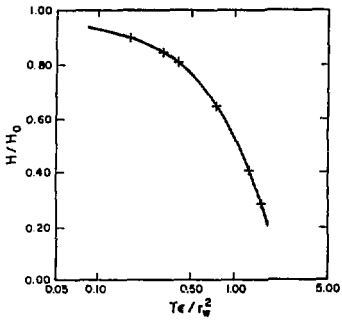

Fig. 7. A possible type curve for a 0.4 meter well. Points represent numerical solutions. The storativity is 1 x 10^{-3}. (XBL 796-7546).

SUMMARY AND CONCLUSIONS

A. The Case of the Packed-off Well

The problem of interpreting the response of aquifers to the earth tides is relatively involved and requires a number of assumptions even in the case of a packed-off well. The relationships presented in the first part of this paper are applicable to packed-off wells and other situations where appreciable flow to the well does not exist. The relationships themselves are relatively simple and are based on fundamental principles and reasonable assumptions. The comparisons of values of aquifer properties determined from the response to earth tides and from the more standard pumping tests for the two California fields are reasonably good. This is especially true in view of the large number of assumptions that must be made in arriving at numerical values in the case of the pump test interpretations as well as in the case of the interpretation of the aquifer response to earth tides.

B. The Case of an Open Well

Having a field situation where the well is open to the atmosphere makes the problem more complicated. In this case there may be an appreciable amount of flow to the well. This flow to the well is seen as either a phase lag between the signal at the well and the earth tide or as a difference in the ratio of the well signal to the tide for the semidiurnal and diurnal components of the tide. The latter is probably the better and more accurate indicator of flow to the well.

Analyses of such situations, however, become involved and are probably best done as case by case studies. The numerical solutions presented in this study show that treating the inverse problem through numerical modeling is at least feasible for any individual situation. Further, it may be possible to simplify the inverse problem through the generation of type curves. It is not likely, however, that general type curves that are applicable to diverse situations would be practical.

REFERENCES

Arditty, Patricia C. and Henry J. Ramey, Jr., Reseponse of a Closed Well-Reservoir System to Stress Induced by Earth Tides, Paper No. 7485, 53rd Annual Fall Technical Conference and exhibition, SPE of AIME, Houston, Texas, October 1-3, 1978.

Bodvarsson, Gunnar, Confined fluids as strain meters, J. Geophys. Res., 75(14), 2711-2718, 1970.

Bredehoeft, J. D., Response of well-aquifer systems to earth tides, J. Geophys. Res., 72(12), 3075-3087, 1967.

Chapman, S., and R. S. Lindzen, Atmospheric Tides, Gordon and Breach, New York, 1970.

Chierici, G. L., et al., The effect of overburden pressure on some petrophysical characteristics of sandstone reservoir rocks, 7th World Petroleum Congress, Mexico City, April 1967.

Cooley, J. W. and J. W. Tukey, An Algorithm for the machine calculation of complex Fourier series, Mathematics of Computation, 19(90), 297-301, 1965.

Cooper, Hilton H. Jr., John D., Bredehoeft, and Istavros S. Papadopulos, Response of a finite-diameter well to an instantaneous charge of water, Water Resources Res., 3(1), 263-269, 1967.

Dale, R. H., Relationship of Groundwater Tides to Ocean Tides: A Digital Simulation Model, Ph.D. Dissertation, University of Hawaii, Honolulu, 150p, 1974.

Edwards, Arthur L., Trump: A computer Program for Transient and Steady-State Temperature Distributions of Multidimensional Systems, Lawrence Livermore Laboratory, Rept. UCRL-14754, Rev. 3, September 1, 1972.

Ferris, J. G., D. B. Knowles, R. H. Brown, and R. W. Stallman, Theory of Aquifer Tests, Geological Survey Water-supply Paper 1536-E, U. S. Gov. Printing Office Washington, 1962.

George, W. O. and F. W. Romberg, Tide producing forces and artesian pressures, Trans. Amer. Geophys. Union, 32, 369-371, 1951.

Grablovitz, G., Sul fenemeno di marea osservatonelle miniere di Dun in Bohemia, Bull. Soc. Adrietica Sci. Naturali Triests, 6, 43, 1880.

Hamming, R. W., Numerical Methods for Scientists and Engineers, 721p, McGraw-Hill, New York, 1973.

Harrison, J. C., New Computer Programs for the Calculation of Earth tides, Cooperative Institute for Research in Environmental Sciences, University of Colorado, Boulder, Colorado, November, 1971.

Klonne, F., Die periodischen schwankengen des wasserspiegels in den inundieten kohlenschachten von Dux in der period von 8 April bis 15 September 1879, Sitzber.Kais. Akad. Wiss., 1880.

Love, A. E. H., Some Problems of Geodynamics, 180p, Cambridge University Press, Cambridge, 1911.

Melchior, P., Sur l'effet des marees terrestes dans les variation de niveau observees dans les puits in particular at sondage de Turnhout (Belgium), Commun. Obs. Roy. Belgique, 108, 7-28, 1956.

Melchior, P., Die Gezeiten in unterirdischen flussigkerten, Erdoel Kohle, 13, 312-317, 1960.

Melchior, P., Earth tides, in Research in Geophysics, vol. 2, edited by H. Odishaw, 183-193, Massachusetts Institute of Technology Press, Cambridge, Mass, 1964.

Melchior, P., The Earth Tides, 458p, Pergamon Press, Oxford, London, 1966.

Morland, L. W., Earth tide effects on flows in horizontal permeable elastic layers connected to wells, Geophys. J. Roy. Astro. Soc., 51(2), 371-385, 1977.

Narasimhan, T. N., A Unified Numerical Model for Saturated-Unsaturated Groundwater Flow, Ph.D. Dissertation, University of California, Berkeley, February, 1975.

Narasimhan, T. N., D. G. McEdwards and P. A. Witherspoon, Results of Reservoir Evaluation Tests, 1976 East Mesa Geothermal Field, CA., Lawrence Berkeley Laboratory, University of California, Rept. LBL-6369, July 1977a.

Narasimhan, T. N., R. C. Schroeder, C. G. Goranson, D. G. McEdwards, D. A. Campbell and J. H. Barkman, Recent Results from Tests on the Republic Geothermal Wells, East Mesa, California, Lawrence Berkeley Laboratory, University of California, Rept. LBL-7017, December, 1977b.

Narasimhan, T. N. and B. Y. Kanehiro, A Note on the Meaning of Storage Coefficient, Lawrence Berkeley Laboratory, University of California, Rept. LBL-8295, January, 1979.

Pekeris, C. L., Note on tides in wells, in Report on Earth Tides, edited by W. D. Lambert, 23-24, U. S. Coast and Geodetic Survey, Spec. Publ. 223, 1940.

Richardson, R. M., Tidal fluctuations of water level observed in wells in east Tennessee, Trans. Am. Geophys. Union, 37, 461-462, 1975.

Rinehart, John S., Alterations of Flow Characteristics within Geothermal Areas by Tidal Forces, University of Colorado, CUMER 75-6, June 1975.

Robinson, T. W., Earth-tides shown by fluctuations of water levels in wells in New Mexico and Iowa, Trans. Am. Geophys. Union, 20, 656-666, 1939.

Stacey, Frank D., Physics of the Earth, 2nd ed., 414p., John Wiley and Sons, New York, 1969.

Swanberg, C. A., The Mesa Geothermal Anomaly, Imperial Valley, California: A Comparison and Evaluation of Results Obtained from Surface Geophysics and Deep Drilling, in Proceedings, Second United Nations Symposium on the Development and Use of Geothermal Resources, Vol. 3, San Francisco, California, May 20-29, 1975.

Takeuchi, H., On the earth tide of the compressible earth of variable density and elasticity, Trans. Am. Geophys. Union, 31, 361-689, 1950.

Theis, C. V., Earth tides as shown by fluctuations of water level in artesian wells in New Mexico, Intern. Union Geodesy and Geophysics, Washington, D. C. (U. S. Geological Survey open-file report, 10p.), 1939.

Todd, David K., Groundwater Hydrology, John Wiley and Sons, New York, 1959.

Werner, P. W., and D. Noren, Progressive waves in nonartesian aquifers, Trans. Am. Geophys. Union, 32(2), 230-244, 1951.

Williams, P. L., Dr. R. Mabey, A. A. R. Zohdy, H. Ackerman, D. B. Hoover, K. L. Pierce and S. S. Oriel, Geology and Geophysics of the Southern Raft River Valley Geothermal Area, Idaho, U.S., 1273-1282, Proc. Second United Nations Symp. on the Development and Use of Geothermal Resources, San Pancisco, California.

Witherspoon, P. A., T. N. Narasimhan and D. G. McEdwards, Results of Interference Tests from Two Geothermal Reservoirs, Lawrence Berkeley Laboratory, University of California, Rept. LBL-4484, August, 1976.

Young, A., Tidal Phenomena at inland boreholes near Craddock, Trans. Roy. Soc. South Africa, 31, 61-106, 1913.

A DRAWDOWN AND BUILD-UP TYPE CURVE FOR INTERFERENCE TESTING

H. J. Ramey, Jr.
Stanford University
Stanford, California

ABSTRACT

Interference testing is a powerful method for in situ measurement of transmissivity, storativity, and quantitative identification of anisotropy and system boundaries. The log-log type-curve matching procedure can be used for analysis of interference data taken during production or drawdown. Once production is terminated, observation well pressures return toward the initial pressure. This recovery, or pressure build-up, has been interpreted by differencing the extrapolated drawdown and measured build-up. This procedure extracts the "injection" well which causes the build-up. A new type curve for both the drawdown and build-up portion of the test has been prepared. Application of the new type curve shows that the older differencing procedure may obscure detection of system boundaries. The principal of the build-up type curve may be extended to other flow problems.

INTRODUCTION

The initial assessment of geothermal reservoirs usually has two main objectives. One is determination of the deliverability from the reservoir, and the other is estimation of the reserves, or the economically producible amount of steam in the system. Many geothermal reservoirs are complicated by the fact that neither the porosity-thickness product nor producible area are known, either early in the life or after extended production. One means of determining the deliverability is a pressure transient test. Pressure transient tests can be conducted in a short period of time, and early in the life of a geothermal development. However, estimation of steam reserves requires an extended period of production with observation of mean reservoir pressure at various stages of production. Material and energy balance performance matching with a detectable decline in pressure following production is the minimum information for performance matching. Thus it is necessary to produce a reservoir for an extended period of time before performance matching can be accomplished with acceptable risk.

The dilemma is that single-well pressure tests of fairly short duration are needed to provide accurate information on deliverability (permeability thickness or transmissivity) and well condition, while long-term production testing is required to establish reserves. Fortunately, an interference test is a type of pressure transient test that can be accomplished in a reasonable period of time, and yet provide important information concerning apparent reserves early in the life of a geothermal development. At least two wells are required for an interference test. More than two wells is desirable.

The main problem with single-well pressure transient tests is that distances in the reservoir are measured in units of the wellbore radius. A test of an individual well can yield important information concerning the condition of the well, the formation conductivity, and drainage boundaries of the well. However, long periods of production are required prior to pressure build-up testing for boundaries to be evident, when distances are measured in units of wellbore radius. An alternate procedure is to observe pressure effects transmitted between two or more wells. This kind of test is called an interference test. The theory of interference testing was explained by C.V. Theis (1935). A modern discussion of interference testing procedures has been presented by Earlougher (1977). There are many recent publications on this important subject in both the groundwater and the petroleum engineering literatures. An example of application of interference testing to geothermal systems has been published by Chang and Ramey (1979).

One simple basis for interference test analysis is the continuous line source solution. This model assumes that a single well is produced at a constant rate in an infinitely large slab reservoir of constant properties. The pressure effects caused by the producing well may be observed at one or more distant wells, which are not produced but used simply as pressure observation stations. The solution to this problem can be displayed on a piece of log-log coordinate paper. Figure 1 is a type-curve for this problem as used commonly in the petroleum literature. Figure 1 presents the analytical solution for the conventional line-source well (exponential integral solution).

$$p_D = -\frac{1}{2}\,\mathrm{Ei}\left(-\frac{r_D^2}{4t_D}\right), \tag{1}$$

where

$$p_D = \frac{kh}{141.2\,qB\mu}(p_i - p_{r,t}) \tag{2}$$

$$r_D = r/r_w \tag{3}$$

$$t_D = \frac{0.000264kt}{\phi\mu c r_w^2} \tag{4}$$

In Eqs. 2-4, English engineering units are used: permeability in millidarcies, lengths in feet, pressures in psi, viscosity in centipoise, flow rates in stock tank barrels per day, time in hours, porosity in fraction of bulk volume, formation volume factor in reservoir volumes per standard volume, and total system effective compressibility in reciprocal psi.

Figure 1 presents a dimensionless pressure which is directly proportional to an observed pressure drawdown versus the ratio of a

dimensionless time to the dimensionless distance between the production and observation well squared. The dimensionless time is directly proportional to real time, and the dimensionless distance is directly proportional to real distance. An important characteristic of the logarithmic scale is that quantities proportional to the plotted scale are simply displaced linearly along the scale. Thus it is possible to graph the field data observed in an interference test as a pressure drop on the ordinate versus time on the abscissa, and make a direct comparison with the analytic solution represented by Fig. 1. This procedure is called log-log type-curve matching, and has been outlined in detail in many references, such as Earlougher (1977).

Once a set of field data has been matched with the line-source type curve, it is possible to equate the pressure difference point with the dimensionless pressure from the type-curve to make quantitative calculations. In the usual case, the net formation thickness (h), the flowrate (q), the formation volume factor (B), and the viscosity (μ) of the produced fluid would be known. The objective of the pressure matchpoint would be calculation of the effective permeability to the flowing phase (k). From the time matchpoint, it would be possible then to calculate the porosity-compressibility product. In the ordinary case, the porosity would be known, and thus it would be possible to obtain a check on the average compressibility of the formation and fluid. An alternative would be to determine the in-place porosity under the assumption that the average compressibility of the rock-fluid system were known. This step is frequently done in petroleum engineering work as a check upon porosity derived either from core analyses or from well logging methods. In petroleum engineering application, one frequently obtains both effective permeabilities and porosities which agree with information known from other sources. For example, the effective permeability will frequently agree with that obtained from a pressure buildup test on a single well, while the porosity obtained from an interference test will frequently agree with porosities obtained from core analyses.

In the case of interference testing of geothermal systems, analysis is often more complex. In the use of the pressure matchpoint, it is often observed that the net formation thickness for the geothermal system is not known. This may be a result of the fact that the formation has not been fully penetrated by drilling, or that the system is fractured and characteristics are not readily apparent. In this case, the product of permeability and formation thickness is obtained, a useful quantity for deliverability and well condition determination. In the case of the time matchpoint, frequently the porosity is not known. Since the thickness also is not known, there is a dilemma as to the kind of useful calculation available from the time matchpoint. Fortunately, important and useful information can be obtained from the time matchpoint. The product of porosity, compressibility, and thickness can be computed. This product is sufficient to estimate the mass of geothermal fluid in the system per unit area. An estimate of the system area and recovery factor for the fluid is then sufficient to make an initial estimate of the capacity of the system.

The result obtained by this method is definitely preliminary, and should be checked by material-energy balance performance matching as production follows. Several uncertainties have been identified which render the results of the test uncertain. The Theis line-source method depends on a single-phase fluid flow model. There may be carbon dioxide or steam caps in geothermal systems. In this case, the compressibility of the system may be close to that of gas, rather than liquid. Another problem is that geothermal systems are often fractured systems. Recently, Deruyck (1980) studied interference testing in fractured (two-porosity) systems, and Kucuk (1980) has offered a similar study. It appears that this sort of system should be studied further.

Both show that two-porosity system interference results may resemble the Theis curve for a homogeneous system, but the parameters which result from type-curve matching can be uncertain.

We have established the potential importance of an interference test in the early evaluation of geothermal steam systems. Because an interference test involves producing a geothermal system from an initially static condition for some time, it is obvious that the test must eventually be terminated. When this happens, there is an opportunity to obtain additional information as pressures return toward the initial state. Most discussions of interference testing deal mainly with the pressure drawdown period. But the ensuing shut-in period, when pressures recover toward the initial state, can provide important information concerning drainage boundaries of the system. One discussion of this kind of procedure was presented by Ramey in 1975. In general, the procedure involves extrapolating the initial drawdown portion of the test and differencing the pressure recovery from the extrapolation from the drawdown. The result is extraction of the effect of an injection well which caused the pressure shut-in. An example of this kind of differencing is given by Ramey (1975). Fortunately, it is possible to prepare a new log-log type-curve which contains both the drawdown and build-up portions of the test on a single graph.

Pressure-Build-up Type Curves

We consider that a well is produced at constant rate for a period of time, t_p, and then shut in. During the initial drawdown portion, the pressures at adjacent shut-in observation wells are represented by Fig. 1 and Eqs. 1-4. After the producing well is shut in, it is necessary to employ the principle of superposition to generate a relationship which describes the shut-in period properly. This results in:

$$\frac{kh}{141.2\ qB\mu}\left(P_i - P_{ws_{r,t+\Delta t}}\right) = P_D(r_D, t_p+\Delta t) - P_D(r_D, \Delta t) \qquad (5)$$

Equation 5 can be evaluated generally by replacing the dimensionless pressures by their appropriate line-source values for a particular producing time, t_p, and a range of shut-in times, Δt. Fig. 2 presents such a graph. The format is similar to Fig. 1, except the pressure build-up lines are shown as a family of curves dropping below the line-source solution, each displaying the parameter of dimensionless producing time divided by the dimensionless distance squared.

Figure 2 is the general solution for both pressure drawdown and pressure build-up measured at a shut-in observation well caused by a well producing at a constant rate for time, t_p. Obviously, a single type-curve match between field data and Fig. 2 can be made with the match involving both the production and the build-up data.

Field Example

In 1975 Ramey presented several sets of pressure drawdown and build-up interference data. We will select one example from this reference for purposes of discussion. The example will be the production of well 5-D with an interference effect measured in well 1-E, 700 ft away from well 5-D. This test actually involved injection rather than production, but the principle is the same. The injection into well 5-D caused a pressure rise in 1-E, and after shut-in, the pressure rise declined, approaching the initial pressure at an extended period of shut-in.

The details of the field example will not be given completely here. The results for well 1-E were selected by Ramey in 1975 to illustrate the principle of differencing pressure build-up data to extract the effect of the well causing the shut-in. As found in this study, well 1-E appeared to provide a reasonable match with the line-source solution for both the drawdown and pressure build-up data. (See Wenzel, 1942, for rate change differencing.)

Table 1 provides the field data for the example interference fall-off test at well 1-E. Fig. 3 is a log-log type curve of both the drawdown and build-up pressure drops as a function of the total test time. This sort of field data graph can be matched directly with the new drawdown-build-up line-source type-curve presented in Fig. 2. Fig. 4 is an illustration of the kind of match that can be obtained between the well 1-E example and the new drawdown-build-up type curve. In the match shown in Fig. 4, the same matchpoint found by Ramey in 1975 has been maintained. It is evident by comparing the field data with the new type-curve that although the drawdown portion matches the line-source reasonably well, the build-up portion of the curve after shut-in does not appear to match the computed buildup curves in Fig. 2 ideally. This may represent an indication of some sort of boundary effect becoming evident during the build-up portion of the test.

On the other hand, in the 1975 publication by Ramey, the differencing procedure was used to analyze the pressure build-up portion of the test. The build-up portion was found to match the line-source solution reasonably well. We suspect that the differencing procedure involves enough trial and error that data may be forced to match the line-source even when the field data are not a good match for the line-source solution. On the other hand, a number of other field cases have been found which appear to provide reasonably good matches with the new drawdown-build-up type curve shown in Fig. 2.

ACKNOWLEDGMENT

This work was conducted at Stanford University under DOE Grant # LBL Subcontract # 1673500.

REFERENCES

1. Chang, C.R.Y., and Ramey, H.J., Jr.: "Well Interference Test in the Chingshui Geothermal Field," Proc., Fifth Workshop on Geothermal Engineering, Stanford University, Dec. 12-14, 1978, 71.

2. Deruyck, B.G.: "Interference Well Test Analysis for a Naturally Fractured Reservoir," MS report, Stanford University, June 1980.

3. Earlougher, R.C.: Advances in Well Test Analysis, Society of Petroleum Engineers of AIME Monograph No. 5 (1977).

4. Kucuk, F.: "Transient Flow in Naturally Fractured Reservoirs and Its Application to Devonian Gas Shales," paper SPE No. 9397, presented at the 55th Annual Fall Meeting, SPE of AIME, Dallas, Texas, Sept. 21-24, 1980.

5. Theis, C.V.: "The Relation Between the Lowering of the Piezometric Surface and the Rate and Duration of Discharge of a Well Using Groundwater Storage," Trans., AGU (1935), 16, 519.

6. Ramey, H.J., Jr.: "Interference Analysis for Anisotropic Formations--A Case History," Jour. Pet. Tech. (Oct. 1975), 1290.

7. Wenzel, L.K.: "Methods for Determining Permeability of Water Bearing Materials," Geol. Survey Water Supply Paper 887, US Government Printing Office, Washington, 1942, 93.

TABLE 1--FIELD EXAMPLE INTERFERENCE FALL OFF
Well 1-E

Total Time, (hours)*	Δt, (hours)	Δp, (psi)**
27.5		3
47		5
72		11
95		13
115	14	16
125	24	16
142	41	13
192	91	10
215	114	10
240	139	6
295	194	5.8

*t_p + Δt after shut-in at 101 hours
**Actual measured pressure rise

q = 115 b/d
B = 1 res b/Stb
μ = 1 cp
r = 700 ft
h = 25 ft
t_p = 101 hrs

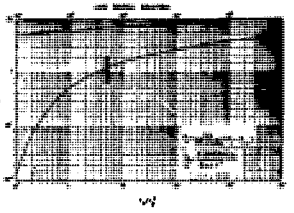

Fig. 1--The Continuous Line-Source Solution Type Curve

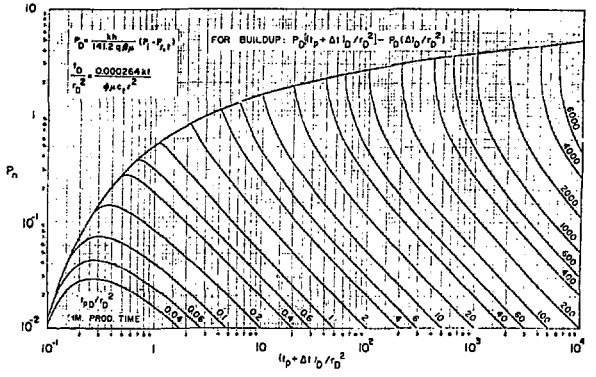

Fig. 2--Drawdown and Buildup Interference Test for a Line Source Well

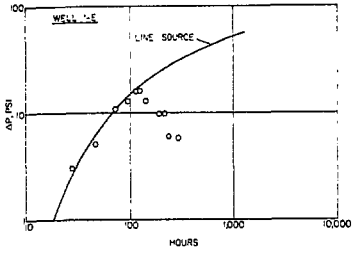

Fig. 3--Field Data Graph for Well 1-E

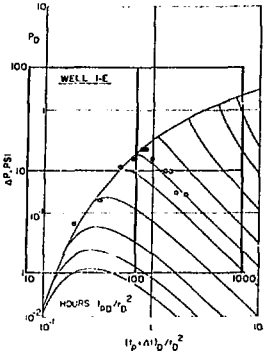

Fig. 4--Type-Curve Match for Well 1-E

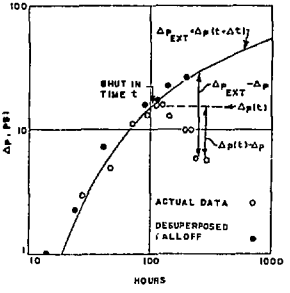

Fig. 5--Field Example Interference Falloff Analysis, Well 1-E

ABSTRACT

MULTIPLE PRESSURE MEASUREMENTS AND WATER SAMPLES IN SMALL DIAMETER DRILL HOLES

S. D. Patton and W. H. Black
Westbay Instruments, Ltd.
West Vancouver, B.C., Canada

Three different types of hydrologic testing in drill holes are noted: 1) packer testing during drilling, 2) packer testing after drilling, and 3) testing and monitoring in permanent casing systems. The Profiler is an example of the first type and MP and CPI casing systems are examples of the third type. The paper describes the development of the Profiler and casing systems which are compatible with wireline drill holes from 60 to 100 mm (2-3/4 to 4") in diameter.

Field installation of the casing systems and methods of obtaining pressure measurements and water samples are described. These techniques include floating the casing into the hole, inflation of packers, backfilling, decontamination pumping using pumping ports, and the use of probes for water sampling and pressure measurements.

Test results from the Profiler and from MP casing installations are presented in the form of diagrams of depth vs. pressure head with depths ranging from 30 to 820 m (100 to 2700 ft). Pressure measurements and pressurized water samples have been obtained from as many as 18 ports in the same drill hole. The paper concludes with a discussion of the advantages and disadvantages of the three types of hydraulic testing in drill holes.

PRESSURE MEASUREMENTS IN LOW PERMEABILITY FORMATIONS

A. F. Veneruso and T. D. McConnell
Sandia National Laboratories
Albuquerque, NM 87185

ABSTRACT

This paper examines the performance requirements and identifies candidate hardware implementations for pressure instrumentation that is needed to provide well test data in low permeability formations. Low permeability values are typically defined to be less than 1 microdarcy and are usually encountered in hard rock formations, such as granite, that are of interest in hot dry rock geothermal, deep exploration drilling, and fluid waste disposal. Groundwater flow in these "tight" formations has been shown to be dominated by flow-through fractures rather than through the formation's intrinsic permeability. In these cases, we cannot use the familiar form of Darcy's law or the usual dimensionless coefficients to estimate the expected scale factors and dynamic responses necessary to properly select and set up the wellbore pressure instrument. This paper shows that the expected instrument responses can be estimated using some recent work by Wang, Narasimhan, and Witherspoon. This paper further describes the minimum electronic capability that the downhole pressure instrument must have in order to provide the required measurement resolution, dynamic range, and transient response. Three specific hardware implementations are presented based on the following transducers: a quartz resonator, a capacitance gauge, and a resistance strain gauge.

INTRODUCTION

Reliable measurements from downhole pressure instruments are essential to provide the reservoir engineer with sufficient data to analyze a reservoir's performance and project future production under various modes of operation. Downhole pressure data is also essential in determining the condition of production and injection wells and their associated formations. In recognition of the importance of pressure measurement to well testing, a significant body of knowledge has been developed to assist both instrumentation and reservior engineers with the design, operation, and interpretation of this instrumentation. However, as new well testing regimes are encountered, it is important to reexamine the basic assumptions and interpretations made concerning pressure instruments to avoid incorrect analyses and conclusions.

As the focus of this symposium demonstrates, there is keen interest in low permeability formations such as those encountered in deep exploration drilling, hot dry rock geothermal, and fluid waste disposal. In these tight formations, permeabilities of less than one microdarcy are typical, whereas, in oil and in geothermal formations the permeability is usually greater than one millidarcy. Groundwater flow in tight formations has been shown to be dominated by flow through fractures rather than through the formation's intrinsic permeability.[1] In these cases we cannot use Darcy's law or the usual dimensionless coefficients to estimate the scale factors and dynamic responses necessary to properly select and operate wellbore pressure instruments. Also, research into low permeability formations may require certain improvements to be made in pressure instrument performance. Each of these issues is explored in the following paragraphs. First, as a basis for comparison, a quick review will be made of pressure measurement in moderate permeability formations, then the behavior of low permeability formations will be examined, and finally the key performance characteristics of four candidate pressure instruments will be reviewed.

PRESSURE INSTRUMENTS FOR MODERATELY PERMEABLE FORMATIONS

The mathematical model describing the flow of fluid in a moderately permeable formation is described by the well-known diffusivity equation[2]:

$$\nabla^2 p = \frac{1}{\kappa} \frac{\partial p}{\partial t} \qquad (1)$$

where κ is the diffusivity. In radial coordinates, Equation 1 is usually expressed as

$$\frac{\partial^2 p}{\partial r^2} + \frac{1}{r} \frac{\partial p}{\partial r} = \frac{1}{\kappa} \frac{\partial p}{\partial t} \qquad (2)$$

where

$$\kappa = \frac{k}{\phi \beta \mu} \ (m^2 s^{-1}) \qquad (3)$$

and k = formation permeability (m^2)

ϕ = formation porosity (dimensionless)

β = fluid compressibility ($m\ s^2\ kg^{-1}$)

μ = fluid viscosity ($kg\ m^{-1}\ s^{-1}$)

The following steady-state radial flow equation[2] completes this simple model:

$$q = \frac{2\pi kh\,(p_e - p_w)}{B\mu \ln(r_e/r_w)} \qquad (4)$$

where

h = formation thickness (m)

B = formation volume factor (dimensionless)

r_e = radius into the formation (m)

r_w = radius of wellbore (m)

p_e = pressure at radius r ($kg\ m^{-1}s^{-2}$)

p_w = pressure in wellbore ($kg\ m^{-1}s^{-2}$)

q = flow rate (m^3s^{-1})

Equations 2, 3, and 4 are typically used by instrumentation and reservior engineers to design well tests and to determine the types of pressure gauges required and the setup of those gauges in terms of the maximum pressure anticipated, the resolution and the time response requirements. For example, Chapter 13 of Reference 2 presents numerous exercises in which typical oil field values for the above parameters are used to determine the instrument's performance requirements. Figure 1 is taken from Reference 2 to indicate a typical pressure-time response in a constant flow rate test.

PRESSURE INSTRUMENTS FOR LOW PERMEABILITY FORMATIONS

Groundwater flow in tight formations has been shown to be dominated by fracture flow rather than flow through the formation's intrinsic permeability. In these circumstances, Equations 1, 2, and 3 are modified through the use of an equivalent permeability[3] that is related to the fractures present. As an example for the ideal case of a single horizontal fracture, Equation 2 is written with

$$\kappa = \frac{k}{\rho\mu} \qquad (5)$$

where

$$k = \frac{(\text{Fracture Width})^2}{12} \qquad (6)$$

Reference 2 gives an excellent analysis of pressure transient response to pulse packer testing in a low permeability, fracture dominated formation. For a given applied pressure pulse, P_N, Figures 2 and 3 (taken from Reference 3) show the response to pulse testing with a normalized ordinate pressure:

$$P_N(t) = \frac{P_{actual}}{P_{applied}} \qquad (7)$$

and a dimensionless wellbore leaking capacity factor, u, that is proportional to the ratio of the wellbore fracture contact area to the wellbore test volume, or equivalently

$$u = \frac{2 \text{ Fracture Width}}{\text{Wellbore's Test Length (or distance between packers)}} \qquad (8)$$

Note that because of the low permeabilities (usually less than 1 microdarcy) in these tight formations, the pressure time history is characterized by extremely large ranges of test time and smaller resolution values when compared to the usual pressure testing in moderate permeability formations. In general, the specifications required here are every bit as stringent, if not more so, than those required for pressure instruments in moderate permeability formations. To obtain useful data, such as given in Figures 2 and 3, the pressure instrument must be appropriately specified; the key parameters of interest are given in Table 1.

In this context, accuracy or measurement precision is defined as the maximum value of the uncertainty in pressure measurement over the entire full scale range of the instrument. Resolution or measurement sensitivity is defined as the smallest (worst case) detectable change in the pressure measurement over the instrument's range. As an example, assume an instrument with the following ratings:

$$P_{max} = 1000 \text{ psi}$$

$$\frac{P_{acc}}{P_{max}} = \pm\ 1\% \text{ of full scale reading}$$

$$\frac{\Delta P_{res}}{P_{max}} = 0.1\%$$

Suppose a particular measurement is obtained of $P_{meas} = 832$. Then the actual pressure is:

$$P_{actual} = 832 \pm \left(\frac{1}{100} \times 1000\right) \text{ psi}$$

$$= 832 \pm 10 \text{ psi}$$

and, if a subsequent change in pressure takes place, we can be certain the measured change is detectable if it is greater than

$$P_{res} = \frac{\pm 0.1}{100} \times 1000 \text{ psi} = \pm 1 \text{ psi}$$

Added to the characteristics listed in Table 1 is the need to establish the instrument's measurement stability over time and over temperature. Measurement drift with time is an important specification because, as shown in Figures 2 and 3, test times can easily range out to 10^6 seconds (11.6 days). Testing can be done at shorter intervals but only at the expense of requiring greater measurement resolution.

Measurement drift with temperature is another important specification tht is often overlooked. In formations of interest, temperatures can range up to 300°C. However, for typical instruments, temperature sensitivities can range from ± 0.01 psi/°C to 1 psi/°C.

If a measurement resolution of ± 0.1 psi is desired then it becomes important to also specify the temperature stability of the instrument--especially if wellbore temperatures are expected to vary during the test. Often it is not sufficient to know only the instrument's temperature. As we shall discuss later, even small temperature gradients on an instrument can result in dramatic errors in measurement.

INSTRUMENT SPECIFICATION GOALS

Table 1 lists a set of pressure instrument specifications that are proposed as design goals for measurement in tight formations. The preceeding analytical results were used along with a range of expected reservoir conditions (i.e., $10^{-8} < a < 10^{-3}$) to provide measurements that would satisfy the interpretation made in Reference 3. Commercially available pressure transducer specifications are listed in Table 2 (from Reference 2).

Inspection of Table 2 indicates that none of the transducers currently available satisfies all the requirements put forth in Table 1. Some may satisfy one requirement or another but none of the commercial instrument's advertised specifications even address all of the needs. Accuracy has not been called out as such because it is not a prime consideration in that it can be determined by the instrument's stability, resolution, and correction for nonlinearities.

There will be specific instances where a particular instrument will satisfy the immediate needs. For instance, an interference test at a moderate temperature would not have any relatively abrupt temperature changes and the Hewlett Packard[4] (HP) model 2811-P pressure gauge system combined with a temperature probe would meet the requirements.

Figure 4 shows the basic element of the generic types of pressure instruments: the resistance strain gauge, the capacitance type transducer, and the two quartz crystal transducers. The HP instrument[4] operates on the principal that a quartz crystal resonator's natural frequency can be changed by applying stress. Two types of resonators are in common use, the shear mode of crystal resonator used in the HP gauge, and the transverse mode used in a gauge built by Paroscientific.[5] The advertised performance characteristics of the HP and Paros gauges are given in Table 3 along with representative strain and capacitance gauges.

Figure 5 indicates the activities that are underway at Sandia to upgrade these transducers for geothermal and geopressure applications; Figures 6 through 8 summarize the key elements of those projects.

As an example of some specific design and development factors, we will briefly review our activity in the quartz transducer area. Over the past 2 years, considerable work has been done[6-8] at Sandia to understand the temperature and pressure behavior of quartz-resonator-type pressure transducers so that they may be applied to geothermal logging.

Ideally, the crystal's resonant frequency should be sensitive to pressure or stress and independent of temperature. Unfortunately, temperature has a very large effect. Figure 9 shows a family of curves of frequency versus temperature for various crystallographic rotations of the common AT-cut crystal. As can be seen, most of the curves have one or two points where the slope is zero. For a particular crystal, this point is referred to as the turning point, and, if the crystal were operated very close to this temperature, very small frequency deviations could be achieved for a small change in temperature.

Figure 10 shows an AT-cut which has been rotated beyond the limit of Figure 9 to achieve a turning point at 275°C. This curve is contrasted with the rotated X-cut, showing the significantly reduced temperature effect of this new cut.

In practice, to achieve the required resolution, it is necessary to have two closely matched crystals, one of which is used to provide a reference frequency to compensate for temperature. Even so, Figure 11 shows that for good pressure resolution the two crystals must be within a few millidegrees of each other or must both be within a few degrees of the turning point.

Figure 12 displays the requirements and approaches being taken by our project to incorporate the above knowledge into the technology applicable to quartz pressure instruments.

CONCLUSIONS

The pressure time history of well tests in low permeability formations is characterized by extremely large ranges of test time. This requires more stringent instrument resolution and stability than the usual pressure testing in moderate permeability formations. It is also important to consider the temperature gradient sensitivity of the instrument; even small temperature gradients in a well test can result in dramatic errors in measurement.

None of the pressure transducers currently available satisfies all the requirements for the entire range of well testing expected in low permeability formations. Some transducers may satisfy some of the requirements, but none of the commercial instruments' advertised specifications even address all of the needs. For example, in cases where there are no abrupt temperature changes, the HP model 2811-B quartz resonator pressure gauge combined with a temperature probe meets most of the performance requirements. However, this instrument has exhibited large errors in the presence of even moderate temperature gradients.

Using the measurement needs identified by reservoir engineers and an understanding of the function and performance limitations of existing pressure instruments, a development project is described that is directed toward correcting the technical deficiencies. The existing instruments are being upgraded with more stable components such as a rotated X-cut quartz crystal for the resonator-type gauges; special electronics are being designed to improve the stability and output signal strength of strain gauge pressure sensors; and improved materials and design configurations are being investigated to upgrade the capacitor type pressure instrument.

REFERENCES

1. Brace, W. F., J. B. Walsh, and W. T. Frangos, "Permeability of Granite Under High Pressure" J. Geophysical Research 73, No. 6, pp. 2225-2236; 1968.

2. Earlougher, R. C. "Advances in Well Test Analysis," Monograph Vol. 5, Society of Petroleum Engineers, New York and Dallas, 1977.

3. Wang, J. S. Y., T. N. Narasimhan, C. F. Tsang, and P. A. Witherspoon, "Transient Flow in Tight Fractures," Invitational Well-Testing Symposium Proceedings, LBL-7027, UC66, TID-4500-R66, Lawrence Berkeley Laboratory, October 19-21, 1977.

4. Karrer, H. E., and J. Leach, "A Quartz Resonator Pressure Transducer," IEEE Trans. Ind. Elec. and Control Instr. IECI-16, p. 44 (1969).

5. Paros, J., "Digital Pressure Transducers," Measurements and Data, Issue 56, Vol. 10, No. 2, March - April 1976.

6. Eernisse, E. P., "Quartz Resonator Pressure Gauges: Design and Fabrication Technology," SAND78-2264, Sandia Laboratories, January 1974.

7. Eernisse, E. P., "Rotated X-Cut Quartz Resonators for High Temperature Application," Proc. 32rd Annual Symposium on Frequency Control, 1978.

8. Eernissee, E. P. "Temperature Dependence of the Force Frequency Effect for the Rotated X-Cut., Proc. 33rd Annual Symposium on Frequency Control, 1979.

Table 1. Pressure instrument requirements for low permeability reservoirs.

• PRESSURE	$P_{max} \geq 7500$ psi
• RESPONSE SPEED	$\left\|\frac{dp}{dt}\right\| \geq 10 \frac{psi}{sec}$
• RESOLUTION	$\|\Delta p\| \leq 0.01$ psi
• TEMPERATURE	$T_{max} \geq 200°C$
• TEMP. STABILITY	$\left\|\frac{\Delta P_{err}}{\Delta Temp}\right\| \leq 0.01 \frac{psi}{°C}$
• TEMP. GRADIENT	$\left\|\frac{\Delta P_{err}}{\Delta Temp/\tau}\right\| \leq 1 \frac{psi}{°C/sec}$
• TIME STABILITY	$\left\|\frac{\Delta P_{err}}{\Delta time}\right\| \leq 10^{-8} \frac{psi}{sec}$

Table 2.

Down-hole pressure gauges (from Earlougher, "Advances in Well Test Analysis")

Section 1: Self-Contained Wireline Gauges

Gauge	Maximum Pressure[1] (psi)	Sensitivity, Percent of Full Scale	Accuracy, Percent of Full Scale	OD (in.)	Approximate Length[2] (in.)	Maximum Service Temperature[3] (°F)	Type Pressure Element[4]	Maximum Time Down Hole[5] (hours)	Approximate Chart Size, $p \times t$ (in.)
Amerada RPG-3	25,000	0.05	0.2	1.25	77	650	B	360	2 × 5
Amerada RPG-4	25,000	0.056	0.2	1	76	650	B	144	1.8 × 5
Amerada RPG-5	20,000	0.05	0.25	1.5	20	450	B	120	2 × 5
Kuster KPG	25,000	0.05	0.2	1.25	66	700	B	360	2 × 5
Kuster K-2	20,000	0.05	0.25	1	41	500	B	120	2 × 3
Kuster K-3	20,000	0.042	0.25	1.25	43	500	B	120	2.4 × 4
Kuster K-4	12,000	0.067	0.25	0.75	42	450	B	?[2]	1.5 × 2.5
Leutert Precision Subsurface Pressure Recorder	6,400	0.005	0.025	1.25	139	300	P	360	9.8 × 3.1
Leutert Precision Subsurface Pressure Recorder	10,000	0.005	0.025	1.42	139	300	P	360	9.8 × 3.1
Sperry-Sun Precision Subsurface Gauge	16,000	0.005	0.05	1.5	108	300	B	672[6]	2.3 × 7.1

Section 2. Permanently Installed, Surface-Recording Gauges

Gauge	Maximum Pressure[1] (psi)	Sensitivity, Percent of Full Scale	Accuracy, Percent of Full Scale	OD (in.)	Approximate Length[2] (in.)	Maximum Service Temperature[3] (°F)	Type Pressure Element[4]	Type Signal[7]	Type Conductor[8]
Amerada EPG-512[9]	10,000	0.002	0.02	1.25	13	300	D	F	S
Amerada SPG-3	25,000	0.04	0.2	1.25	49	350	B	R	S
Flopetrol	10,000	0.001	0.06	1.42	29	257	S	F	S
Lynes Pressure Sentry MK-9PES	10,000	0.2	0.2	1.5	33	300	B	B	S
Maihak SG-2	5,700	0.1	1.0	3.54	11.54	176	D	F	S
Maihak SG-5	5,700	0.1	1.0	1.65	8.43	176	D	F	S
Sperry-Sun Permagauge	10,000	0.005	0.05	1.66	120 or 240	no max	G	G	T
BJ Centrilift-PHD System[10]	3,500		3[11]	N/A[12]	N/A[12]		B	C	P

Section 3. Retrievable Surface-Recording Gauges

Gauge	Maximum Pressure[1] (psi)	Sensitivity, Percent of Full Scale	Accuracy, Percent of Full Scale	OD (in.)	Approximate Length[2] (in.)	Maximum Service Temperature[3] (°F)	Type Pressure Element[4]	Type Signal[7]	Type Conductor[8]
Amerada EPG-512[9]	10,000	0.002	0.02	1.25	13	300	Q	F	S
Amerada SPG-3	25,000	0.04	0.2	1.25	49	350	B	R	S
Flopetrol[13]	10,000	0.001	0.06	1.42	29	257	S	F	S
Hewlett Packard HP-2811B	12,000	0.00009[14]	0.025[15]	1.44	39	302	Q	F	S
Kuster PSR	5,000	0.04	0.02	1.38	36	212	Q	F	S
Lynes Sentry MK-9PES	10,000	0.2	0.2	1.5	33	300	B	B	S
Maihak SG-3	5,700	0.1	1.0			176	D	F	S
Sperry-Sun Surface Recording	15,000	0.006	0.05	1.5	72	300	B	D	S

*Other gauges are available — no endorsement is implied by inclusion in this table. Data are from information supplied by the manufacturer and other sources believed to be reliable, although we have been careful in assembling this table, neither the author nor SPE-AIME can guarantee accuracy of the data supplied. The reader should contact the manufacturer for specifics. Blank values could not be obtained by the author.

1. Normally, elements are available in several ranges, with the lowest being about 0 to 500 or 0 to 1,000 psi.
2. Length may vary depending on tool configuration; value is approximate nominal length without weight sections.
3. Normally, temperature above which gauge cannot be used, not maximum temperature for normal calibration.
4. B — Bourdon tube
   D — Diaphragm
   G — Gas chamber with transducer at surface
   P — Rotating piston
   Q — Oscillating quartz crystal
   S — Strain gauge
5. Time depends on clock chosen. Clocks normally come in several ranges, starting as low as about 3 hours.
6. Clock is electronic without mechanical linkage to recorder.
7. B — Binary signal
   C — Current
   D — Digital
   F — Frequency
   G — Gas column to surface
   R — Resistance
8. P — Normal power cable for pump, no special conductor
   S — Single-conductor armored cable, ground return
   T — ¼-in.-OD steel tubing
9. Also measures temperature to an accuracy of 0.1 °F and a sensitivity of 0.01 °F.
10. Part of the BJ Centrilift submersible pump. Gauge is an integral part of the motor assembly.
11. Approximately 3 percent of reading.
12. Imbedded in pump motor assembly.
13. Flopetrol has under development a slick-line retrievable surface-recording gauge. The gauge is set in a side pocket mandrel; a conductor cable goes from the mandrel to the surface on the outside of the tubing.
14. Sensitivity is constant across the entire pressure range: 0.01 psi with nominal 1-second count time, 0.001 psi with nominal 10-second count time.
15. Accuracy, if temperature is known within 1°C: ±0.5 psi to 2,000 psi; ±0.025 percent of reading above 2,000 psi.

Table 3. Manufacturers' specifications for three types of pressure gauges.

Specification	Hewlett Packard Quartz Pressure Tool	GRC Capacitive Pres/Temp Tool	Paros Quartz Pressure Gage	CEC Pressure Strain Gage
Max Pressure (psi)	11,000	10,000	5,000	10,000
Accuracy (±%)	.025①	.05	--	②
Resolution (±%)	.0001	.01	--	②
Hysteresis & non-repeatability (±%)	.004	.02	0.02	0.25
Operating Range (°F)	32 to 302	32 to 300 (calibrated)	-65 to 225	75 to 400 (compensated)
Thermal Shift (%/°F)	③	0.005③	.004	0.02
Sensitivity to Thermal Shift Rate (%/°F/min)	--	.0075	--	--

① Requires that temperature is known to ± 1.8°F

② Hysteresis and nonrepeatability include accuracy and resolution

③ Thermal shift is corrected to obtain indicated accuracy

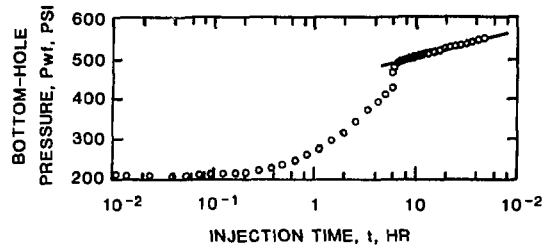

Figure 1. Calculated injectivity pressure response for Example 13.2 in Ref. 2.

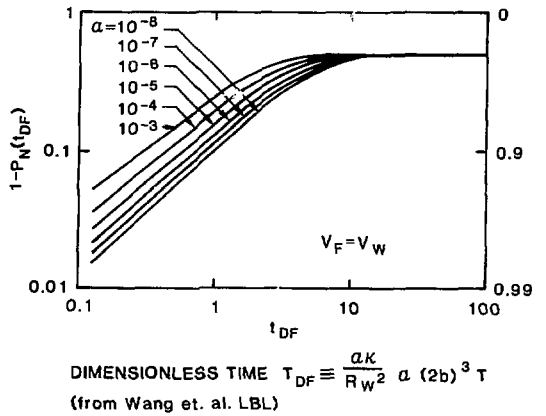

Figure 2. Type curves at early time for a finite fracture volume (from Earlougher, Ref.2).

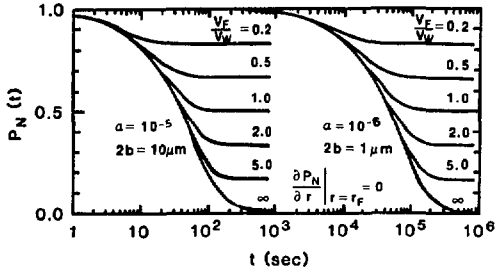

CLOSED FRACTURE BOUNDRY

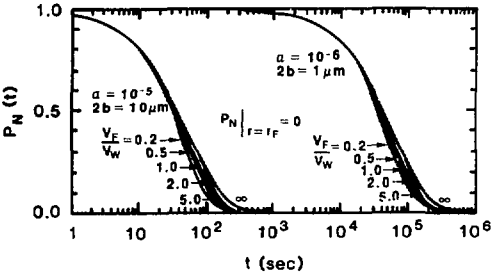

OPEN FRACTURE BOUNDRY

$V_F/V_W \equiv$ FRACTURE-WELLBORE VOLUME

$2b \equiv$ FRACTURE WIDTH

$a \equiv$ DIMENSIONLESS LEAKING CAPACITY

Figure 3. Normalized pressure decays (from Wang et al., Ref. 3).

RESISTIVE STRAIN GAUGE–Resistor bridge pattern on diaphragm changed by deflection.

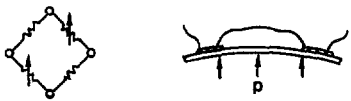

$\frac{\Delta \Omega}{\Delta p}$ (CEC)

CAPACITIVE TRANSDUCER– Capacitance changed by deflection of diaphragm.

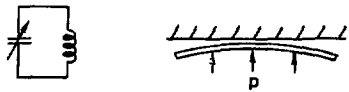

$\frac{\Delta c}{\Delta p}$ (GRC)

SHEAR MODE QUARTZ RESONATOR–Stress in quartz causes resonant frequency shift

$\frac{\Delta f}{\Delta p}$ (H.P.)

TRANSVERSE MODE QUARTZ RESONATOR–Stress in vibrating element causes change of frequency

$\frac{\Delta f}{\Delta p}$ (PAROS)

Figure 4. Types of gauges in common use.

- GEOTHERMAL - 7500 PSI, 275°C, ± .01 PSI

  1. DEVELOP QUARTZ CRYSTAL GAGE SIMILAR TO H.P.
  2. JOINT PROGRAM TO HARDEN COMMERCIAL CAPACITIVE OR STRAIN GAGE TOOL. (LESS RESOLUTION)
  3. ADD HIGH TEMPERATURE BOURDON TUBE GAGE TO EXISTING GEOTHERMAL TEMPERATURE TOOL CIRCUITRY. (LOW RESOLUTION)

- GEOPRESSURE - 20,000 PSI, 200°C, ± 0.1 PSI

  1. DEVELOP CIRCUITRY FOR STRAIN GAGE TOOL ON JOINT PROGRAM WITH LBL.
  2. JOINT DEVELOPMENT PROGRAM WITH A MANUFACTURER TO HARDEN THEIR EXISTING CAPACITIVE GAGE TOOL.
  3. MODIFY EXISTING H.P. PRESSURE TOOL FOR OPERATION IN THIS ENVIRONMENT.

Figure 5. Sandia/DOE pressure instrumentation program.

OBJECTIVE - TO DEVELOP AN ACCURATE, MEDIUM RESOLUTION LOGGING TOOL FOR USE IN GEOPRESSURE WELLS UP TO 20,000 PSI AND 200°C

CAPABILITIES - ACCURACY OF ± 5 PSI
RESOLUTION OF ± 0.1 PSI
(OVER PERIOD OF 5 DAYS)

APPROACH - ADAPT A COMMERCIALLY AVAILABLE STRAIN GAUGE TRANSDUCER TO SPECIAL 200°C CIRCUITRY

Figure 6. Geopressure logging tool using a strain gauge pressure transducer.

- STRAIN GAGE TRANSDUCER - BELL & HOWELL, CEC DIVISION STRAIN GAGE MODEL 1000, HAVING SPUTTERED GAGE PATTERNS. A SPECIAL GAGE WILL BE REQUIRED FOR 20,000 PSI.

- CIRCUITRY - SPECIALLY DESIGNED VCO AND CHOPPER-STABILIZED DC AMPLIFIER CIRCUITS ARE BEING DESIGNED EMPLOYING HARRIS 2600 HIGH TEMPERATURE OPERATIONAL AMPLIFIERS. THESE CIRCUITS WILL BE COMPATIBLE WITH THE NEW HARRIS 300°C OP AMP NOW UNDER DEVELOPMENT.

- READOUT - TEMPERATURE, PRESSURE, AND FLOW WILL BE MULTIPLEXED AND SURFACE INSTRUMENTATION WILL BE USED FOR TEMPERATURE, CORRECTED PRESSURE, AND FLOW INDICATION.

- PARTICIPANTS - LBL: TOOL HARDWARE, TESTING AND RESERVOIR ENGINEERING SUPPORT

  SANDIA: ELECTRONIC DEVELOPMENT, FABRICATION, AND TEST SUPPORT

Figure 7. Geopressure and pressure instrumentation development at Sandia.

OBJECTIVE - TO ENHANCE THE CAPABILITIES OF A STANDARD COMMERCIAL PRESSURE TOOL TO SATISFY THE GEOPRESSURE ENVIRONMENT OF 20,000 PSI AND 200°C.

CAPABILITIES - ACCURACY OF ± 2 PSI
RESOLUTION OF ± 0.05 PSI
(OVER PERIOD OF 5 DAYS)

APPROACH - TO APPLY SANDIA AND COMMERCIAL TECHNOLOGY, AS APPLICABLE, TO EXTEND THE APPROPRIATE CAPABILITIES. THIS WORK IS BEING DONE AS A JOINT DEVELOPMENT EFFORT WITH THE MANUFACTURER.

Figure 8. Geopressure logging tool using a capacitive diaphragm transducer.

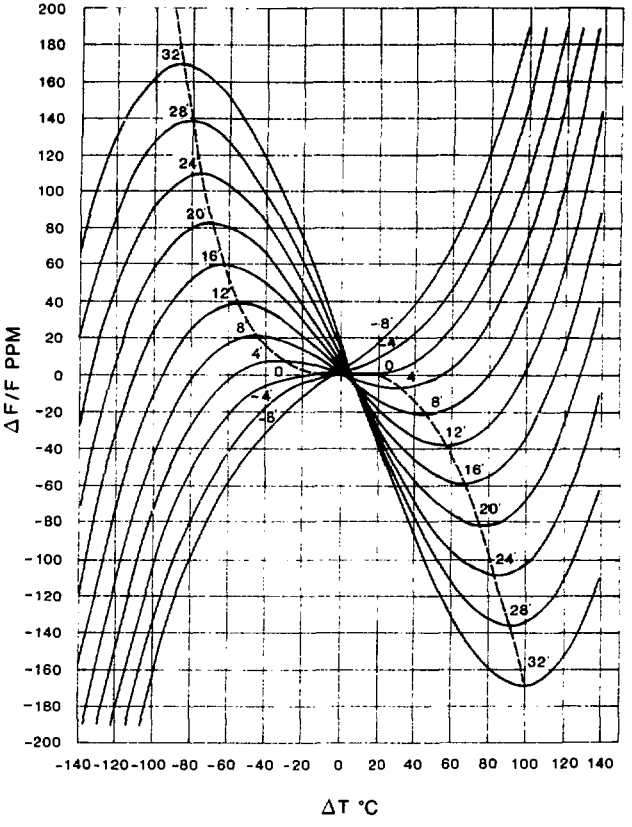

Figure 9. Frequency-temperature curves of AT-cut crystal.

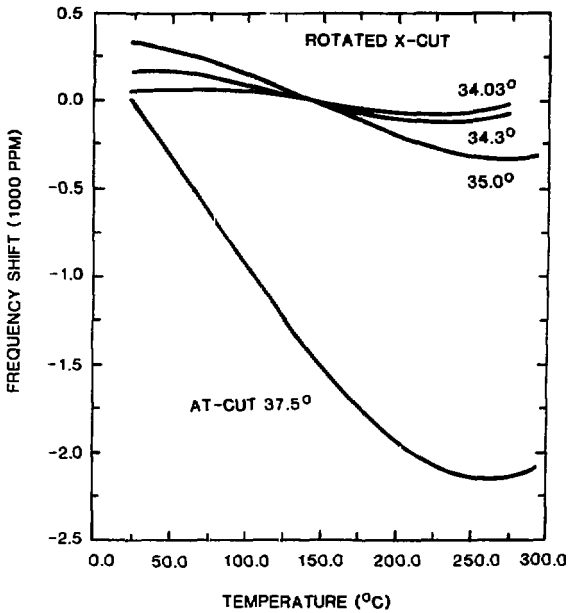

Figure 10. Measured frequency versus temperature characteristics for the rotated X-cut (The typical AT-cut chosen for a 275°C turning point is shown for comparison).

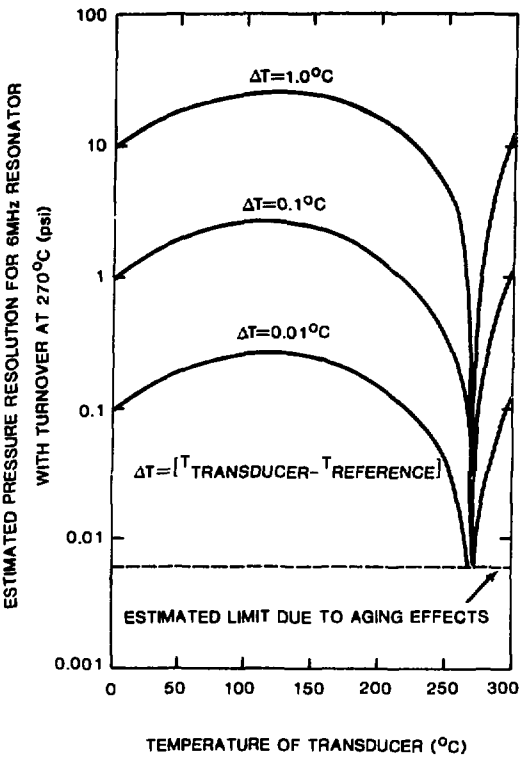

Figure 11. Estimated pressure resolution versus temperature for rotated X-cut crystals.

REQUIREMENT - MINIMIZE FREQUENCY SHIFT DUE TO TEMPERATURE.

1. FREQUENCY SHIFT OF CRYSTAL RESONATORS MUST BE MINIMIZED
2. OVERALL THERMAL INTERACTIONS MUST BE MINIMIZED
3. OSCILLATOR CIRCUITS MUST BE VERY STABLE
4. TURNING POINT OF CRYSTAL MUST BE INDEPENDENT OF PRESSURE

APPROACH

1. SELECT CRYSTALLOGRAPHIC AXIS TO MINIMIZE FIRST AND SECOND DERIVATIVES OF FREQ. VS. TEMP. CHARACTERISTIC AT 275°C
2. USE TWO IDENTICAL CRYSTALS, COUPLE THEM THERMALLY FOR TRACKING, AND ENCLOSE IN TEMPERATURE CONTROLLED OVEN
3. USE PIERCE TYPE OSCILLATOR CIRCUIT WITH AUTOMATIC GAIN CONTROL AND ENCLOSE IN OVEN
4. INVESTIGATE CONFIGURATIONAL CHANGES TO MINIMIZE SHIFT OF TURNING POINT CAUSED BY PRESSURE

Figure 12. Quartz crystal transducer development program.

INSTRUMENTATION FOR DETERMINING ROCK MASS PERMEABILITY BY HYDRO-PNEUMATIC PRESSURE TESTING

W. O. Miller
U. S. Army Engineer Waterways Experiment Station
Vicksburg, Mississippi

The Waterways Experiment Station (WES) has a research project underway which has the goals of developing better analytical techniques for interpreting and evaluating rock mass permeability as well as determining and describing the phenomena that control the flow of water through a rock mass. As a by-product of this investigation, new and improved instrumentation has been developed for use in the field of pressure testing.

The requirements for accurate measurements of rock mass permeability in low-permeability environments are precision, repeatability, and reliability. At the initiation of this study, a detailed review of existing pressure test equipment was made, and as a result, new instrumentation was developed by WES which eliminates many problems noted in earlier systems. Some of the problems which were noted in existing systems were the unreliability of electronic transducers in the testing environment; the inability to verify or cross-check downhole pressure measurements; a difficulty in maintaining or assuring a positive packer to test section differential pressure; and very long packer inflation and deflation times in deep borings. The time required for inflation and deflation ranged between 15 and 20 minutes in deep borings (1500 to 2000 feet) when a supply of compressed air on the surface was used for packer inflation. It was also noted that perforated pipe was frequently used in the test sections which constituted a source of excessive friction losses if high flow rates were attained.

In order to eliminate the problems encountered with existing pressure test equipment, a downhole control unit, Figures 1 and 2, was designed for conducting tests in NX boreholes. The unit maintains a preset minimum differential pressure between the packers and the test section, and controls inflation and deflation of the packers. The packer response to inflation and deflation commands is greatly increased in deep borings since the control unit is located downhole, and inflation is accomplished with the testing fluid (which is normally either water or air). For increased flexibility, the control unit was designed with the capacity for operating as either a single- or double-packer system by the use of simple ground surface control commands.

Within the control unit four transducers (rated from 0 to 3000 psi) are used to measure packer pressure, test section pressure, and the pressures above and below the packers. Redundancy was designed into the system by interfacing three of the downhole pressure sensing points (above packer, test section, and below packer) through a nine-way valve to three transducers. In the event of a transducer failure during testing, a critical pressure sensing point can be moved to another transducer with simple ground surface controls. With such flexibility, a test can be continued as long as one of the three interfaced transducers is functioning. Additionally, this capability provides the ability to verify pressure measurements by changing transducers while a test is in progress. The electronic components of the unit are protected from the testing environment with a waterproof housing and O-ring seals.

To reduce friction losses in the test section at high flow rates, stainless steel, wire-wrapped, keystone-slotted well screen is used in lieu of perforated pipe. For NX boreholes, the test section screens currently being used are 1-3/4 inch in diameter and have a No. 80 slot, i.e. 0.080-inch slot width.

To facilitate the control and monitoring of any pressure test, various uphole systems have been designed and assembled. Constant pressure tests are controlled with a specially fabricated pressure regulating by-pass valve, Figure 3. The flow rate is monitored with flow meter manifolds, Figure 4, capable of measuring water flow rates from 0.03 to 250 gpm, and air flow rates from 0.15 to 750 cfm. If constant flow tests are conducted, they are controlled with a specially designed automated flow control valve, Figure 5, which monitors the flow meter output and maintains the desired flow rate with a regulating valve.

An uphole control system, Figure 6, has been designed and constructed to monitor test data and operate the downhole control unit. Control and monitoring of the downhole electronics is accomplished with a single, multiconductor, waterproof signal transmission cable, Figure 7. A programmable data acquisition system, Figure 8, has been interfaced with the uphole control system to provide a permanent record of test data. Data which are currently monitored and recorded at a test well are test section pressure, pressure above the test section, packer pressure, line pressure on the ground surface, and flow rate. The data acquisition system, however, has expansion capabilities for reading up to 1000 data points (either strain gage or analog signals). With the above monitoring capacity, a complete three-dimensional array of piezometers may be installed around a pressure test well for the purpose of describing the pressure bulb generated. Since data reduction techniques in pressure testing are a function of the assumed flow pattern from the well, a knowledge of the pressure bulb generated by a test is very useful.

Various components of the pressure testing system have been tested individually. The automated flow control valve, flow meters, and data acquisition system, along with transducers designed specifically for water level measurements, have been field tested in a series of field pumping tests and have proven to be very successful to date. The downhole control unit and the uphole control

system have been tested extensively in the laboratory. One field test, Figure 9, has been conducted to date with the complete pressure testing system. All components checked out satisfactorily in the testing environment.

The entire system is ready for field application, with the following exceptions. Prior to performing an air pressure test, thermocouples must be installed in the downhole control unit for measuring fluid temperature in the test section as well as in the flow meter manifold to measure uphole fluid temperature. All the necessary monitoring and recording provisions have been included in the existing instrumentation for temperature measurements and installation of the sensors is the only remaining requirement.

The equipment and instrumentation which have been developed provide the accuracy and reliability required for an evaluation of pressure testing data and techniques. The primary emphasis of future work will be directed toward developing interpretative techniques, using pressure test and geologic data, which provide a better understanding of the phenomena which control the movement of water (or air) through rock masses.

Initial pressure tests (water and air) will be conducted at well-defined or geologically predictable sites. Rock coring as well as borehole logging will be conducted at each site to accurately determine the geologic features and fissure characteristics which could control flow through the rock mass. In the interim, a modeling effort is being initiated which will identify and delineate the relative contribution of the various geologic features which control the overall permeability. If the model studies reveal flows which are significantly different than the usual assumption of flow in continuous porous media, a discontinuum approach to data reduction will be made. The end product would be formulas which better reflect the boundary conditions and provide a means of possibly integrating geologic and pressure test data for a more accurate evaluation of the permeability.

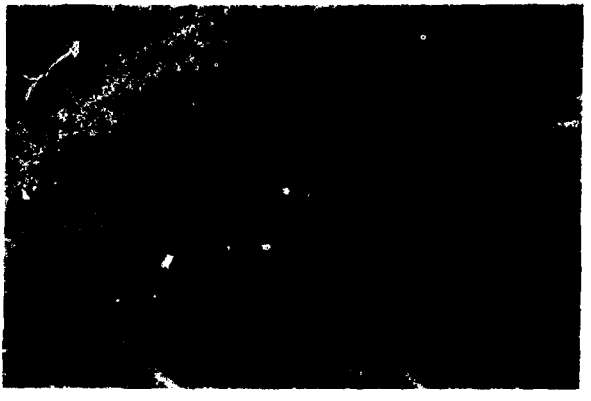

Fig. 1. Downhole control unit with packers and screen.

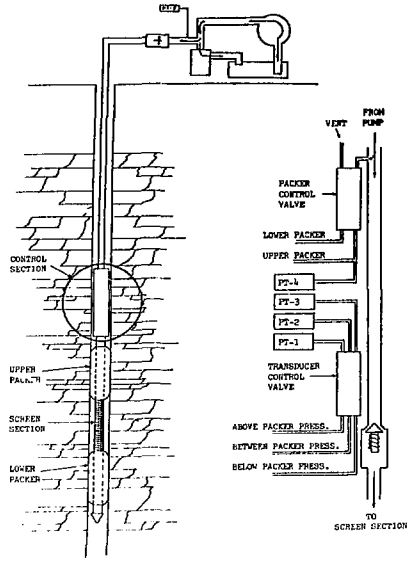

Fig. 2. Downhole control unit schematic.

Fig. 4. Flow meter manifold with pressure regulator.

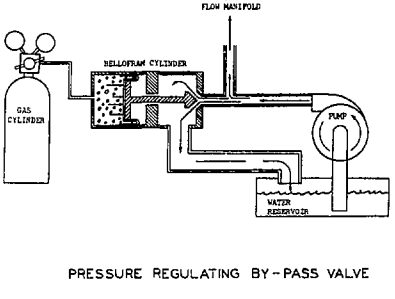

Fig. 3. Pressure regulating by-pass valve schematic.

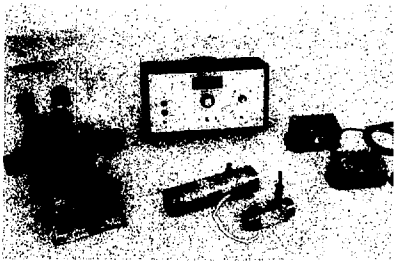

Fig. 5. Automated flow control valve with flow meters and instrumentation.

Fig. 6. Uphole control system for hydro-pneumatic pressure test equipment.

Fig. 8. Uphole control system, data acquisition system, and 50-channel expansion unit.

Fig. 7. Signal transmission cable.

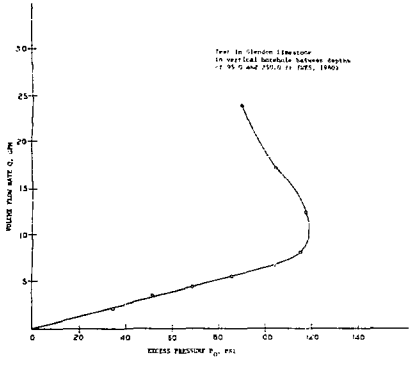

Fig. 9. Single-packer pressure test data.

ABSTRACT

FRACTURE CHARACTERIZATION IN CRYSTALLINE ROCK WITH THE BOREHOLE TELEVIEWER

Mark D. Zoback
Office of Earthquake Studies
U. S. Geological Survey
Menlo Park, California

The borehole televiewer is an ultrasonic device originally developed by Mobil Oil Corp. to map the smoothness of well bores and casing. Planar fractures that intersect uncased boreholes are easily detected with the tool and as the tool contains a fluxgate magnetometer, it is straight-forward in reconstructing the strikes and dips of the fractures. Results are reported from studies that have been done in eight wells drilled into granitic rocks. Six of the wells are in California; the depth of these wells is about 250 m. In South Carolina data are available from two wells approximately 1.1 km deep. The following generalizations characterize the data:

1) Although moderate decreases in fracture density with depth are observed, this effect is not dramatic, even in the deeper wells.

2) In some cases a predominant fracture trend persists over the entire depth range of the well; in other cases distinct fracture sets are limited to a particular depth range.

3) Correlation between the televiewer and sonic velocity logs is generally good; zones of dense fracturing have much lower velocity and a progressive decrease in fracture density with depth correlates with a moderate increase in velocity. In some zones of little apparent fracturing, however, low velocities are sometimes observed suggesting the presence of microfractures or undetected fractures.

ABSTRACT

DOWNHOLE DOUBLE PACKER INSTRUMENTATION WITH HIGH PRESSURE RESOLUTION CAPABILITY AND IMMEDIATE SURFACE MONITORING ABOVE, BELOW AND IN THE STRADDLED INTERVAL

K. G. Kennedy, W. Miller and R. R. Phillips
Science Applications, Inc.
Albuquerque, New Mexico

Surface monitoring of transient and static test data is essential for effective utilization of high cost downhole testing instrumentation. Science Applications, Inc. (SAI) and Lynes, Inc. have developed design and testing methods for allowing this type of monitoring. We recently tested basalt rocks to depths of about 1500 m (4500 feet) on a project funded by Rockwell Hanford Operations in Richland, Washington.

The downhole instrumentation consists of a modified version of the Lynes 'Treat and Test Tool' Packer Assembly, integrated with a sensor carrier located just above the top packer that contains three quartz pressure transducers ported above, below and into the straddled interval. A shut-in tool is located above the carrier; it is closed to prevent disturbing the formation pressure when the tool is run into the well.

Downhole multiplexing of the frequency signals allows rapid transmission of both pressure and temperature data to surface processing equipment, where it is printed, displayed, recorded and plotted, utilizing Hewlett-Packard microprocessing equipment.

The 0 to 5000 psi quartz pressure tranducers have a demonstrated resolution of $\pm$0.01 psi and an accuracy of about $\pm$2.5 psi.

The water-inflatable rubber packers provide excellent borehole sealing capability using a packer inflation pressure typically 1500 psi above the downhole pressure. The inflation procedure, however, can create a 'squeeze' or overpressure in the interval between the packers. This is undesirable in testing low permeability zones and can create extensive interpretation problems and delays.

The instrumentation package is particularly well suited to conduct instantaneous pulse or slug tests and drill stem-type tests. Incorporating a shut-in tool just above the packer and downhole electronics assembly allows much more versatility in testing than would an open conduit connecting the formation with the surface.

When testing in open hole conditions with multilayered aquifers, additional packers installed below and above the double packer system would be an improvement in the method for documenting fluid movement in the rock around the packers.

LIST OF PARTICIPANTS

AAMODT, Lee
Los Alamos National Laboratory
P. O. Box 1663
Los Alamos, New Mexico 87544
(505) 667-5048

ABOU-SAYED, Ahmed
TerraTek, Inc.
University Research Park
420 Wakara Way
Salt Lake City, Utah 84108
(801) 582-2220

AGARWAL, Ram G.
Amoco Production Co.
P. O. Box 591
Tulsa, Oklahoma
(918) 664-3042

AHMED, Usman
TerraTek, Inc.
University Research Park
420 Wakara Way
Salt Lake City, Utah 84108
(801) 582-2220

ALLMAN, David W.
University of Idaho
209 Taylor, #13
Moscow, Idaho 83843
(209) 882-7977

ALMEN, Karl-Erik
Geological Survey of Sweden
Sveriges geologiska undersokning
Vretgrand 18
S-753 22 Uppsala
SWEDEN
018/15 56 40

ANDERSON, Merlin
Halliburton Services
905 Alice
P. O. Box 1431
Duncan, Oklahoma 73533
(405) 251-3137

ANDERSON, Terry O.
Halliburton Services
P. O. Box 1431
Duncan, Oklahoma 73533
(405) 251-3271

ARELLANO, Victor M.
Interior Internado Palmira
Apartado Posta 475
Cuernavaca, Morelos
MEXICO

BANKS, Don
Waterways Experiment Station
P. O. Box 631
Vicksburg, Mississippi 39180
(601) 634-2630
FTS 542-630

BASLER, James A.
U.S. Geological Survey
Water Resources Division
505 Marquette N.W.
P. O. Box 26659
Albuquerque, New Mexico 87125
(505) 766-2810
FTS 474-2246

BENSON, Sally
Lawrence Berkeley Laboratory
Bldg. 90/1106
1 Cyclotron Road
Berkeley, California 94720
(415) 486-5875
FTS 451-5875

BENTLEY, Michael E.
Bureau of Economic Geology
University of Texas
Box X, University Station
Austin, Texas 78712
(512) 471-1534

BLACK, John H.
Institute of Geological Sciences
Building 151
Harwell Laboratory
Didcot, Oxon
ENGLAND
0235 24141 x 2232

BLACK, Bill (W.H.)
Westbay Instruments Ltd.
265 - 25th Street
West Vancouver, B.C.
Canada V3L 4G2
(604) 926-8541

BLUM, Justin
Woodward-Clyde Consultants
#3 Embarcadero Center, Ste. 700
San Francisco, California 94111
(415) 956-7070

BÖDVARSSON, Gudmundur
Lawrence Berkeley Laboratory
Bldg. 90/1024D
1 Cyclotron Road
Berkeley, California 94720
(415) 486-5350
FTS 451-5350

BÖDVARSSON, Mary
Lawrence Berkeley Laboratory
Bldg. 90/1024D
1 Cyclotron Road
Berkeley, California 94720
(415) 486-5350
FTS 451-5350

BRANAGAN, Paul
CER Corporation
4370 S. Maryland Parkway
Las Vegas, Nevada 89109
(202) 735-7136

BRIGHAM, William E.
Stanford University
Petroleum Engineering Dept.
Stanford, California 94305
(415) 497-1774

BURNS, Floyd L.
Batelle
Office of Nuclear Waste Isolation
505 King Avenue
Columbus, Ohio 43201

CARLSSON, Leif
Geological Survey of Sweden
Sveriges geologiska undersökning
Vretgrand 18
S-753 22 Uppsala
SWEDEN
018/15 56 40

CHRISTENSEN, Chris
Nuclear Waste Experimental Programs
Division 4512
Sandia Laboratories
Albuquerque, New Mexico 87185
(505) 264-9930

COHEN, Lewis
Lawrence Berkeley Laboratory
Bldg. 90/1106
1 Cyclotron Road
Berkeley, California 94720
(415) 486-6457
FTS 451-6457

CORDOBA, Francisco
Interior Internado Palmira
Apartado Posta 475
Cuernavaca, Morelos
MEXICO

COTNER, Gene
CER Corporation
P. O. Box 15090
Las Vegas, Nevada 89114
(702) 735-7136

DERBY, James A.
Halliburton Services
P. O. Box 1431
Duncan, Oklahoma 73533
(415) 251-3271

DOE, Thomas
Lawrence Berkeley Laboratory
Bldg. 90/1106
1 Cyclotron Road
Berkeley, California 94720
(415) 486-6778
FTS 451-6778

FARRELL, Clifford
Bechtel Incorporated
50 Beale Street
San Francisco, California
(415) 764-5655

FILBEY, Gil
Go Wireline Services
2730 Gundry
Long Beach, California 90805
(213) 426-6559

GALE, John E.
Dept. of Earth Sciences
University of Waterloo
Waterloo, Ontario
N2L 3G1
(519) 885-1211, ext. 3464

GILMAN, Jeffrey A.
Woodward-Clyde Consultants
#3 Embarcadero Center
San Francisco, California 94111
(415) 956-7070, ext. 437

GORANSON, Colin
Lawrence Berkeley Laboratory
Bldg. 90/1024A
1 Cyclotron Road
Berkeley, California 94720
(415) 486-6657
FTS 451-6657

GOYAL, Keshav P.
Lawrence Berkeley Laboratory
Bldg. 90/1024D
1 Cyclotron Road
Berkeley, California 94720
(415) 486-5400
FTS 451-5400

GRAHAM, David L.
University of Idaho
Rt. 4, Box 291-A #20
Moscow, Idaho 83813
(208) 885-7977

GRISAK, Gerry
Environment Canada
502 Booth Street
Ottawa
Ontario, Canada
K1V 8H2
(613) 995-4020

GUVANASEN, Varuttama
Lawrence Berkeley Laboratory
Bldg. 90/1106
1 Cyclotron Road
Berkeley, California 94720
(415) 486-6001
FTS 451-6001

HANSON, Jonathan
Lawrence Livermore Laboratory
Box 808, L-220
Livermore, California 94530
(415) 422-6509

HARRISON, Roger
Eureka Energy
215 Market Street
San Francisco, California 94106

HAWS, Jerr
Oil Recovery Department
Research Division
Marathon Oil Company
7400 South Broadway
P. O. Box 269
Littleton, Colorado 80160
(303) 794-2601

HERRGOTT, John G.
Hewlett Packard
690 East Middlefield Road
Mountain View, California 94042
(415) 969-0880

HORNE, Roland N.
Dept. of Petroleum Engineering
Stanford University
Stanford, California 94305
(415) 497-9595

HSIEH, Chih-Hang
Conoco, Inc.
125 Roadrunner Drive
Ponca City, Oklahoma 74601
(405) 765-8905

HSIEH, Paul
University of Arizona
Dept. of Hydrology
Tucson, Arizona 85719
(602) 626-3131

HSU, Sungnan
Halliburton Services
Drawer 1431
Duncan, Oklahoma 73533
(405) 251-3350

IGLESIAS, Eduardo R.
Lawrence Berkeley Laboratory
Bldg. 90/1024G
1 Cyclotron Road
Berkeley, California 94720
(415) 486-5943
FTS 451-5943

IRVINE, Jeffrey
Lawrence Berkeley Laboratory
Bldg. 90/1106
1 Cyclotron Road
Berkeley, California 94720
(415) 486-6789
FTS 451-6789

JAMIESON, I.
Enthalpy Inc.
320 College Ave., Ste. 305
Santa Rosa, California 95401
(707) 542-6429

KAM, James T.
Science Applications Inc.
200 Lomas N.W., Ste 600
Albuquerque, New Mexico 87102
(505) 247-0381

KANEHIRO, Brian
Lawrence Berkeley Laboratory
Bldg. 90/1106
1 Cyclotron Road
Berkeley, California 94720
(415) 486-4717
FTS 451-4717

KATZ, Donald L.
University of Michigan
Ann Arbor, Michigan 48104

KEENEY, Ronald C.
Radian Corporation
8500 Shoal Creek
Austin, Texas 78
(512) 454-4797

KENNEDY, Keith G.
Science Applications, Inc.
200 Lomas N.W., Ste. 600
Albuquerque, New Mexico 87102
(505) 247-0381

KIHARA, Deane
University of Hawaii
2540 Dole Street
Honolulu, Hawaii 96822
(808) 948-7167

KING, M. S.
Engineering Geoscience
University of California
Berkeley, California 94720
(415) 642-3157

KUNZMAN, William J.
Marathon Oil Company
7400 South Broadway
Littleton, Colorado 80160
(303) 794-2601

LEE, Pat
Gartner Lee Associates Ltd.
Toronto Buttonville Airport
Markham
Ontario Canada L3P 3J9
(416) 297-4600

LICHTNER, Peter
Lawrence Berkeley Laboratory
Bldg. 90/1140
1 Cyclotron Road
Berkeley, California 94720
(415) 486-5298
FTS 451-5298

LIPPMANN, Marcelo
Lawrence Berkeley Laboratory
Bldg. 90/1012E
1 Cyclotron Road
Berkeley, California 94720
(415) 486-5035
FTS 451-5035

LONG, Jane
Lawrence Berkeley Laboratory
Bldg. 90/1106
1 Cyclotron Road
Berkeley, California 94720
(415) 486-6697
FTS 451-6697

LUNDY, Don
Brown and Caldwell
Consulting Engineers
1501 N. Broadway
Walnut Creek, California 94596

McEDWARDS, Donald G.
Harding Lawson Associate
7655 Redwood Boulevard
P. O. Box 578
Novato, Calfornia 94747
(415) 892-0821

MAEDER, Paul F.
Brown University
Providence, Rhode Island 07912
(401) 863-7655

MANGOLD, Donald C.
Lawrence Berkeley Laboratory
Bldg. 90/1024F
1 Cyclotron Road
Berkeley, California 94720
(415) 486-6459
FTS 451-6459

MEHRAN, Mohsen
Lawrence Berkeley Laboratory
Bldg. 90K
1 Cyclotron Road
Berkeley, California 94720
(415) 486-5655

MERCER, Jerry W.
U.S. Geological Survey
Water Resources Division
505 Marquette N.W.
P. O. Box 26659
Albuquerque, New Mexico 87125
(505) 766-2810
FTS 474-2246

MEYER, Charles F.
G. E. TEMPO
P. O. Drawer QQ
Santa Barbara, California 93102
(805) 965-0551

MILLER, Billy R.
Lynes, Inc.
P. O. Box 12486
Houston, Texas 77017
(713) 790-9132

MILLER, Constance W.
Lawrence Berkeley Laboratory
Bldg. 90/1042
1 Cyclotron Road
Berkeley, California 94720
(415) 486-6454
FTS 451-6454

MILLER, Frank G.
Stanford University
Petroleum Engineering Dept.
Stanford, California 94305
(415) 497-2938

MILLER, W. O. "Yogi"
U.S. Army Engineers
Waterways Experiment Station
P. O. Box 631
Vicksburg, Mississippi 39180
(601) 634-2117

MOLLY, Martin W.
U.S. Department of Energy
Division of Geothermal Energy
San Francisco Operations Office
1333 Broadway
Oakland, California 94612
(415) 273-7943
FTS 536-7943

MOUNT, Russell
Hydro-Search, Inc.
333 Flint Street
Reno, Nevada 89501
(702) 322-4173

NARASIMHAN, T. N.
Lawrence Berkeley Laboratory
Bldg. 90/1012D
1 Cyclotron Road
Berkeley, California 94720
(415) 486-5655
FTW 451-5655

NELSON, Phillip
Lawrence Berkeley Laboratory
Bldg. 90/1070
1 Cyclotron Road
Berkeley, California 94720
(415) 486-6758
FTS 451-6758

NEUMAN, Shlomo P.
University of Arizona
7632 Calle Cabo
Tucson, Arizona 85715
(602) 885-3482

O'BRIEN, Maura
Lawrence Berkeley Laboratory
Bldg. 90/1042
1 Cyclotron Road
Berkeley, California 94720
(415) 486-4745
FTS 451-4745

OLSON, Karl R.
Lawrence Berkeley Laboratory
Bldg. 90/1106
1 Cyclotron Road
Berkeley, California 94720
(415) 486-6129
FTS 451-6129

O'SULLIVAN, M. J.
Lawrence Berkeley Laboratory
Bldg. 90/1024C
1 Cyclotron Road
Berkeley, California 94720
(415) 486-6452
FTS 451-6452

PALEN, Walter A.
University of California
Bldg. 90/1024D
Berkeley, California 94720
(415) 486-5350
FTS 451-5350

PALMA, Julio Cesar
Instituto Nacional Elect. (I.N.D.E.)
San Jose Villa Nueva, Guatemala
Guatemala, C.A.
460 712 ext. 19

PAPADOPULOS, Stavros S.
S. S. Papadopulos & Associates
8216 Scotch Bend Way
Potomac, Maryland 20854
(301) 983-9119

PATTON, Frank
Westbay Instruments Ltd.
#2-265 - 25th Street
West Vancouver, B.C.
Canada V7V 4H9
(604) 926-8541

PAULSSON, Björn
Lawrence Berkeley Laboratory
Bldg. 90/1070
1 Cyclotron Road
Berkeley, California 94720
(415) 486-6789
FTS 451-6789

PELKA, Walter
RWTH Aachen
Elsass-Str. 88
D-5100 Aachen
West Germany

PETERSON, Ed
Systems, Science & Software
3398 Carmel Mountain Road
San Diego, California 92038
(714) 453-0060

PHILIP, John F.
Lawrence Berkeley Laboratory
Bldg. 90/1012A
1 Cyclotron Road
Berkeley, California 94720
(415) 486-6468
FTS 451-6468

POPIELAK, Roman
D'Appolonia Consulting Engineers, Inc.
P. O. Box 22417
7400 South Alton Court
Denver, Colorado 80222
(303) 771-3464

PRATT, Howard R.
TerraTek
University Research Park
420 Wakara Way
Salt Lake City, Utah 84108
(801) 582-2220

PRUESS, Karsten
Lawrence Berkeley Laboratory
Bldg. 90/1042E
1 Cyclotron Road
Berkeley, California 94720
(415) 486-6106
FTS 451-6106

RACHIELE, Richard
Lawrence Berkeley Laboratory
Bldg. 90/1106
1 Cyclotron Road
Berkeley, California 94720
(415) 486-6789
FTS 451-6789

RAMEY, J. H.
Stanford University
Petroleum Engineering Dept.
Stanford, California 94305
(415) 497-1774

RAPIER, Pascal M.
Lawrence Berkeley Laboratory
Bldg. 90/1070G
1 Cyclotron Road
Berkeley, California 94720
(415) 486-4708
FTS 451-4708

REDA, Daniel C.
Sandia Laboratories
9508 Admiral Nimitz N.E.
Albuquerque, New Mexico 87111
(505) 844-4916

REMER, Janet
Lawrence Berkeley Laboratory
Bldg. 90/1070
1 Cyclotron Road
Berkeley, California 94720
(415) 486-4450
FTS 451-4450

ROGERS, Leah
Lawrence Livermore Laboratory
East Avenue
Livermore, California 94550
(415) 422-3538

ROGERS, Leo A.
Institute of Gas Technology
3424 South State Street
Chicago, Illinois 60616
(312) 567-5292

ROCKAR, Evelyn M.
Institute of Gas Technology
3424 South State Street
ITT Center
Chicago, Illinois 60616
(312) 567-5825

SAARI, Kari
University of California
440 Davis Hall
Berkeley, California 94720
(415) 642-6557

SANYAL, Subir K.
Stanford University
Stanford, California 94305
(415) 497-0691

SAREM, A. M. Sam
Union Science & Technology Division
Union Oil Company of California
376 South Valencia Avenue
Brea, California 92621
(714) 528-7201

SCHLEMMER, A. E.
Texas Eastern Corporation
P. O. Box 2521
Houston, Texas 77001
(713) 759-5466

SCHROEDER, Ron C.
Lawrence Berkeley Laboratory
Bldg. 90/1012C
1 Cyclotron Road
Berkeley, California 94720
(415) 486-5560
FTS 451-5560

SCHWARZ, Werner J.
Lawrence Berkeley Laboratory
Bldg. 90/1070
1 Cyclotron Road
Berkeley, California 94720
(415) 486-4706
FTS 451-4706

SEKI, Arthur
Hawaii Natural Energy Institute
University of Hawaii at Manoa
2540 Dole Street
Honolulu, Hawaii 96822
(808) 948-8890

SIMPSON, E. S.
University of Arizona
Department of Hydrology
Tucson, Arizona 85721
(602) 626-1855

SMITH, Donald A.
University of Idaho
849 Kennett Avenue
Moscow, Idaho 83843
(208) 882-0792

SPANE, Frank A., Jr.
Rockwell Hanford Operations
P. O. Box 800
Richland, Washington 99352
(509) 942-2615

STEPHENSON, Dale E.
D'Appolonia Consulting Engineers, Inc.
2340 Alamo S.E., Ste. 306
Albuquerque, New Mexico 87112
(505) 842-0835

STERBENTZ, Rebecca
Lawrence Berkeley Laboratory
Bldg. 90K
1 Cyclotron Road
Berkeley, California 94720
(415) 486-6696
FTS 451-6696

STONE, Randolph
Lawrence Livermore Laboratory
P. O. Box 808
Livermore, California 94550
(415) 422-6499

STRISOWER, Beverly
Lawrence Berkeley Laboratory
Bldg. 90/1046
1 Cyclotron Road
Berkeley, California 94720
(415) 486-6658
FTS 451-6658

STROMDAHL, A. W.
Lawrence Berkeley Laboratory
Bldg. 90/1070
1 Cyclotron Road
Berkeley, California 94720
(415) 486-6708
FTS 451-6708

TEILMAN, Maren
IECO
180 Howard Street
San Francisco, California 94105
(415) 442-7300

THIERY, Dominique P.
BRGM
BP 6009 Orleans
France 45018

THOMPSON, Glenn
University of Arizona
Dept. of Hydrology
Tucson, Arizona 85721
(602) 626-4208

THUR, William
Lawrence Berkeley Laboratory
Bldg. 90/1070
1 Cyclotron Road
Berkeley, California 94720
(415) 486-4381
FTS 451-4381

TSANG, Chin Fu
Lawrence Berkeley Laboratory
Bldg. 90/1012H
1 Cyclotron Road
Berkeley, California 94720
(415) 486-5782
FTS 451-5782

UPDEGRAFF, C. David
Science Applications
200 Lomas Bldv. N.W.
Albuquerque, New Mexico 87112
(505) 247-0381

VECHIL, Jack
Go Wireline Services
5024 Airport Drive
Bakersfield, California 93308
(805) 399-9541

VENERUSO, A. F.
Sandia Laboratories
P. O. Box 5800
Albuquerque, New Mexico 87185
(505) 844-9162

VON BRIESEN, Roy
Johns Hopkins University
Johns Hopkins Road
Laurel, Maryland 20810
(301) 953-7100

VONDER HAAR, Stephen
Lawrence Berkeley Laboratory
Bldg. 90/1024D
1 Cyclotron Road
Berkeley, California 94720
(415) 486-5350
FTS 451-5350

WANG, Joseph S. Y.
Lawrence Berkeley Laboratory
Bldg. 90/1012G
1 Cyclotron Road
Berkeley, California 94720
(415) 486-6753
FTS 451-6753

WITHERSPOON, Paul A.
Lawrence Berkeley Laboratory
Bldg. 90/1106
1 Cyclotron Road
Berkeley, California 94720
(415) 486-5082
FTS 451-5082

WOLLENBERG, Harold
Lawrence Berkeley Laboratory
Bldg. 90/1046
1 Cyclotron Road
Berkeley, California 94720
(415) 486-5344
FTS 451-5344

YANES-MORENO, Alberto
Apartado Postal 475
Cuernavaca Mor.
MEXICO

YU, Kwang
Johns Hopkins University Applied Physics Lab.
1 Johns Hopkins Road
Laurel, MD 20910
(301) 953-7100

YUEN, Paul
University of Hawaii
Hwaiii Natural Energy Institute
2540 Oole Street
Honolulu, Hawaii 96822
(808) 948-8890

ZAIS, Dr. Elliot J.
Elliot Zais & Associates, Inc.
7915 N.W. Siskin Drive
Corvallis, Oregon 97330
(503) 757-9795

ZOBACK, Mark
U. S. Geological Survey
345 Middlefield Rd.
Menlo Park, California 94025

NAME INDEX

C = Committee
A = Author
Ch = Chairman

U.S.GPO:1981:789-009/5718